AD-A076 023 TRW INC CLEVELAND OHIO F/G 11/2
ULTRASONIC DETECTION OF SURFACE FLAWS IN GAS TURBINE CERAMICS.(U)
AUG 79 T DERKACS , I M MATAY N62269-77-C-0136
UNCLASSIFIED TRW-ER-7980-F NADC-76369-30 NL

1 OF 2
AD A076023

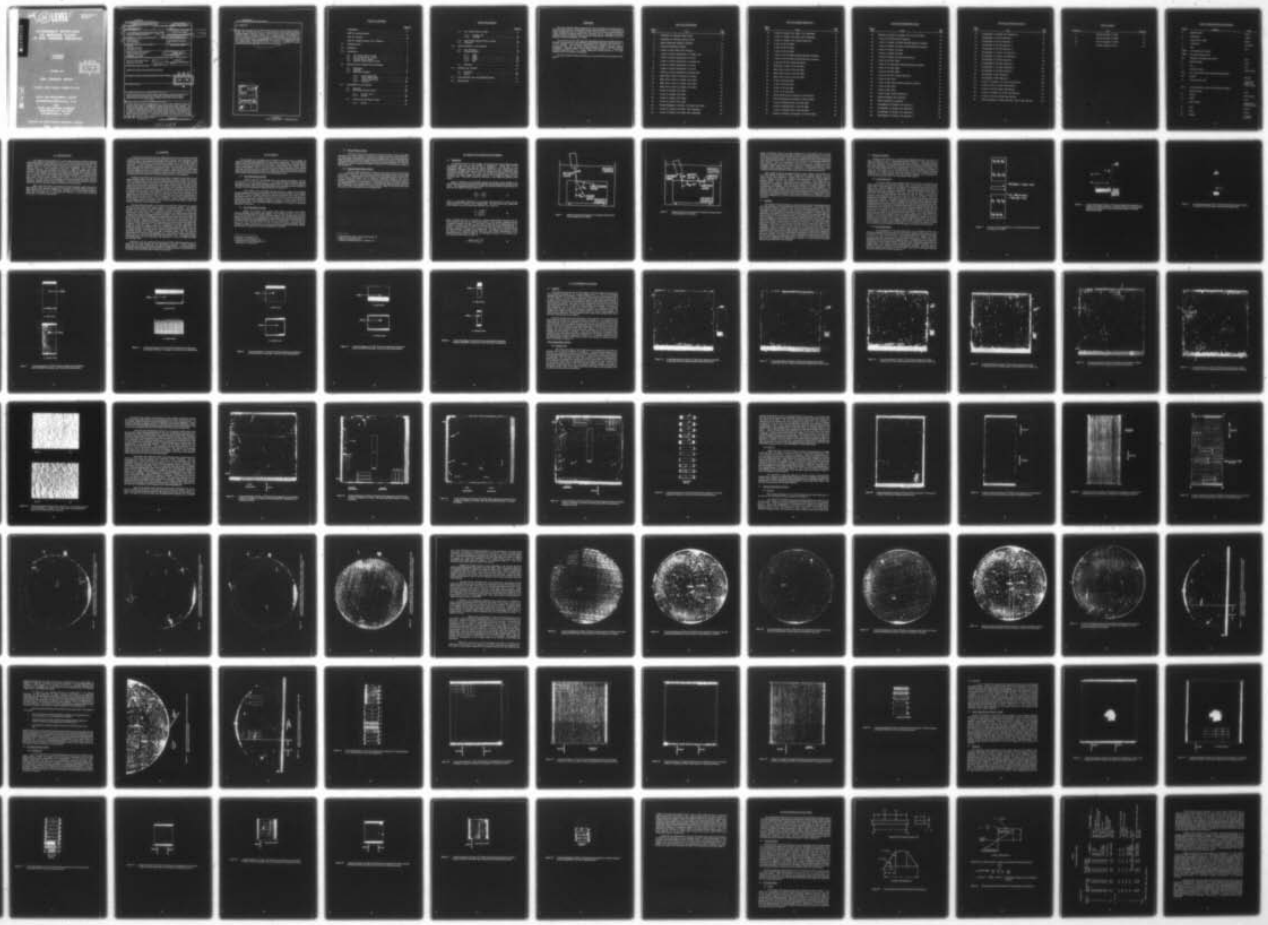

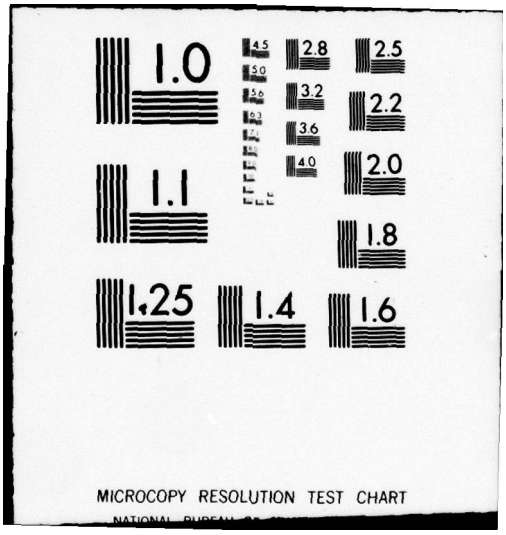
1.0
1.1
1.25
1.4
1.6
1.8
2.0
2.2
2.5
2.8
3.2
3.6
4.0
4.5
5.0
5.6
MICROCOPY RESOLUTION TEST CHART

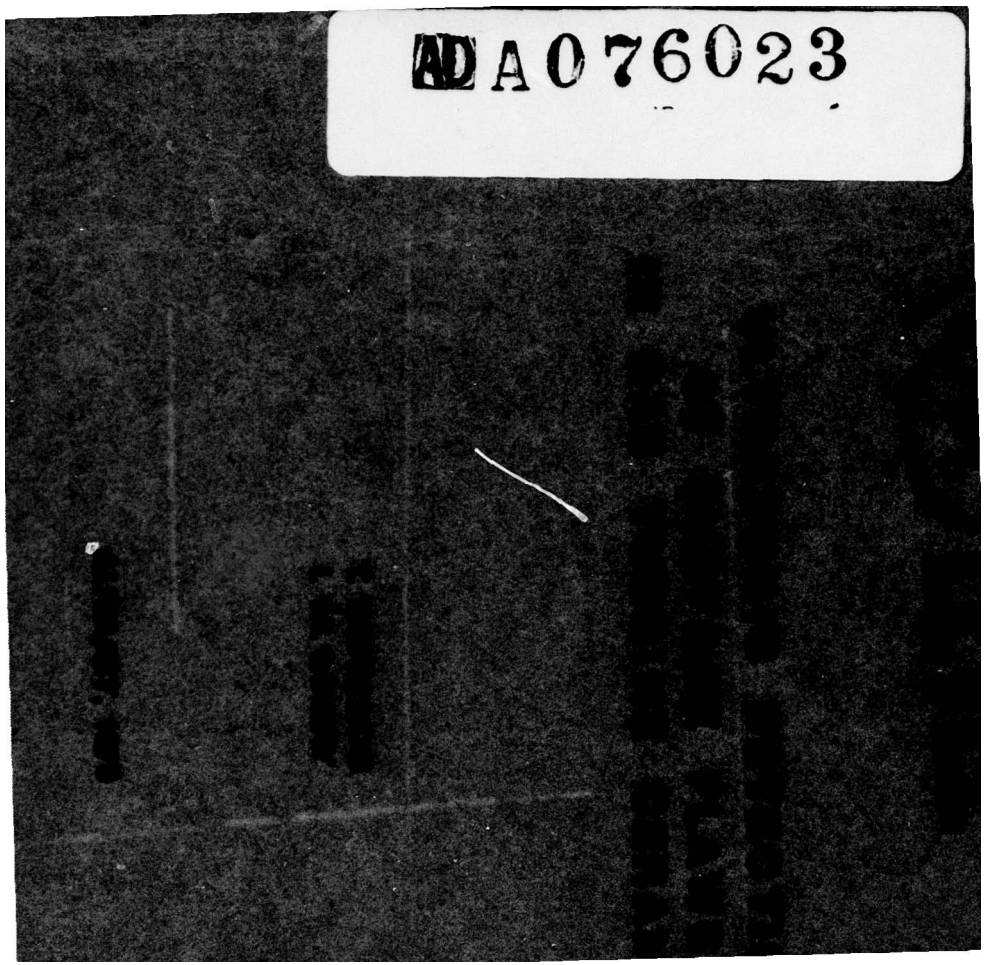
AD A076023

Unclassified

SECURITY CLASSIFICATION OF THIS PAGE (When Data Entered)

REPORT DOCUMENTATION PAGE	READ INSTRUCTIONS BEFORE COMPLETING FORM
1. REPORT NUMBER: NADC-76369-30	2. GOVT ACCESSION NO. / 3. RECIPIENT'S CATALOG NUMBER
4. TITLE (and Subtitle): ULTRASONIC DETECTION OF SURFACE FLAWS IN GAS TURBINE CERAMICS	5. TYPE OF REPORT & PERIOD COVERED: Final Technical Report, 13 Sep 77 - 12 Dec 78
	6. PERFORMING ORG. REPORT NUMBER: TRW-ER-7986-F
7. AUTHOR(s): Thomas Derkacs, Istvan M. Matay	8. CONTRACT OR GRANT NUMBER(s): N62269-77-C-0136
9. PERFORMING ORGANIZATION NAME AND ADDRESS: TRW Inc., 23555 Euclid Avenue, Cleveland, OH 44117	10. PROGRAM ELEMENT, PROJECT, TASK AREA & WORK UNIT NUMBERS
11. CONTROLLING OFFICE NAME AND ADDRESS: Naval Air Systems Command, Department of the Navy, Washington, DC 20361	12. REPORT DATE: August 1979; 13. NUMBER OF PAGES: 123
14. MONITORING AGENCY NAME & ADDRESS (if different from Controlling Office): Naval Air Development Center, Warminster, PA 18974	15. SECURITY CLASS. (of this report): Unclassified; 15a. DECLASSIFICATION/DOWNGRADING SCHEDULE

16. DISTRIBUTION STATEMENT (of this Report)

Approved for public release; distribution unlimited.

DDC RECEIVED NOV 1 1979 B

17. DISTRIBUTION STATEMENT (of the abstract entered in Block 20, if different from Report)

18. SUPPLEMENTARY NOTES

19. KEY WORDS (Continue on reverse side if necessary and identify by block number)

Nondestructive Evaluation (NDE); ceramics; high frequency ultrasonics; surface waves; flexural strength; hot pressed silicon nitride; reaction bonded silicon nitride; hot pressed silicon carbide; sintered silicon carbide; surface flaws; fracture origins.

20. ABSTRACT (Continue on reverse side if necessary and identify by block number)

A 45 MHz ultrasonic surface wave technique was developed and evaluated for detection of small surface flaws of <100 microns (0.004 inches) in gas turbine quality ceramics. The surface wave technique, which employs conventional immersion C-scan recording, was evaluated on hot pressed silicon nitride and silicon carbide of two sources each, and also on reaction bonded silicon nitride and sintered silicon carbide. These evaluations included tests on specimens run in a burner rig to simulate the effects on NDE of a gas turbine operating environment. Conventional mechanical tests were also run to verify

DD FORM 1 JAN 73 1473 EDITION OF 1 NOV 65 IS OBSOLETE S/N 0102-014-6601

Unclassified

SECURITY CLASSIFICATION OF THIS PAGE (When Data Entered)

349550

20. ABSTRACT

defect sizes and types and to correlate flexural strength with ultrasonic inspection results. The technique was found to be quite sensitive to surface conditions such as grinding damage, as well as to defects. Flexural strength was correlated qualitatively with the extent of ultrasonic response from machining damage. The sensitivity to defects was found to be limited by the depth of machining damage and the focal spot size of the ultrasonic beam. For the 580 μm (0.023 inch) diameter focal spot size used, the smallest defect verified metallurgically was equivalent to a 30 μm (0.0012 inch) deep semi-circular crack. Specimens run in the burner rig were found to become uninspectable because of beading of fused silica on the surface.

microns

TABLE OF CONTENTS

TABLE OF CONTENTS

FOREWORD

This Final Technical Report describes the work performed for the Department of the Navy under Naval Air Development Center Contract N62269-77-C-0136 during the period 13 September 1977 to 12 December 1978. The work involved the development of a high frequency ultrasonic surface wave technique and its evaluation on ceramic materials, under the technical direction of Mr. Irving Machlin, AIR-52031B, Naval Air Systems Command, Washington, DC 20361.

This contract with the TRW Materials Technology Laboratory of TRW Equipment, TRW Inc., was carried out in the Materials Development Department directed by Dr. I. J. Toth, Manager. TRW personnel contributing to this program, and their areas of involvement, were: Mr. I. M. Matay, Program Manager and Mr. T. Derkacs, Principle Investigator. Technical support to this program was provided by Mr. J. Touhalisky, ultrasonic inspections, Mr. C. A. Tyndall, mechanical testing; and Mr. W. G. Curtis, scanning electron microscope fractography.

This Final Technical Report has been given an internal TRW report number of ER-7980-F.

LIST OF ILLUSTRATIONS

LIST OF ILLUSTRATIONS (Cont.)

LIST OF ILLUSTRATIONS (Cont'd)

LIST OF ILLUSTRATIONS (Cont'd)

LIST OF TABLES

LIST OF ABBREVIATIONS AND SYMBOLS

Symbol	Quantity	Unit
b	specimen width	meter
C	temperature	Celsius
o	temperature or angle	degree
F	temperature	Fahrenheit
g	mass	gram
HPSiC	hot pressed silicon carbide	-
HPSN	hot pressed silicon nitride	-
Hz	frequency of oscillation per second	hertz
h	specimen height	meter
hr	time	hour
I	moment of inertia	quadric meter
IDS	hot pressed silicon nitride internal defect standard	-
ksi	pressure	1000 psi
K	stress intensity factor	newtons per square root of cubic meter
LDS	hot pressed silicon nitride laser drilled hole standard	-
l	specimen length	meter
M	moment	newton-meter
m	length	meter
μ	shear modulus	meganewtons per square meter
N	force	newton
P	force	newton
psi	pressure	pounds per sq. inch

LIST OF ABBREVIATIONS AND SYMBOLS (Cont'd)

Symbol	Quantity	Unit
RBSN	reaction bonded silicon nitride	-
RPM	angular velocity	revolutions per minute
ρ	density	grams per cubic centimeter
SEM	scanning electron microscope	-
SSiC	sintered silicon carbide	-
σ	Poisson's ratio	-
σ_b	stress on specimen tensile surface	meganewtons per sq. meter
σ_y	stress at defect location	meganewton
θ	angle of incident ultrasonic beam	degree
θ_L	angle of incident ultrasonic longitudinal wave	degree
θ_s	angle of refracted ultrasonic shear wave	degree
θ_1	angle of incident wave	degree
θ_2	angle of refracted wave	degree
V_K	ultrasonic longitudinal wave velocity	meters per second
V_s	ultrasonic shear wave velocity	meters per second
V_1	wave velocity in medium 1	meters per second
V_2	wave velocity in medium 2	meters per second
v	velocity of sound	meters per second
X	magnification	-
x	distance from end of specimen	meter
Y	coordinate along billet edge	meter

PREFIXES

Decimal multiples and submultiples of the engineering units listed above are formed by means of the following prefixes:

Symbol	Prefix	Multiplication Factor
M	mega	10^{6}
K	kilo	10^{3}
c	centi	10^{-2}
m	milli	10^{-3}
μ	micro	10^{-6}
n	nano	10^{-9}

1.0 INTRODUCTION

The purpose of this program is to develop high frequency ultrasonic evaluation techniques capable of detecting defects in the 10 to 100 μm (0.0004 to 0.004 inch) size range in gas turbine quality ceramics, such as silicon nitride and silicon carbide. The present contract is the third one-year contract in this program. In the first year's contract (Ref. 1), a high frequency (25-45 MHz), longitudinal wave mode, pulse-reflection technique was developed and applied to a range of candidate gas turbine ceramics. This technique was shown to be capable of detecting voids at least as small as 25 μm (0.001 inches) and also high density inclusions, although of a somewhat larger size. It was also shown to be capable of detecting the porosity in a material that is not fully dense, such as reaction bonded silicon nitride. In the second year's contract (Ref. 2), a 45 MHz shear wave technique was developed which provides improved sensitivity, reduces the back surface deadband to 40 μm (0.0016 inches) and provides correlation between inspection results and four-point-bend test data.

Effort under this contract was directed towards developing a high frequency (45 MHz) surface wave inspection technique for detection of surface defects, in order to allow inspection of the 40 μm (0.0016 inch) deadband left by the previously developed shear wave technique; and to investigate the effects of a gas turbine operating environment on material inspectability.

2.0 SUMMARY

In order to detect surface and near surface defects that are beyond the capability of the Navy/TRW previously developed longitudinal and shear wave techniques, a high frequency surface wave inspection technique was developed. The technique utilizes a focused 45 MHz transducer in the pulse-echo immersion mode at an incident angle of about 18°. A short waterpath, and the focused beam, were used to overcome the limitations normally associated with immersion surface wave testing, and to allow a C-scan recording to be made of the inspection results. Knoop and Vicker's indentations and laser drilled holes were investigated as possible surface reference defects. While the laser drilled hole looks most promising, because its size is most easily controlled and verified, an entirely satisfactory reference standard has yet to be developed.

Ultrasonic evaluations were performed on billets of Ceralloy 147A and NC-132 hot pressed silicon nitride, NC-350 reaction bonded silicon nitride, Ceralloy 146 and NC-230A hot pressed silicon carbide, and boron-doped sintered silicon carbide. On Ceralloy 147A and NC-350 billets, comparisons were made between shear and surface wave results and between as-received surfaces and surfaces machined with a 320 grit diamond wheel to remove surface irregularities. The surface wave technique was found to be extremely sensitive to surface condition, detecting many surface defects that could not be detected by the shear wave technique, as well as the surface texture left by machining. The limitation on sensitivity to defects was found to be a function of the signal-to-noise ratio between the pulse from the defect and the general background of pulses from the surface texture. This is controlled by the extent of general surface damage and by the focal spot size of the transducer. Surface damage as shallow as 15 μm (0.0006 inches) was detected when it was as wide as the 580 μm (0.023 inch) diameter focal spot of the ultrasonic beam.

Four-point-bend specimens of the various materials were machined to encompass defects and also areas with varying degrees of machining damage. The flexural strengths of the specimens were determined from four-point-bend tests and the fracture surfaces were examined using a scanning electron microscope to locate and characterize fracture origins. A qualitative correlation was found between ultrasonic response from machining damage and flexural strength. In the NC-350 billet, which had an unmachined surface containing shallow, parallel surface lines made by cutting in the green state, there was no correlation between response from the surface lines and flexural strength. Specimens containing 1 and 50 kg Vicker's indentations were also tested to measure flexural strength and determine the crack size from the indentation. In general, it was found that a 1 kg Vicker's indentation is strength controlling, even though its ultrasonic response cannot be distinguished above the signal from the machining damage. This identifies the need for an improved signal-to-noise ratio, such as could be achieved by having a smaller acoustic focal spot size. In specimens with low machining damage, the smallest strength controlling defect that was detected ultrasonically and verified by fractography was a near surface inclusion equivalent in surface area to a 30 μm (0.0012 inch) deep semi-circular crack. The largest strength controlling defect that was undetected was equivalent to a 15 μm (0.0006 inch) deep semi-circular crack.

Specimens of all the materials except sintered silicon carbide were also run in a burner rig test using standard jet fuel contaminated with salt. Periodic ultrasonic inspections were made to determine the effect on inspectability. It was found that the specimens became progressively more difficult to inspect because of contamination of the surface with fused silica which beaded on the surface.

3.0 MATERIALS

The materials for this program were selected to cover as much as possible the range of materials being considered for gas turbine applications. They included hot pressed silicon nitride (HPSN) from two sources, hot pressed silicon carbide (HPSiC) from two sources, boron-doped sintered silicon carbide (SSiC) and reaction bonded silicon nitride (RBSN). Some of the material was purchased especially for this contract and some consisted of billets or portions of billets of material that had been evaluated using ultrasonic longitudinal and shear wave inspections under TRW's previous contracts. These materials are described in detail in the following sections.

3.1 Hot Pressed Silicon Nitride

Billets of NC-132[+] and Ceralloy 147A* were used in this program. The NC-132 was an 11 x 5 x 0.6 cm (4-5/16 x 6 x 1/4 inch) size billet of Norton's standard materials left over from TRW's previous program (Ref. 2), where it was machined to flat surfaces with a 320 grit diamond wheel except for some deep pits near a corner on one side. It had a manufacturer measured density of 3.28 g/cm^3.

The Ceralloy 147A purchased for this contract is made from 99 weight percent alpha-silicon nitride powder (AME[‡] CP85) and one percent MgO. The powder is ground for 72 hours in tungsten carbide and then hot pressed for two hours at 1750^{o}C and 4000 psi (Ref. 3). The Ceralloy 147A was a 15 x 15 x 0.8 cm (6 x 6 x 5/16 inch) size billet with a manufacturer measured density of 3.2 g/cm^3. It was received with the as-pressed surface and, after preliminary inspection, machined to a flat surface with a 320 grit diamond wheel. The as-pressed surface is discussed in the section on ultrasonic inspection of this billet.

3.2 Hot Pressed Silicon Carbide

Billets of NC-203A[+] and Ceralloy 146* HPSiC, available from TRW's previous contracts, were used in this program. The NC-203A was a 15 x 15 x 0.7 cm (6 x 6 x 9/32 inch) size billet of Norton's standard material with a manufacturer measured density of 3.32 g/cm^3. It was machined to a flat surface with a 320 grit diamond wheel and was found by ultrasonic longitudinal and shear wave inspection to be generally free of defects except for a large defective area near the center (Ref. 2). The Ceralloy 146 was a 14 x 14 x 0.64 cm (5-1/2 x 5-1/2 x 1/4 inch) size billet purchased already machined in TRW's initial contract. It was made from 98 weight percent silicon carbide and two percent Al_2O_3 (Ref. 3), and had a density of 3.24 g/cm^3.

+ Norton Co., Worchester, MA
* Ceradyne, Inc., Chatsworth, CA
‡ Advanced Materials Engineering, Ltd., Gateshead, Co. Durham, UK

3.3 Sintered Silicon Carbide

A 5.0 x 4.6 x 0.64 cm (2 x 1-13/16 x 1/4 inch) size billet of boron doped, SSiC provided by the General Electric Company‡ was available from the previous contract. The material was cold pressed from beta-silicon carbide powder with small additions of boron and carbon and sintered at approximately 2100°C for 30 minutes. The final billet density was 93.5 percent of theoretical, and based on previous experience the billet was expected to contain a number of irregularly shaped pores with dimensions as large as 200 μm (Ref. 4).

3.4 Reaction Bonded Silicon Nitride

NC-350+ RBSN material was evaluated in the initial contract and was found to be a poor material for high frequency ultrasonic inspection because of many large pores (Ref. 1). Although part of this material was still available, recent work on NC-350 for Garrett/AiResearch[x] (Ref. 5) indicates a significant change in more recent material. Therefore, a 19.1 cm (7.5 inch) diameter by 0.5 cm (7/32 inch) thick billet of NC-350 was purchased for this program. As received, both sides of the billet contained fine parallel lines with a spacing of about 2 mm (0.080 inch) running entirely across the part. According to the manufacturer, these lines are created in the green state when the billet is cut to thickness from a much larger billet.

---

‡ General Electric R&D Center, Schenectady, NY
+ Norton Co., Worchester, MA
x AiResearch Manufacturing Co., Phoenix, AZ

4.0 SURFACE WAVE INSPECTION TECHNIQUE

4.1 Background

An ultrasonic beam traveling through a material can have several different modes of vibration, each with its own velocity of propagation. Among these are the longitudinal mode in which particles vibrate transverse to the direction of wave propagation. Although a liquid will not support a shear wave, when a longitudinal wave is incident at an angle other than normal to the interface between two materials, mode conversion generally occurs. Shear waves can therefore be generated in a material immersed in a liquid couplant by proper selection of the angle of incidence of the ultrasonic beam. This mode conversion, therefore, is one method to generate shear waves.

Figure 1 illustrates the relationship between an ultrasonic beam incident at the interface between two materials and the resulting refracted longitudinal and shear wave beams. The relationship between the incident and refracted beams is governed by the same law that applies in optics, Snell's law:

$$\frac{\sin\theta_1}{V_1} = \frac{\sin\theta_2}{V_2} \qquad (1)$$

where θ_1 is the angle of incidence, θ_2 is the angle of refraction, and V_1 and V_2 are the acoustic velocities in media 1 and 2, respectively. The ratio between the longitudinal wave velocity, V_L, and the shear wave velocity, V_S, is given by:

$$\frac{V_S}{V_L} = \sqrt{\frac{1-2\sigma}{2(1-\sigma)}} \qquad (2)$$

Since σ, Poisson's ratio for the medium, is a number usually between zero and one, the shear velocity is less than the longitudinal velocity. It is, therefore, possible to select an angle of incidence such that θ_L, the angle of refraction of the longitudinal wave in medium 2, is greater than 90°, and only the shear wave will remain in the material. If, however, θ_S is selected to be 90° or greater, then the shear wave is excluded from the part and a surface, or Raleigh wave is generated. The surface wave will travel along the surface of the material creating reflections from defects perpendicular to the material surface, as shown in Figure 2. The propagation velocity, v, of a surface wave in an isotropic solid is given by (Ref. 6):

$$v = \left(\frac{0.87 + 1.12}{1 + \sigma}\right) \cdot \sqrt{\frac{\mu}{\rho}} \qquad (3)$$

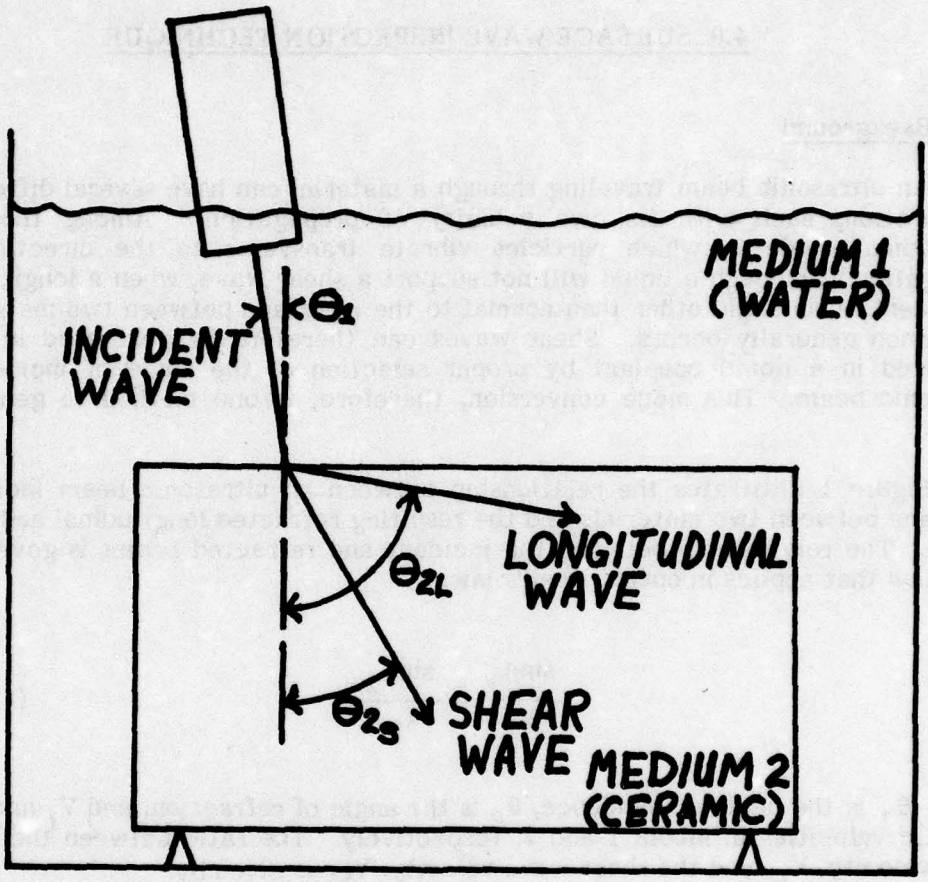

Figure 1. **Diagram Showing the Generation of Ultrasonic Shear Waves at the Interface of Two Media.**

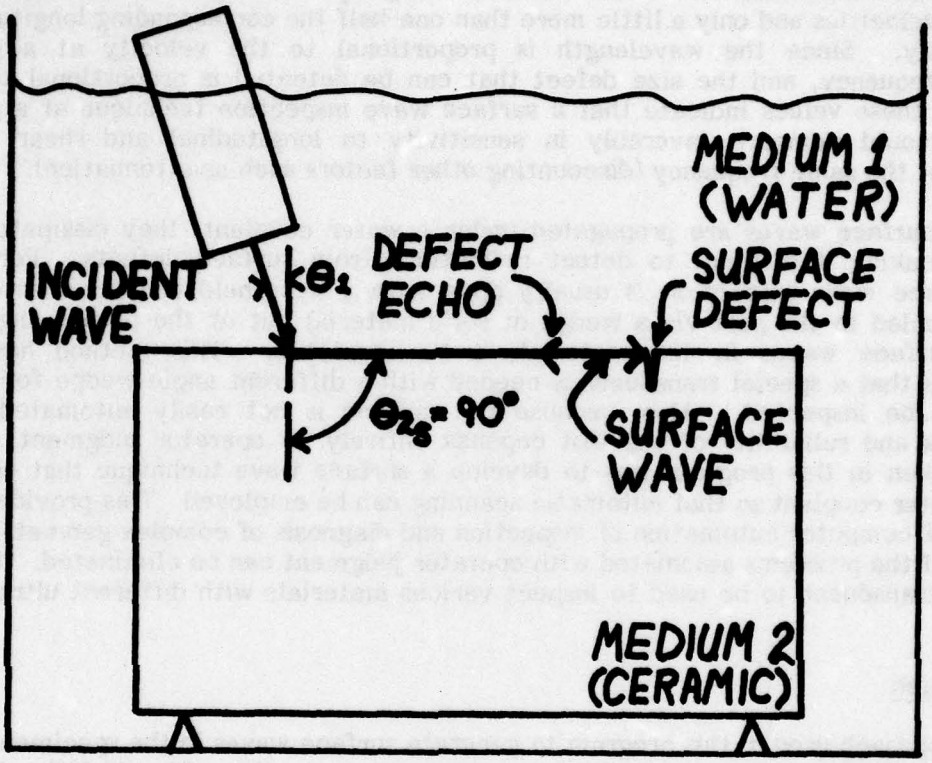

Figure 2. **Diagram Showing the Generation of Ultrasonic Surface Waves at the Interface of Two Media.**

where σ is Poisson's ratio, μ is the shear modulus and ρ is the density of the material. Based on the values available for these properties in the literature (Refs. 7, 8 and 9), the surface wave velocity is about 5600 m/s for hot pressed silicon nitride and 7100 m/s for hot pressed silicon carbide. These values are slightly lower than the corresponding shear wave velocities and only a little more than one-half the corresponding longitudinal wave velocity. Since the wavelength is proportional to the velocity at a given ultrasonic frequency, and the size defect that can be detected is proportional to the wavelength, these values indicate that a surface wave inspection technique at a given frequency should compare favorably in sensitivity to longitudinal and shear wave techniques at the same frequency (discounting other factors such as attenuation).

When surface waves are propagated under a water couplant, they dissipate into the water making it difficult to detect reflections from surface defects. For this reason surface wave inspection is usually done with a hand-held contact transducer which is coupled to the part via a wedge of solid material cut at the proper angle to generate surface waves in the material to be inspected. This method has the disadvantage that a special transducer is needed with a different angle wedge for each material to be inspected. Also, because the method is not easily automated, the thoroughness and reliability of the test depends entirely on operator judgment. The approach taken in this program was to develop a surface wave technique that can be used in a water couplant so that automatic scanning can be employed. This provides the capability of computer automation of inspection and diagnosis of complex geometries so that many of the problems associated with operator judgment can be eliminated. It also allows one transducer to be used to inspect various materials with different ultrasonic velocities.

4.2 Approach

The approach used in this program to generate surface waves in the specimens was the mode conversion technique described in the previous section. The 45 MHz, 2-inch focal length ultrasonic transducer, high frequency ultrasonic instrument and C-scan recording tank were used again as they were used for longitudinal and shear wave inspections. This equipment is described in detail in reference 1. Surface waves are generated in the ceramic specimen by tilting the transducer to provide an incident beam angle of about 18° to the specimen surface. (The value given is for HPSN. The angle will vary slightly for other materials of slightly different surface wave velocity). The water path distance is selected so that the ultrasonic surface wave travels only a short distance on the part surface before it reaches its focal point. The instrument defect gate's time window is set so its duration coincides with the focal point location of the transducer. The beam is scanned over the entire surface of the part, and a C-scan recording is made of defects as they occur at the transducer focal point. The technique's uniqueness is that the highly concentrated surface wave beam of the focused transducer is set to travel only a short distance on the part surface before reaching the defect to be detected, thereby minimizing the dissipation of surface wave energy into the water couplant. The rest of the acoustic interrogation beam travels in the water, but in a less attenuative longitudinal mode of vibration. The following sections, which deal with the inspection and metallurgical evaluation of various ceramic materials, illustrate the sensitivity of the technique.

4.3 Reference Standards

Ultrasonic flaw detection is a comparative measurement means. In order to be able to estimate the size of ultrasonically detected defects, it is necessary to have a reference standard to use in calibrating instrument sensitivity. For longitudinal and shear wave inspection, where internal defects must be detected, reference standards have been made either by seeding the material with defects of known size (Refs. 1 and 7), or by laser drilling holes in the material (Ref. 2). In either case it is difficult to verify the exact nature of the artificial defects without destroying the reference standards. For surface defects, laser drilled holes as well as the indentations from either Knoop or Vicker's hardness testers are possible candidates for reference defects. All three of these possibilities were investigated in this program.

4.3.1 Knoop Indentations

It has been shown that controlled crack-like flaws can be introduced into silicon nitride (Ref. 10) and silicon carbide (Ref. 11) by means of Knoop hardness indentations. Reasonable loads, in the range of 500 to 3000g, will produce cracks in the range of 20 to 100 μm (0.0008 to 0.004 inches). To investigate such flaws for use as ultrasonic surface wave reference standards, a specimen was indented using loads of 1000, 2000 and 3000g standards on each side. One side of the 3.5 x 5.4 x 0.64 cm (1 5/16 x 2 1/8 x 1/4 inch) specimen was polished so that the indents could easily be examined microscopically and the other side was left as machined. When the indentations were made in the specimen, the first set was put in at an angle that made access to them difficult. Therefore, a second set was made. Figure 3 shows the final configuration. Figure 4 is a C-scan recording of a 45 MHz shear wave inspection made looking through the material with the polished side down after the indents were made. Comparison of the C-scan with microscopic examination of the surface reveals that two Knoop cracks were detected, one in the set that is properly aligned with the edge and one in the set at an angle. In each set the defect (labeled K1 and K2 in Figure 4) is the largest one. A number of natural defects were also detected. Shear wave inspection of the as-machined side of the specimen did not detect any of the Knoop indentations. Surface wave inspection failed to detect the Knoop indentations on either side of the specimen. Even on the polished side, the general background of indications from the surface texture was found to be too great to allow these small defects to be detected. These results are similar to the findings of Khuri-Yakub, et al (Ref. 12), who reported that the ability to detect Knoop indentations in NC-132 HPSN was limited to about 60 μm (0.0024 inches) in depth by the size distribution of naturally occurring cracks.

4.3.2 Laser Drilled Holes

An investigation of the laser drilled hole as an ultrasonic surface wave reference standard was made using the laser drilled standard (LDS) which was used successfully for shear wave inspection. As reported in Reference 2, page 5, the LDS is a 4.9 x 1.3 x 0.64 cm (1.9 x 0.52 x 0.25 inch) specimen of Ceralloy 147A HPSN containing eight laser drilled holes of various diameters and depths. Two of these holes, designated F and H, go all the way through the part. A 45 MHz surface wave inspection was performed on the bottom surface of the LDS which is penetrated only by the two through holes. The resulting C-scan recording shown in Figure 5 contains only the indication for Hole F, which is 125 μm (0.005 inches) in diameter. Hole H is very near the bottom edge of the specimen as seen in Figure 5 and is lost in the larger indication caused by reflection from the end of the part.

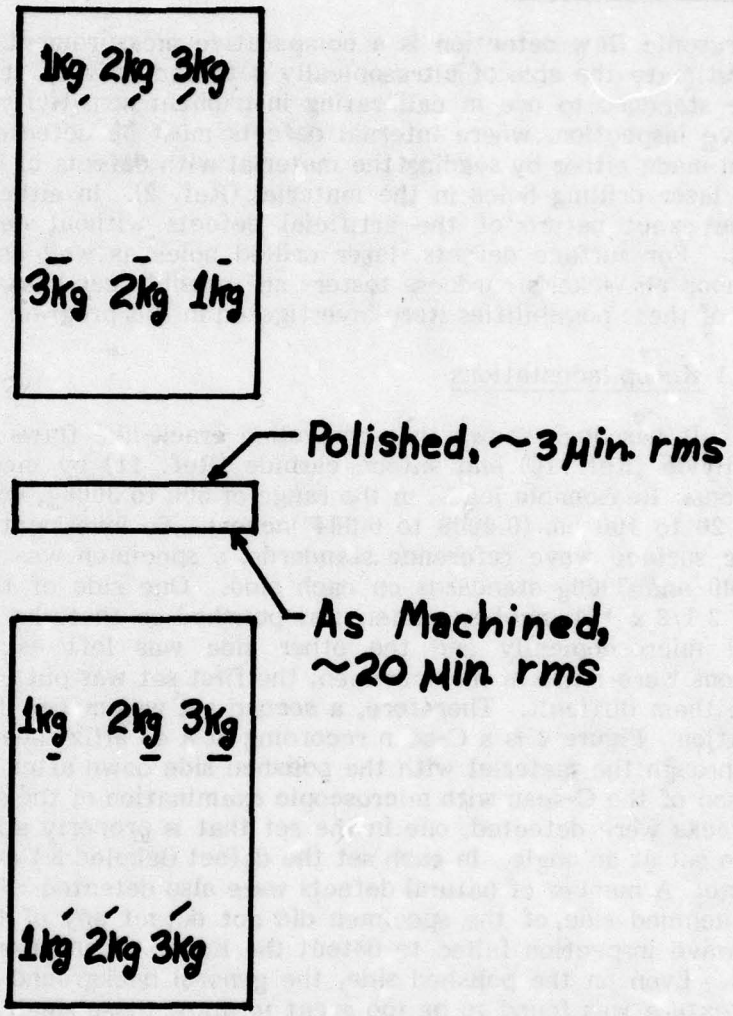

Figure 3. **Location of Knoop Indentations in Preliminary Reference Standard of Ceralloy 147A HPSN.**

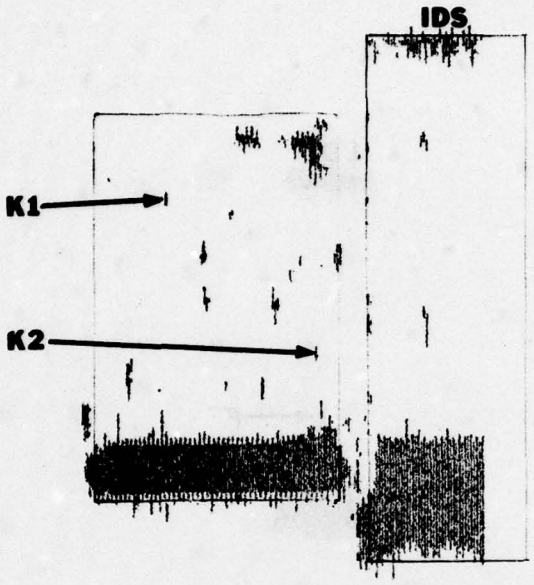

Figure 4. C-scan Recording of 45 MHz, 11° Ultrasonic Shear Wave Inspection of Ceralloy 147A HPSN Preliminary Reference Standard Containing Knoop Indentations (Polished Side Down; Polished Side Inspected Through Material Thickness).

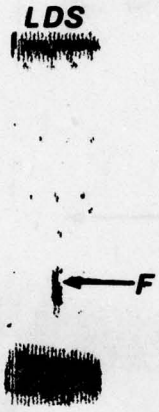

Figure 5. C-scan Recording of 45 MHz, 18° Ultrasonic Surface Wave Inspection of Ceralloy 147A HPSN Laser Drilled Hole Standard (LDS).

Hole F has some limitations as a reference defect. It is larger than the defects of interest in this program and is round, rather than cracklike in shape. These limitations are not serious however. A round reference defect is like a surface pit and can be correlated with an equivalent size crack. Also, since laser drilling tends to make tapered holes, it should be possible to make a much smaller diameter hole, since it does not need to be very deep. The tip of a laser drilled hole can be 40 μm (0.0016) or less (Ref. 2). A major advantage of the laser drilled holes is that its actual size can be measured without destroying the specimen.

4.3.3 Vicker's Indentations

The third type of reference defects investigated were Vicker's indentations. This work was initiated as a result of success in another program (Ref. 13) in which Vicker's indentations, made by another laboratory with loads of 1, 5, 10, 20 and 50 kg in NC-132 HPSN, were detected by the surface wave technique. Vicker's notches of 1 and 50 kg were made in a specimen of each of the six materials used in this program, including NC-132 HPSN. These specimens were inspected using the 45 MHz ultrasonic surface wave technique, and also using a 45 MHz ultrasonic shear wave technique with the transducer focused through the material from the opposite side. The results of these inspections are shown in Figures 6 through 11. In each case the 50 kg defect was easily detected, but the 1 kg defect was not. This inability to detect the 1 kg indentations could be a result of a number of factors, including differences in surface finish between these specimens and the one previously tested, and differences in hardness causing different defect sizes. During four-point-bend testing, Vicker's indentations were placed in a number of specimens which were otherwise defect free, in order to determine the size defects involved in these tests. These results are described in Section 6.

4.3.4 Discussion

The work done to date on reference defects for ultrasonic surface wave inspection of ceramics is only a preliminary review of possible techniques. Considerable additional work is needed to establish the reliability with which defects of a desired size can be made and measured. Both Knoop and Vicker's indentations have the disadvantage that the size defect produced with a given load depends on the hardness of the material. Although the size of the indentation can be measured on the surface, there is no way to directly measure the size of the crack propagating down from the indentation. Therefore, the size of the reference defect would have to be inferred from empirical results. For this reason the laser drilled hole seems a more promising reference defect. Through careful control of the operating parameters, it should be possible to drill a hole close to the desired size. Furthermore, the actual size hole drilled can be subsequently measured. Although the round holes used in this program can be mathematically related to an equivalent crack, it is also possible by use of special lenses to produce a long, narrow slot more like a crack.

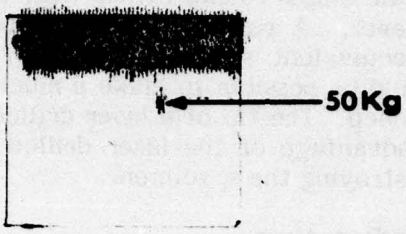

a. Shear Wave

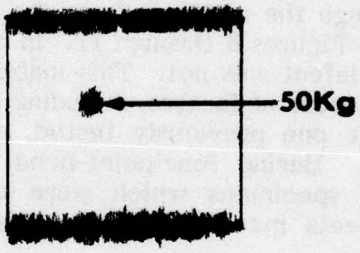

b. Surface Wave

Figure 6. **C-scan Recordings of 45 MHz Ultrasonic Inspections of Specimen of Ceralloy 147A HPSN Containing 1 and 50 kg Vicker's Indentations.**

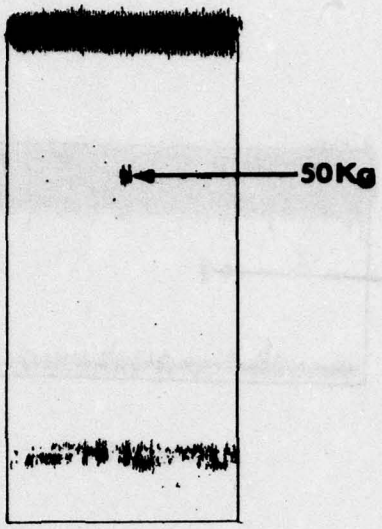

a. Shear Wave

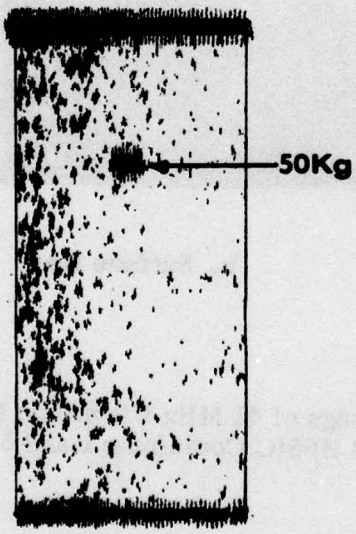

b. Surface Wave

Figure 7. C-scan Recordings of 45 MHz Ultrasonic Inspections of Specimen of NC-350 RBSN Containing 1 and 50 kg Vicker's Indentations.

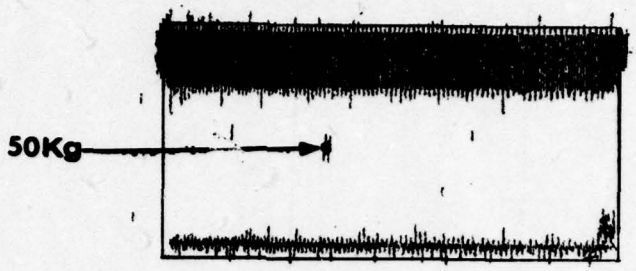

a. Shear Wave

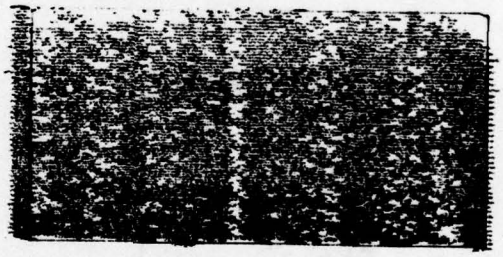

b. Surface Wave

Figure 8. C-scan Recordings of 45 MHz Ultrasonic Inspections of Specimen of Ceralloy 146 HPSiC Containing 1 and 50 kg Vicker's Indentations.

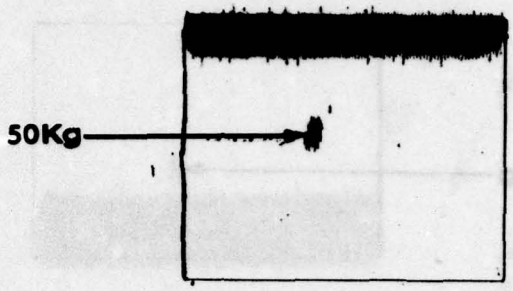

a. Shear Wave

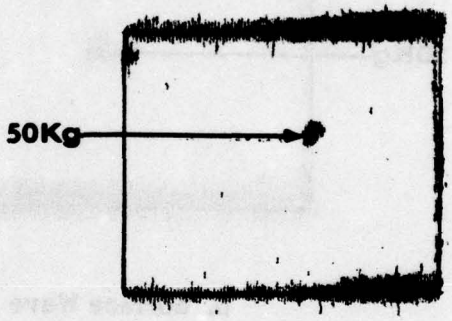

b. Surface Wave

Figure 9. C-scan Recordings of 45 MHz Ultrasonic Inspections of Specimen of NC-230 HPSiC Containing 1 and 50 kg Vicker's Indentations.

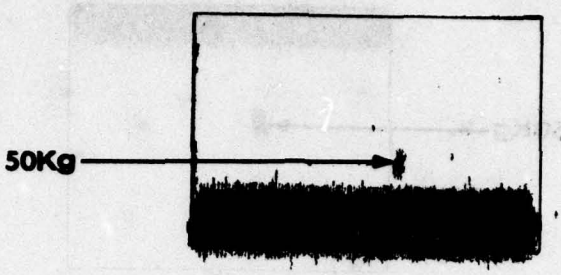

a. Shear Wave

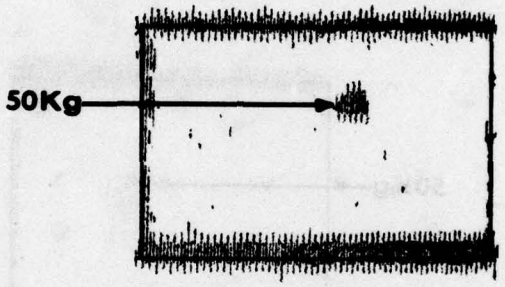

b. Surface Wave

Figure 10. C-scan Recordings of 45 MHz Ultrasonic Inspections of Specimen of NC-132 HPSN Containing 1 and 50 kg Vicker's Indentations.

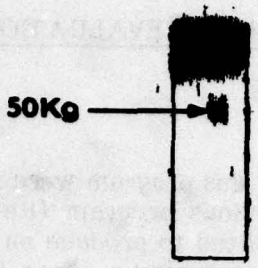

a. Shear Wave

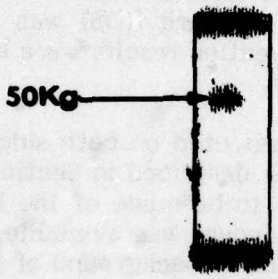

b. Surface Wave

Figure 11. C-scan Recordings of 45 MHz Ultrasonic Inspections of Specimen of Boron Doped SSiC Containing 1 and 50 kg Vicker's Indentations.

5.0 ULTRASONIC EVALUATIONS

5.1 Approach

The materials purchased new for this program were first inspected using the shear wave technique developed in the previous program (Ref. 2). This is an immersion technique in which the transducer is tilted to produce an incident beam angle of about 11° (for HPSN) at the top surface, producing a shear beam within the part that is focused at the back surface. The technique is capable of detecting internal defects in the bottom half of the part and surface defects that penetrate more than 40 μm (0.0016 inches) below the surface. This inspection was repeated for both sides of the part from two orientations 90° apart, in order to provide complete part coverage. The purpose of these inspections was to evaluate the material quality in comparison to previous samples and to provide a basis of comparison with surface wave inspection results. The Ceralloy 147A HPSN internal defect standard (IDS) was used in each inspection to assure uniform sensitivity. Similar inspection results were already available (Ref. 2) for the other materials used in the program.

All of the materials were also inspected on both sides from two orientations 90° apart, using the surface wave technique described in Section 4.0. The purpose of these inspections was to allow an evaluation to be made of the type and size of defect that can be detected. Since no reference standard was available, the sensitivity was set just below the level that would cause a general background of indications from the surface texture. The 130 μm (0.0052 inches) penetration depth of the 45 MHz surface wave overlaps the region inspected by the shear wave technique, so that some correlation between the two methods is expected. The defects detected by the surface wave techniques were then evaluated by other techniques, some of which are described in this section and some of which are described in Section 7.0. In addition, portions of all of the billets except the SSiC, which was too small, were selected for burner rig testing, which is described in Section 6.0.

5.2 Hot Pressed Silicon Nitride

5.2.1 Ceralloy 147A

The C-scan recordings of the 45 MHz shear wave inspections of the billet of Ceralloy 147A are shown in Figures 12 through 15. As with previous samples of this material, these scans show a large number of defect indications. Figures 16 through 19 show the corresponding surface wave inspections. These scans also show large numbers of indications. The two types of scans were compared by means of transparencies. Since the shear wave inspection is performed from the opposite side of the surface than the surface wave inspection, the transparency of the shear wave C-scan is turned over on the surface wave C-scan so that the reference notches coincide. This type of comparison revealed that only a few of the defect indications correspond between the two types of scans. Most of the defects detected by the surface wave technique were not detected by the shear wave technique.

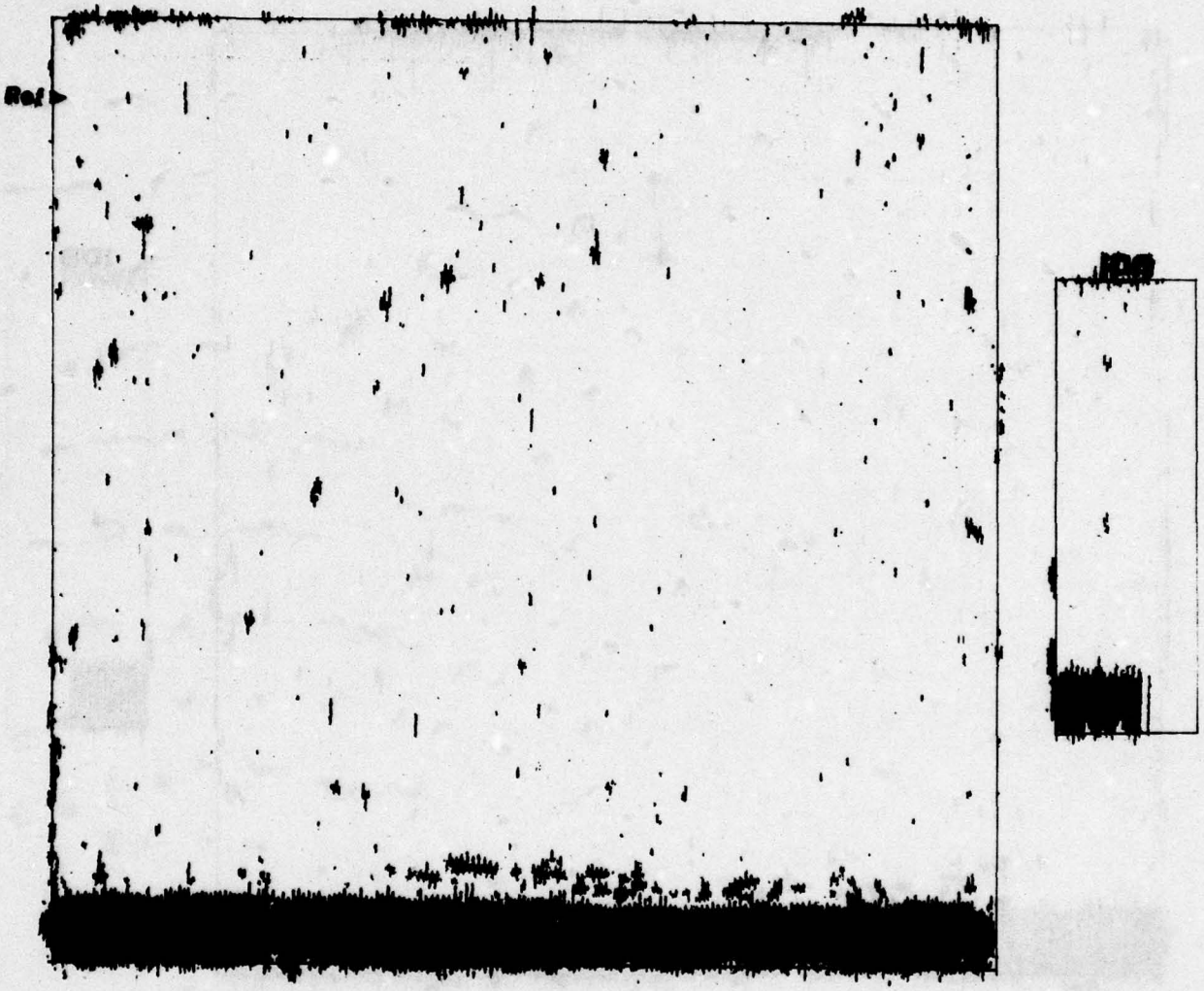

Figure 12. C-scan Recording of 45 MHz, 11° Shear Wave Inspection of Billet of Ceralloy 147A Hot Pressed Silicon Nitride (Notch Down).

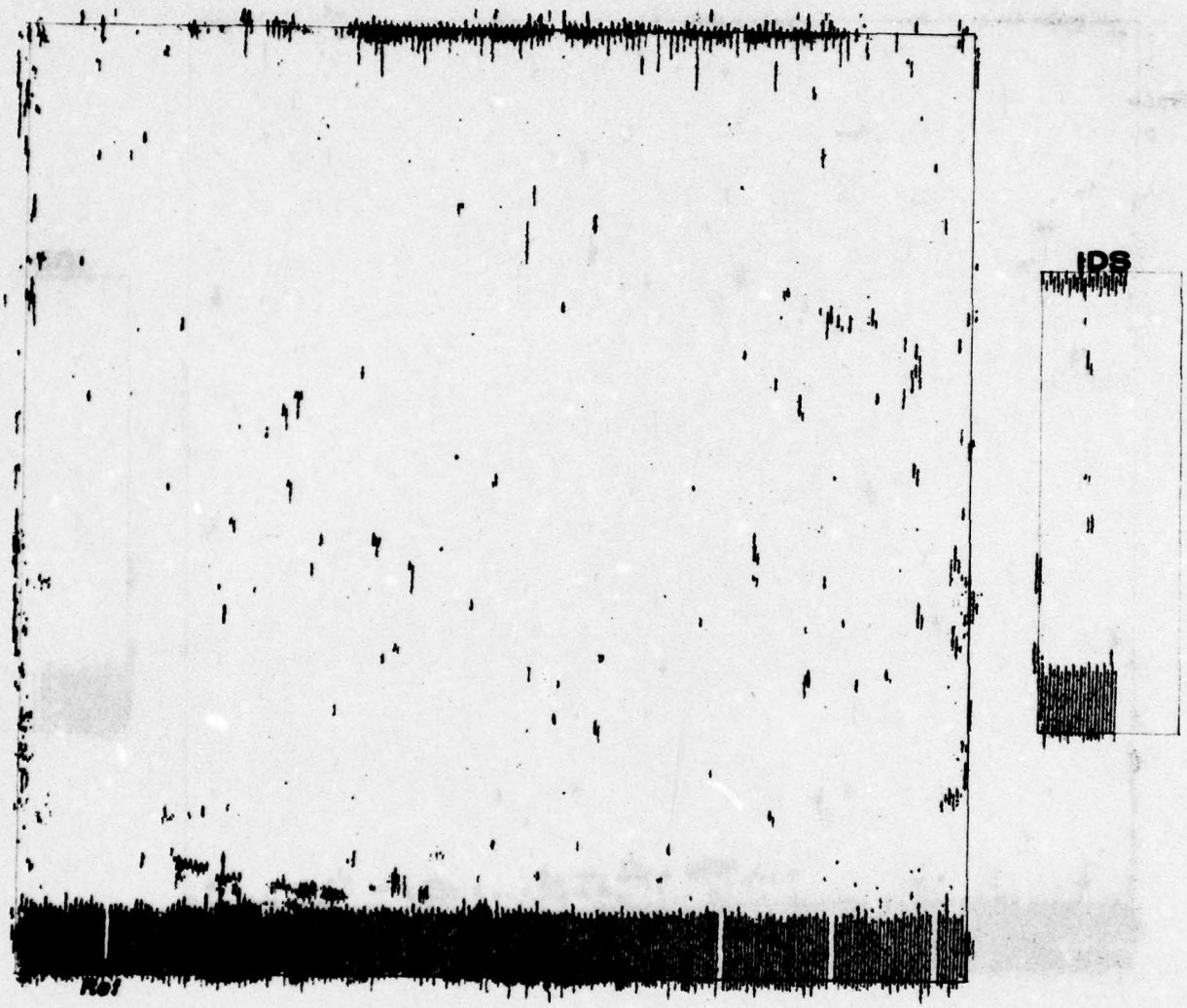

Figure 13. C-scan Recording of 45 MHz, 11° Shear Wave Inspection of Billet of Ceralloy 147A Hot Pressed Silicon Nitride (Rotated 90°, Notch Down).

Figure 14. **C-scan Recording of 45 MHz, 11° Shear Wave Inspection of Billet of Ceralloy 147A Hot Pressed Silicon Nitride (Turned Over, Notch Up).**

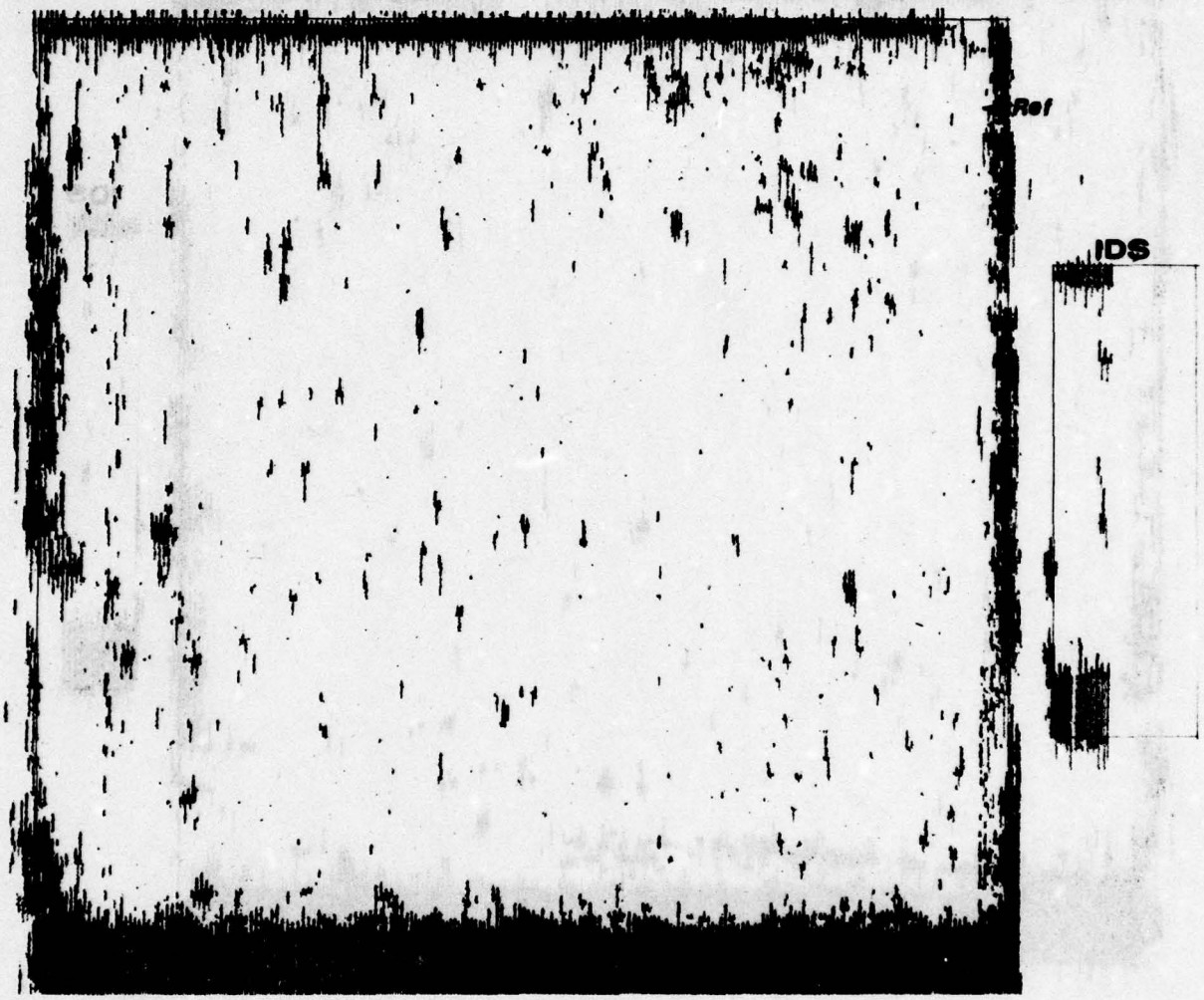

Figure 15. C-scan Recording of 45 MHz, 11° Shear Wave Inspection of Billet of Ceralloy 147A Hot Pressed Silicon Nitride (Rotated 90°, Notch Up).

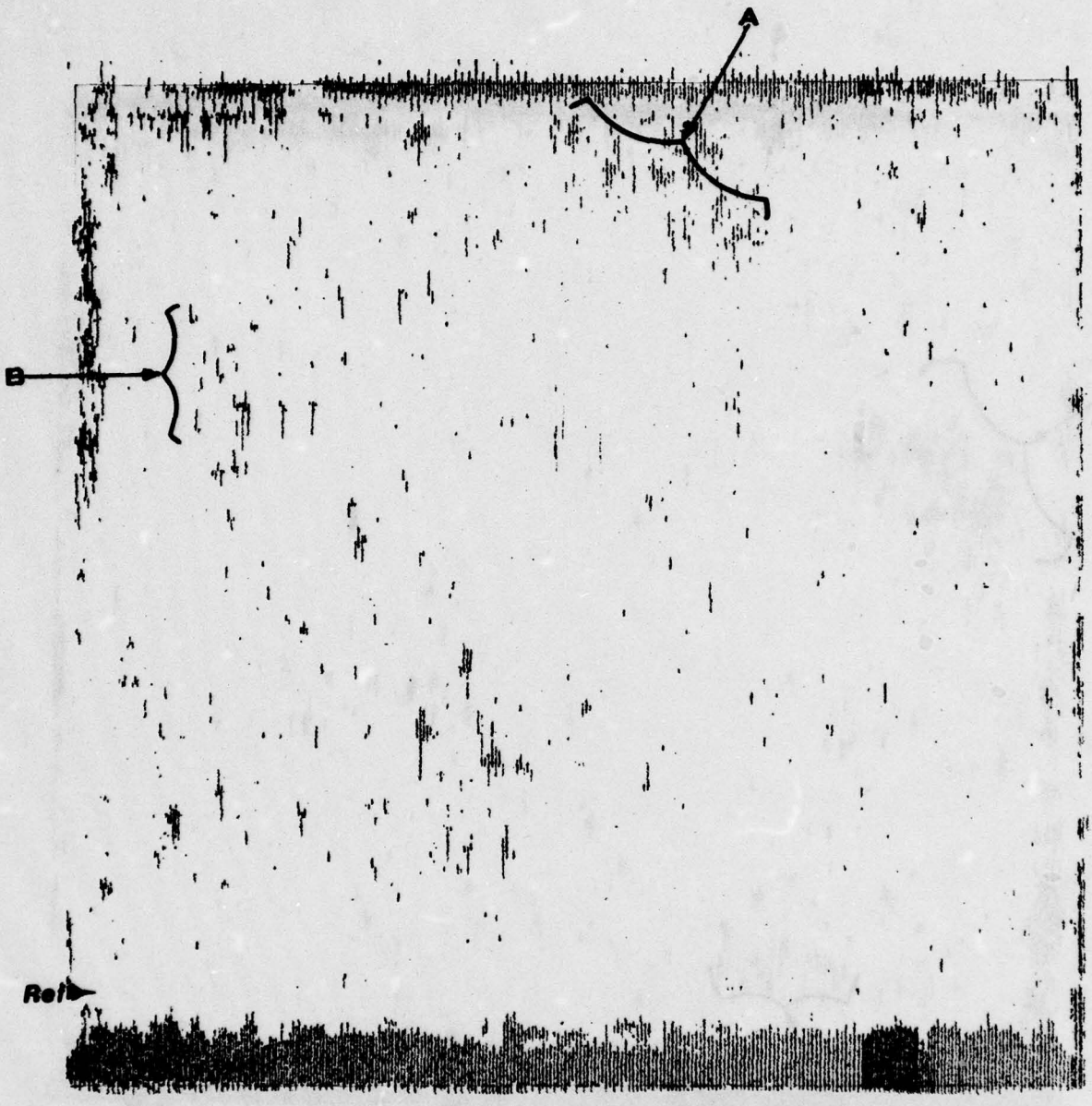

Figure 16. **C-scan Recording of 45 MHz, 18° Surface Wave Inspection of Billet of Ceralloy 147A Hot Pressed Silicon Nitride (Notch Up).**

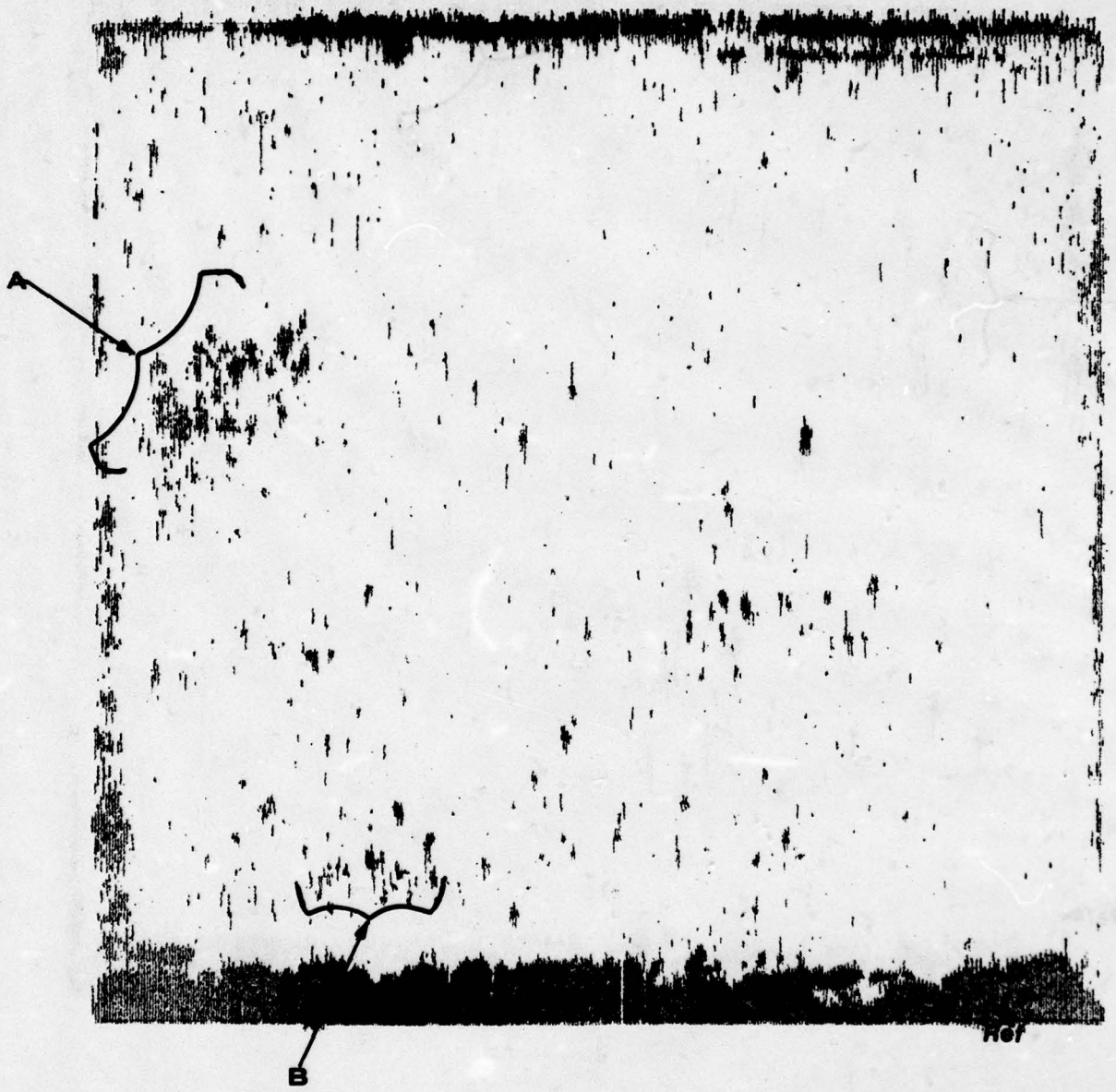

Figure 17. C-scan Recording of 45 MHz, 18° Surface Wave Inspection of Billet of Ceralloy 147A Hot Pressed Silicon Nitride (Rotated 90°, Notch Up).

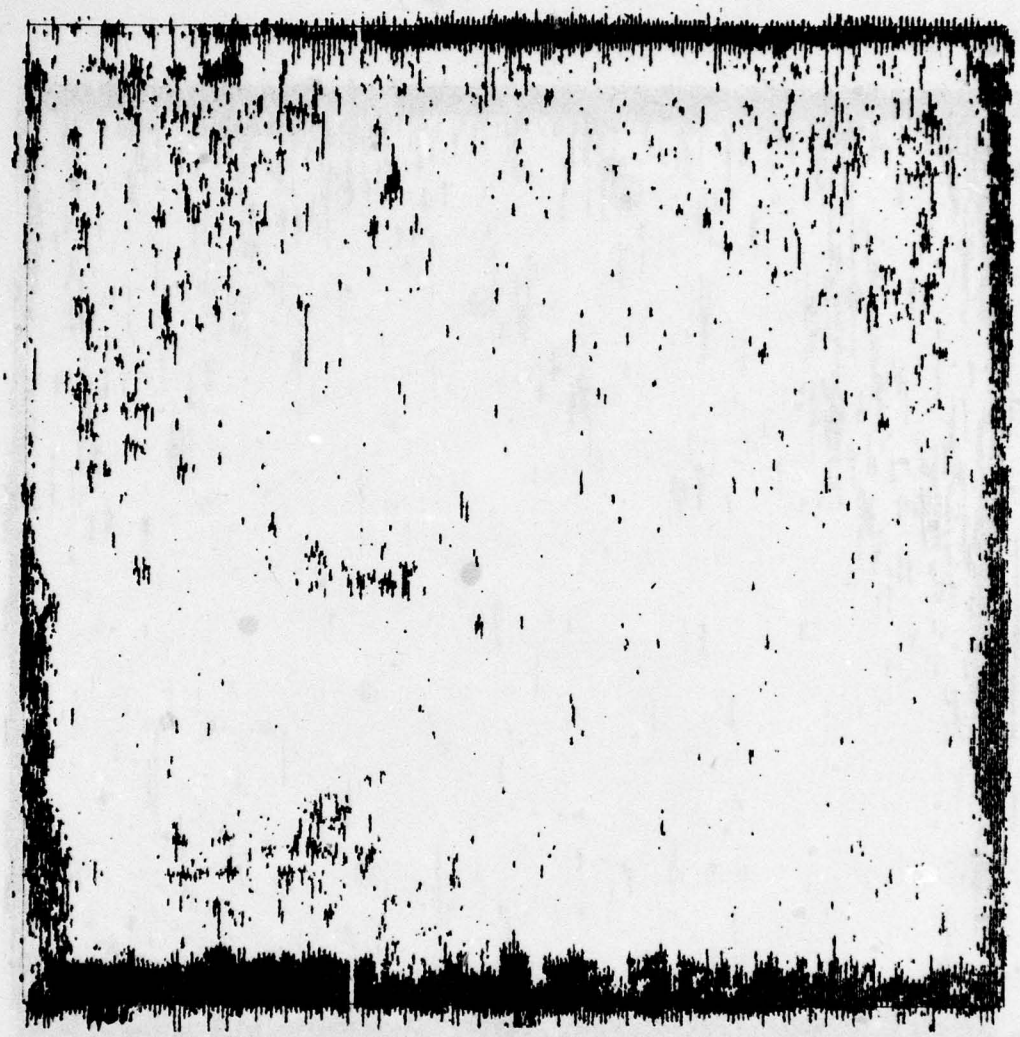

Figure 18. C-scan Recording of 45 MHz, 18° Surface Wave Inspection of Billet of Ceralloy 147A Hot Pressed Silicon Nitride (Turned Over, Notch Down).

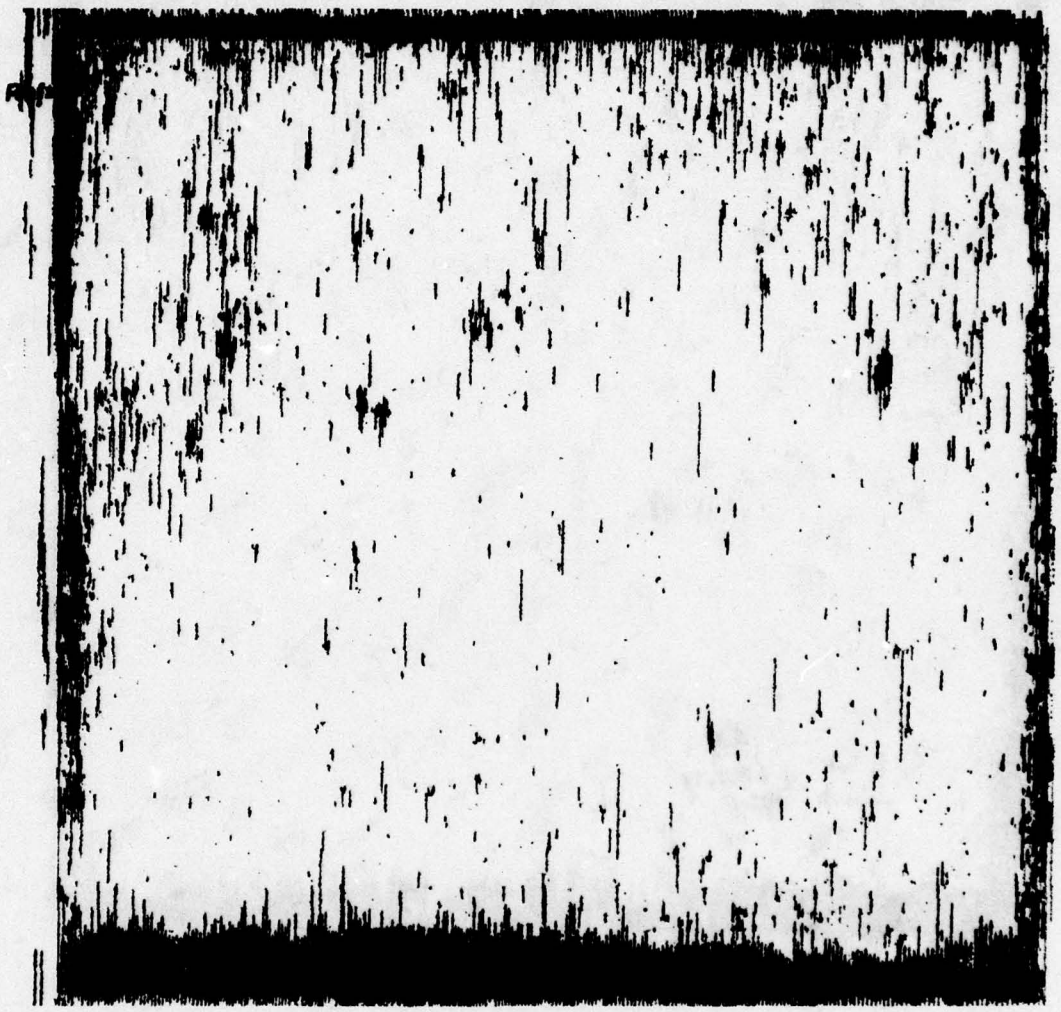

Figure 19. C-scan Recording of 45 MHz, 18° Surface Wave Inspection of Billet of Ceralloy 147A Hot Pressed Silicon Nitride (Rotated 90°, Notch Down).

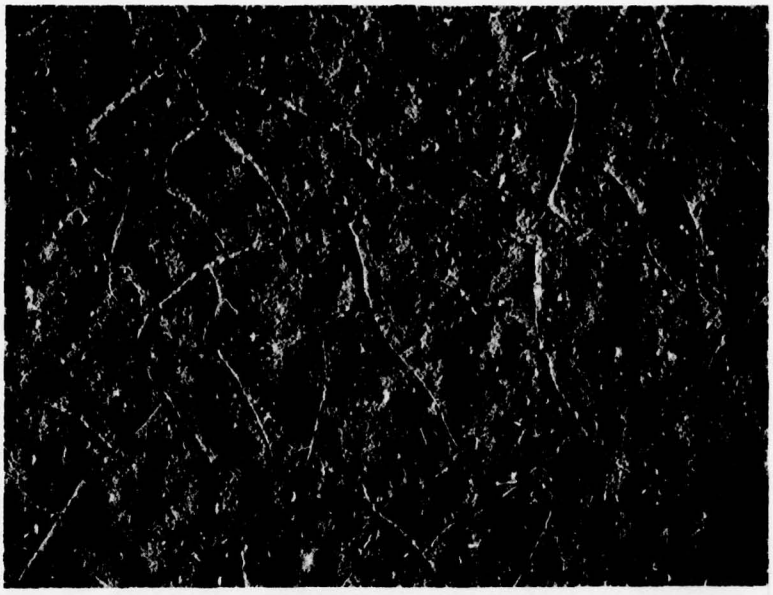

Area A 7X

Area B 7X

Figure 20. Photomacrographs Showing Surface Condition of Two Typical Areas of As-Pressed Billet of Ceralloy 147A HPSN, Where Large Numbers of Surface Wave Indications Were Detected.

Evaluation of the surface wave inspection results showed a correlation between the areas showing large numbers of defect indications and visible surface features. As an example, Figure 20 shows 7X photomacrographs of two areas, designated A and B, which are indicated on Figures 16 and 17. Figure 20 shows that the indications in areas A and B were caused by high concentrations of randomly oriented surface creases. Such creases were not present in areas of the surface where there were no indications.

This billet was subsequently machined to a 20 microinch surface using a 320 grit diamond wheel running perpendicular to the side containing the reference notch. Approximately 1000 μm (0.040 inches) were removed from the total billet thickness to provide a smooth surface on both sides. Figures 21 through 24 show C-scan recordings of 45 MHz surface wave inspections made on both sides at two orientations 90^{o} apart after machining. These inspection results show a few scattered surface defects,as well as some sensitivity to the surface texture left by machining, only on those scans made perpendicular to the machining direction. Arrows in the figures indicate both the grinding and scanning directions. The sensitivity could have been increased so that Figures 21 and 24, which were scanned perpendiular to the direction of machining, would have shown the surface texture due to grinding. However, in order to allow larger defects to be detected, the sensitivity was reduced so that only a few indications were detected from the most severe grinding damage.

The surface wave inspection results after machining were compared with the results of both shear and surface wave inspections before machining. This was accomplished by making transparencies of one set of C-scan recordings and then overlaying them on the other C-scan recordings to look for common indications. No significant correlation was found between the corresponding surface wave inspections made before and after machining. This is as expected, since the amount of material removed during machining was much greater than the 130 μm (0.0052 inch) penetration depth of the 45 MHz surface wave. A correlation was found, however, between a number of the surface wave indications and the corresponding shear wave inspection made before machining. Those indications in Figures 21 through 24 that show an obvious correlation with indications in Figures 12 through 15 are labeled with letters from A through K in the figures where they appear. This correlation indicates that the machining operations exposed internal defects to the surface, which previously could only be detected by the shear wave technique. It is not known whether other defects, indicated by the surface wave inspection results after machining, were undetected by the shear wave techniques or were produced by the machining operation.

Based on the surface wave inspection results after machining, areas of the billet were selected for burner rig testing and for four-point-bend testing. Figures 22 and 24 show how these specimens relate to the inspection results on the two sides of the billet. In Figure 22 it can be seen that four-point-bend specimens were machined

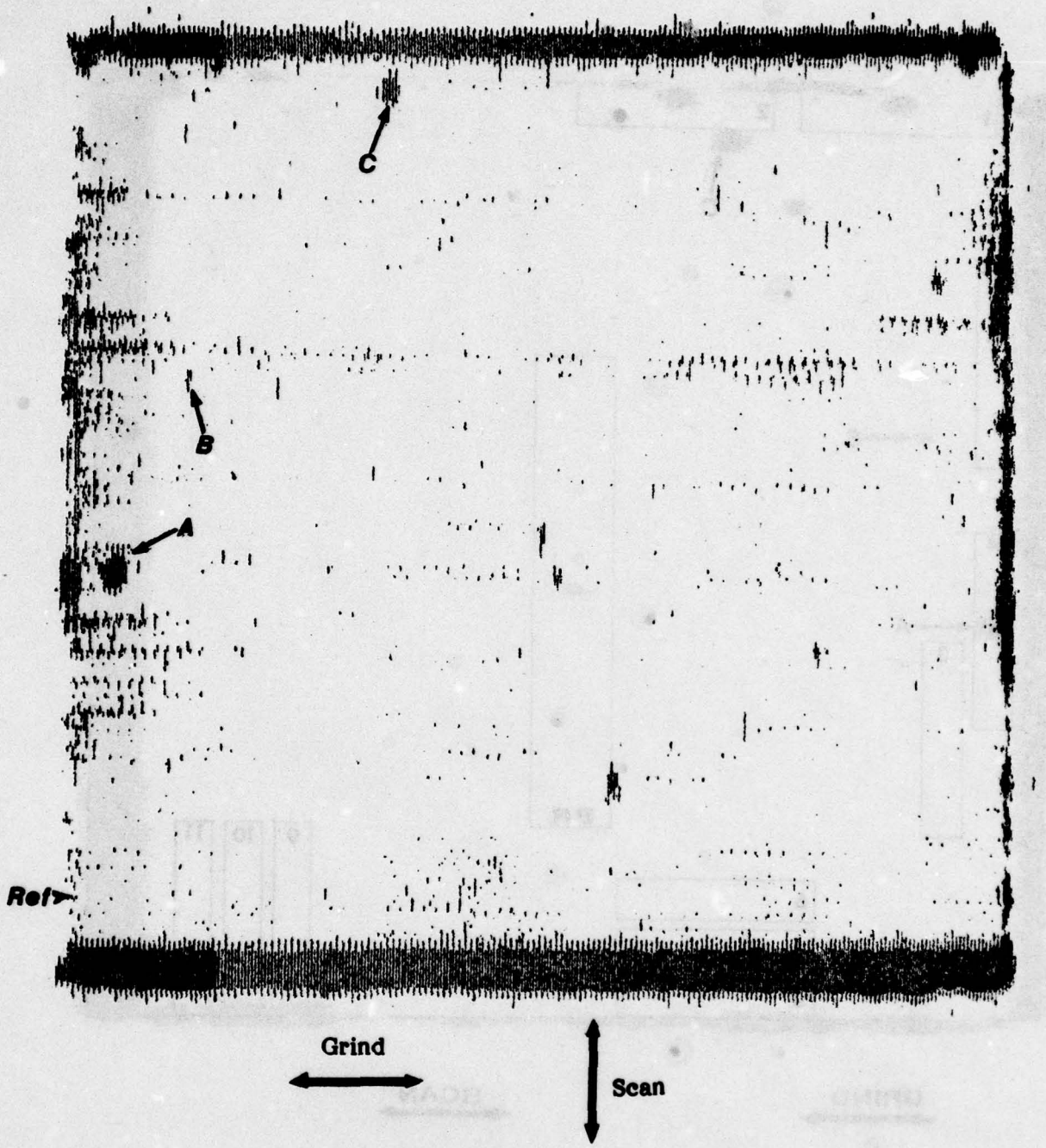

Figure 21. C-scan Recording of 45 MHz, 18° Surface Wave Inspection of Top Surface of Billet of Ceralloy 147A HPSN After Machining (Scan Perpendicular to Grinding Direction).

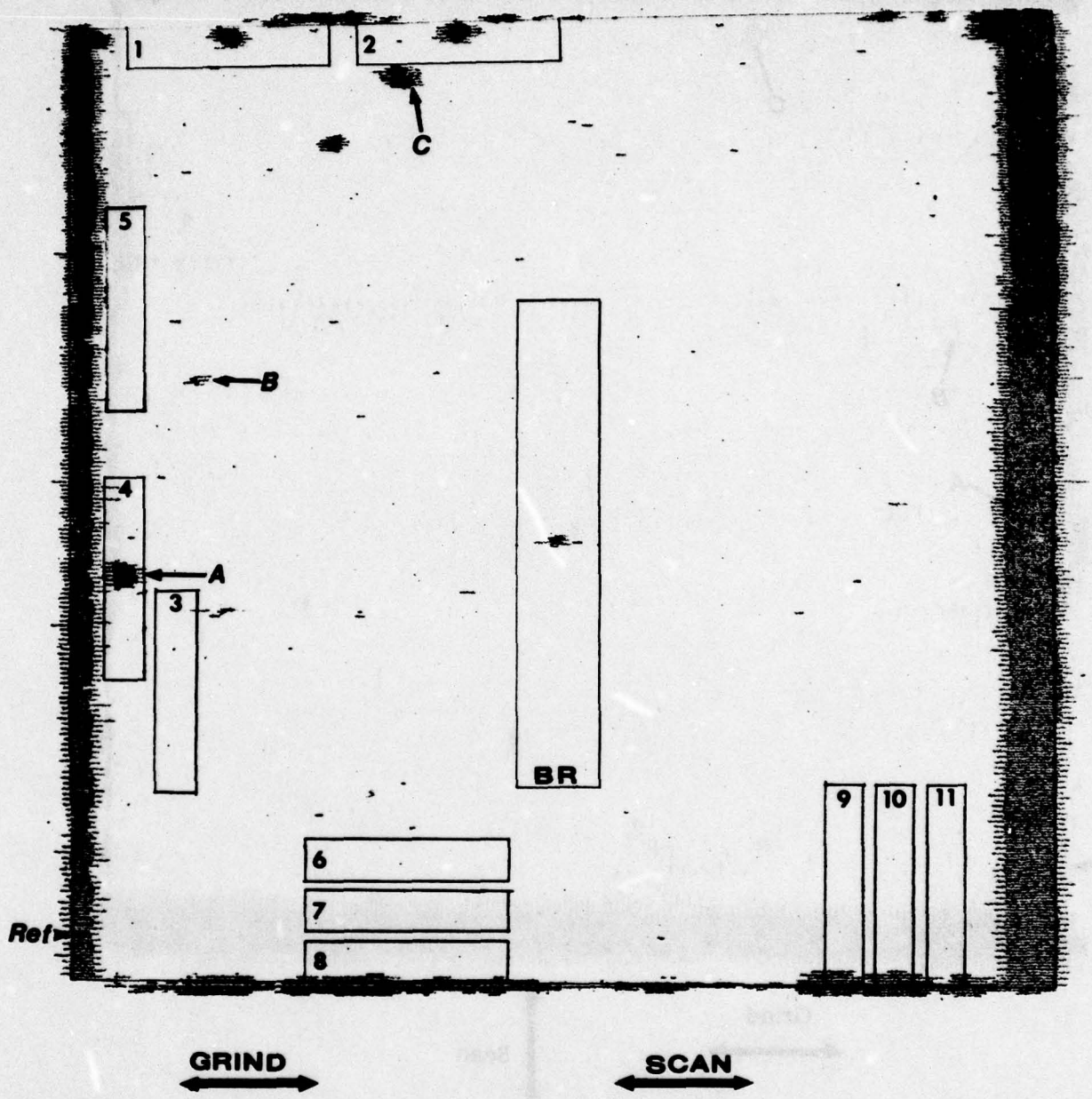

Figure 22. C-scan Recording of 45 MHz, 18° Surface Wave Inspection of Top Surface of Billet of Ceralloy 147A HPSN After Machining (Scan Parallel to Grinding Direction).

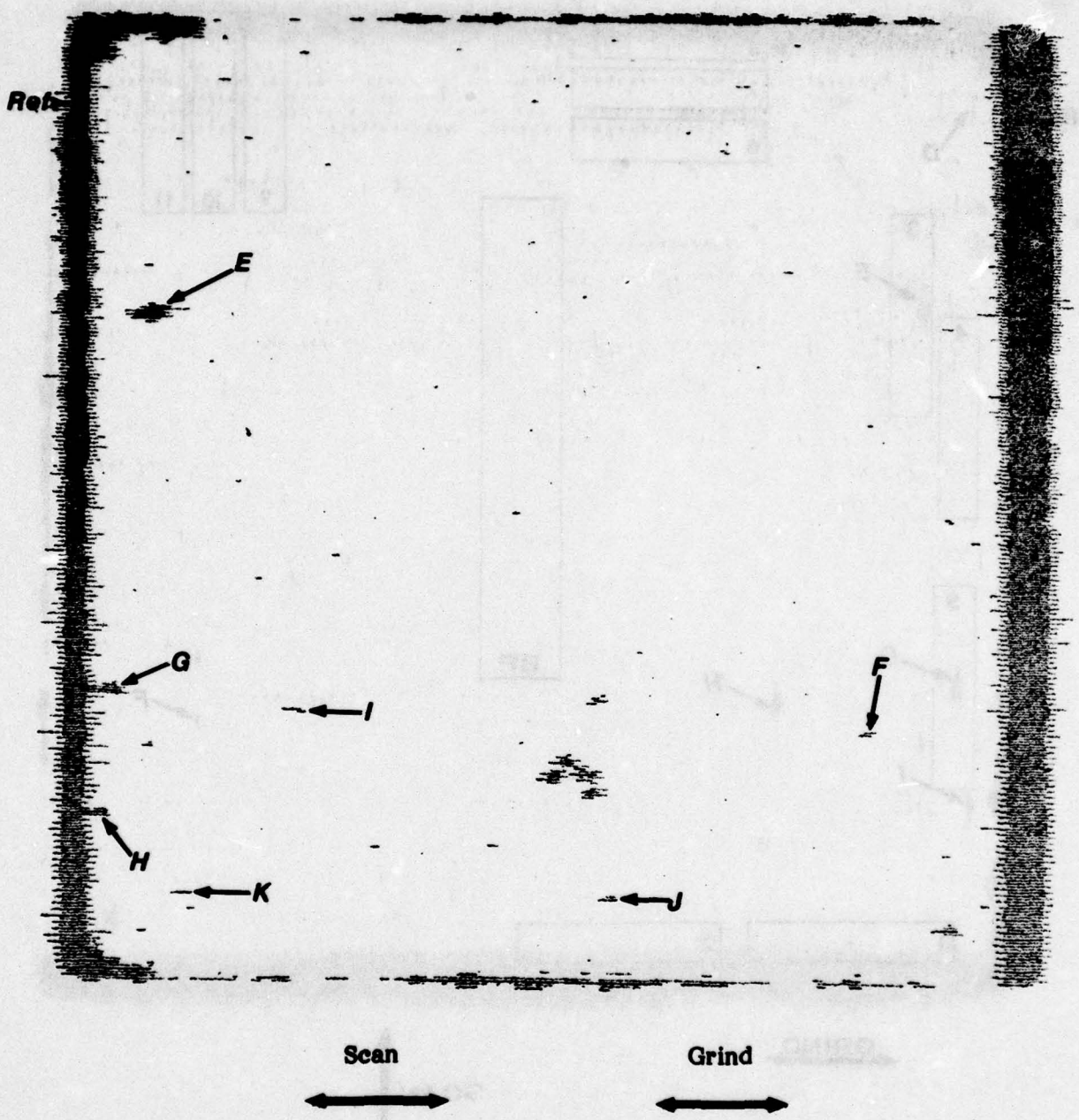

Figure 23. C-scan Recording of 45 MHz, 18° Surface Wave Inspection of Bottom Surface of Billet of Ceralloy 147A HPSN After Machining (Scan Parallel to Grinding Direction).

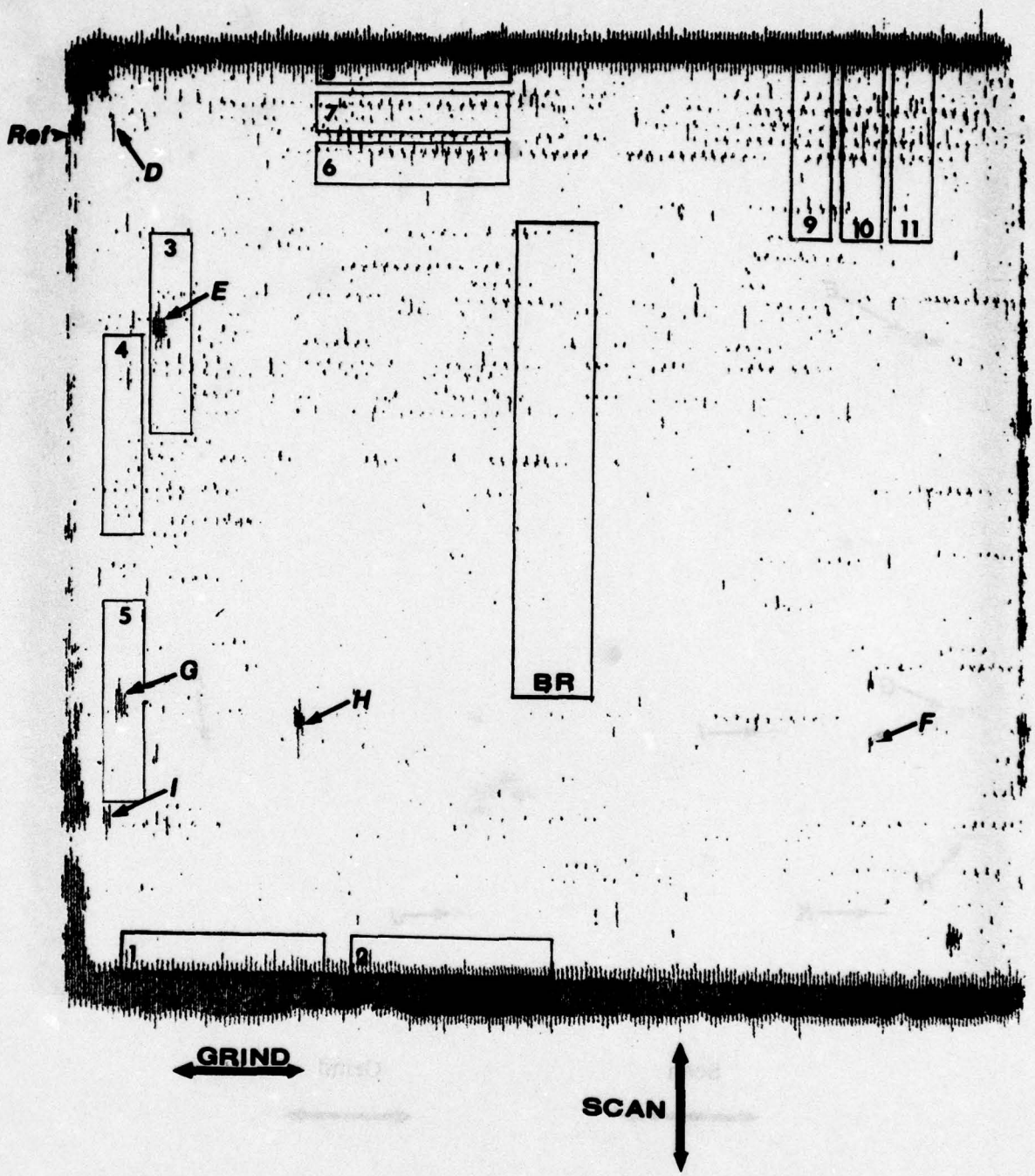

Figure 24. C-scan Recording of 45 MHz, 18° Surface Wave Inspection of Bottom Surface of Billet of Ceralloy 147A HPSN After Machining (Scan Perpendicular to Grinding Direction).

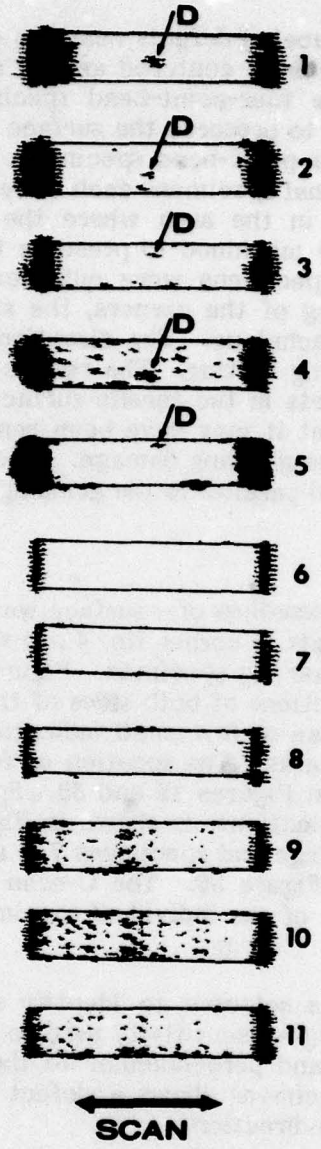

Figure 25. C-scan Recording of 45 MHz, 18° Surface Wave Inspection of Tensile Surfaces of Ceralloy 147A HPSN Four-Point-Bend Specimens.

centered around defect A and two unlabeled defects near the edge. It can also be seen that the burner rig specimen was machined centered around an unlabeled defect near the center of the billet. The three four-point-bend specimens were machined to thickness from the opposite side so as to preserve the surface that is up in this figure. In Figure 24 it can be seen that four-point-bend specimens were machined centered around defects E and G. Three additional specimens each were machined parallel to and perpendicular to the grinding marks in the area where the grinding marks are the heaviest. These eight specimens were machined to preserve the surface shown in this figure. After the four-point-bend specimens were cut from the billet, but before machining to thickness and chamfering of the corners, the surfaces of interest were reinspected using the surface wave technique. The direction of scan was selected to identify strength limiting defects during testing. The results are shown in Figure 25. Specimens 1 through 5 show the defects in the tensile surface, although the defect in specimen 5 is so close to the edge that it may have been removed by chamfering the edge. Specimens 9, 10 and 11 show the grinding damage. Specimens 6, 7 and 8 are free of indications because they are scanned parallel to the grinding damage.

5.2.2 NC-132

Figure 26 shows a C-scan recordings of a surface wave inspection of the billet of NC-132 HPSN. The cluster of defects in corner No. 4 are shallow surface pits. This corner was cut off and used as a burner rig specimen. Figures 27 through 30 show C-scan recordings of surface wave inspections of both sides of the remainder of the billet from two orientations each. Other than of few small indications in Figure 29, the only defects detected were the grinding marks. The location of four-point-bend specimens made from this billet are indicated in Figures 29 and 30. Specimens 1, 2 and 3 were centered around very small defect indications, as shown in Figure 29. Specimens 4, 5, and 6 run parallel to the grinding damage and specimens 7, 8 and 9 run perpendicular to the grinding damage, as is shown in Figure 30. The C-scan recording of the surface wave inspection of the tensile surface of the individual specimens is shown in Figure 31 prior to machining to final thickness.

The direction of scan was selected to identify strength limiting defects during testing. Despite a somewhat higher sensitivity used to emphasize the difference between the specimens cut parallel and perpendicular to the grinding direction, only specimen No. 2 of the defective specimens shows a defect larger than those in the defect-free specimens cut in the same direction.

5.3 Reaction Bonded Silicon Nitride

5.3.1 NC-350

The C-scan recordings of the 45 MHz ultrasonic shear wave inspections of the billet of NC-350 RBSN are shown in Figures 32 through 35.

The Ceralloy 147A HPSN internal defect standard (IDS) is also shown in each of these scans. Unlike the NC-350 purchased several years ago (Ref. 1), this material does not show a general background of indications which obscures the signals from defects. Rather, the background is very clean and a number of internal defect indications can be seen. The exception to this is Figure 35. This C-scan shows extensive indications which are caused by the surface texture on the bottom side of the

Figure 26. C-scan Recording of 45 MHz, 18° Surface Wave Inspection of Top Surface of Billet of NC-132 Hot Pressed Silicon Nitride.

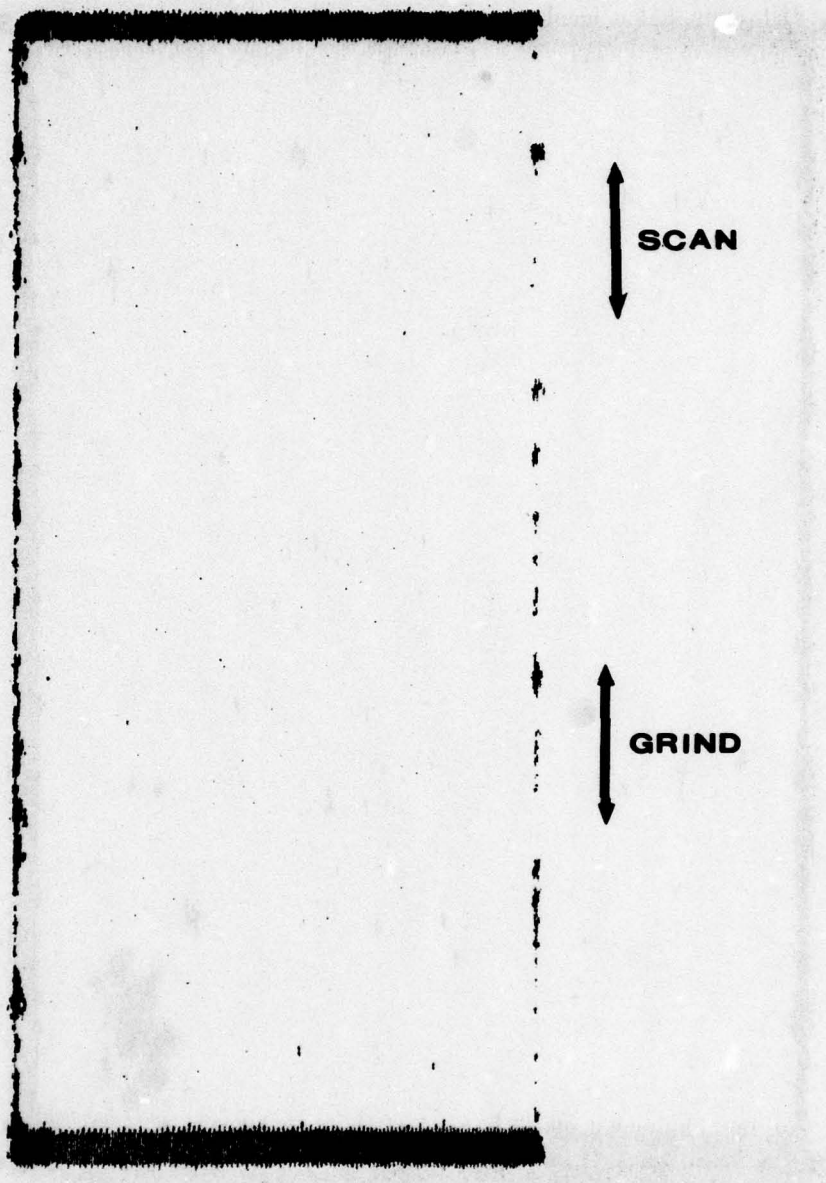

Figure 27. C-scan Recording of 45 MHz, 18° Surface Wave Inspection of Top Surface of Billet of NC-132 HPSN (Scan Parallel to Grinding Direction).

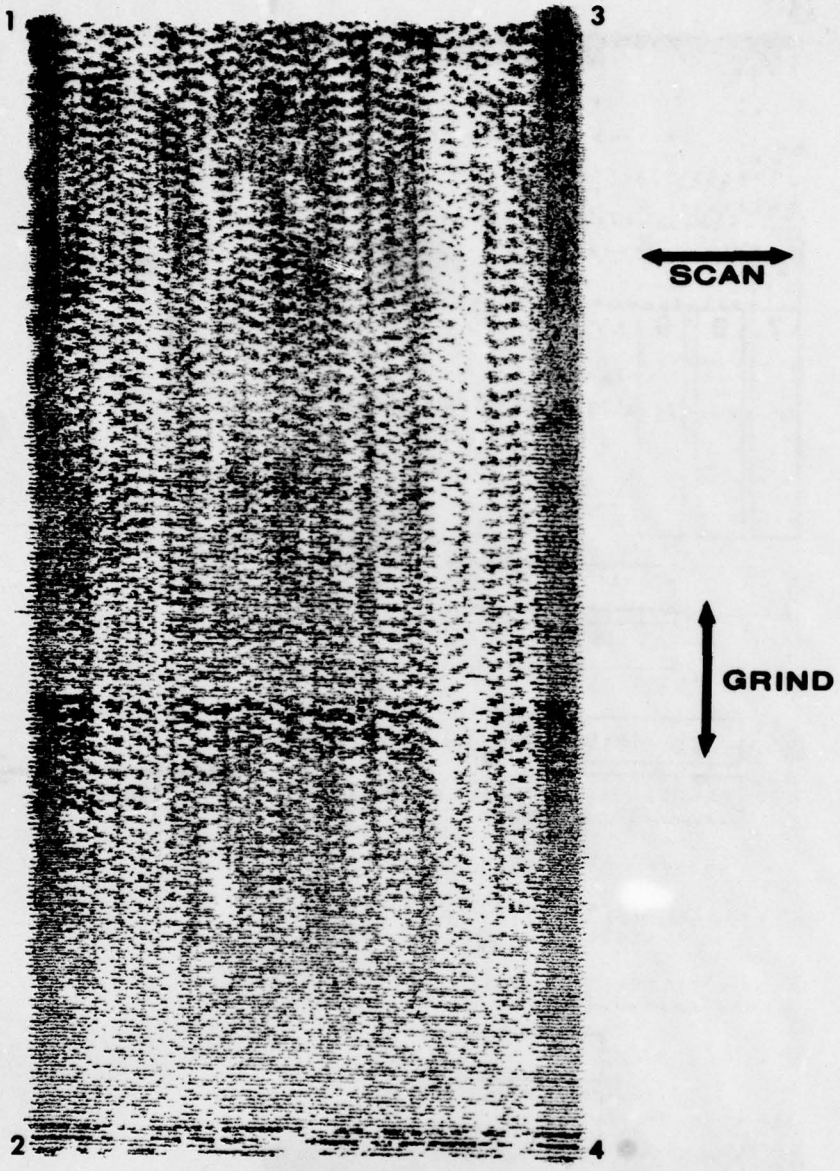

Figure 28. C-scan Recording of 45 MHz, 18° Surface Wave Inspection of Top Surface of Billet of NC-132 HPSN (Scan Perpendicular to Grinding Direction).

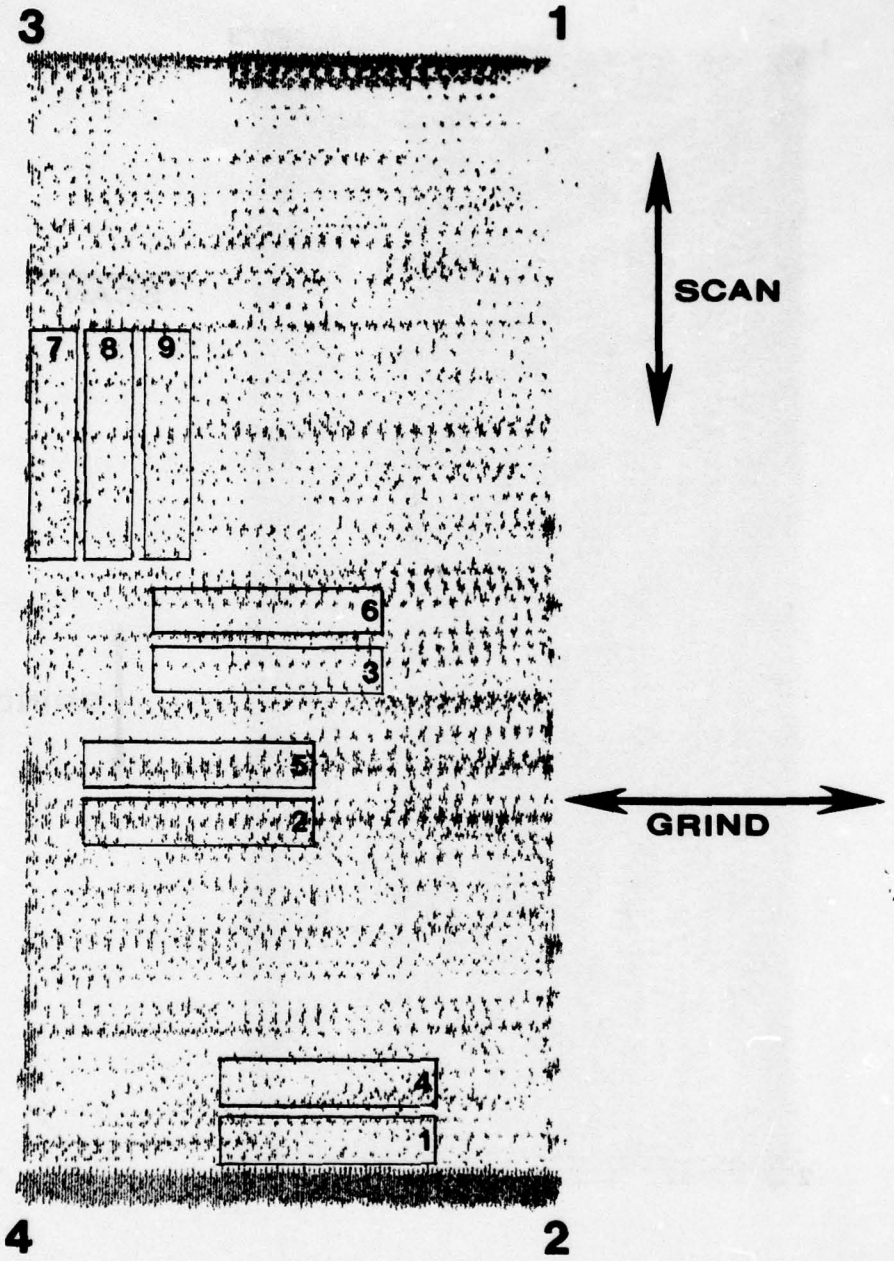

Figure 29. C-scan Recording of 45 MHz, 18° Surface Wave Inspection of Top Surface of Billet of NC-132 HPSN (Scan Parallel to Grinding Direction).

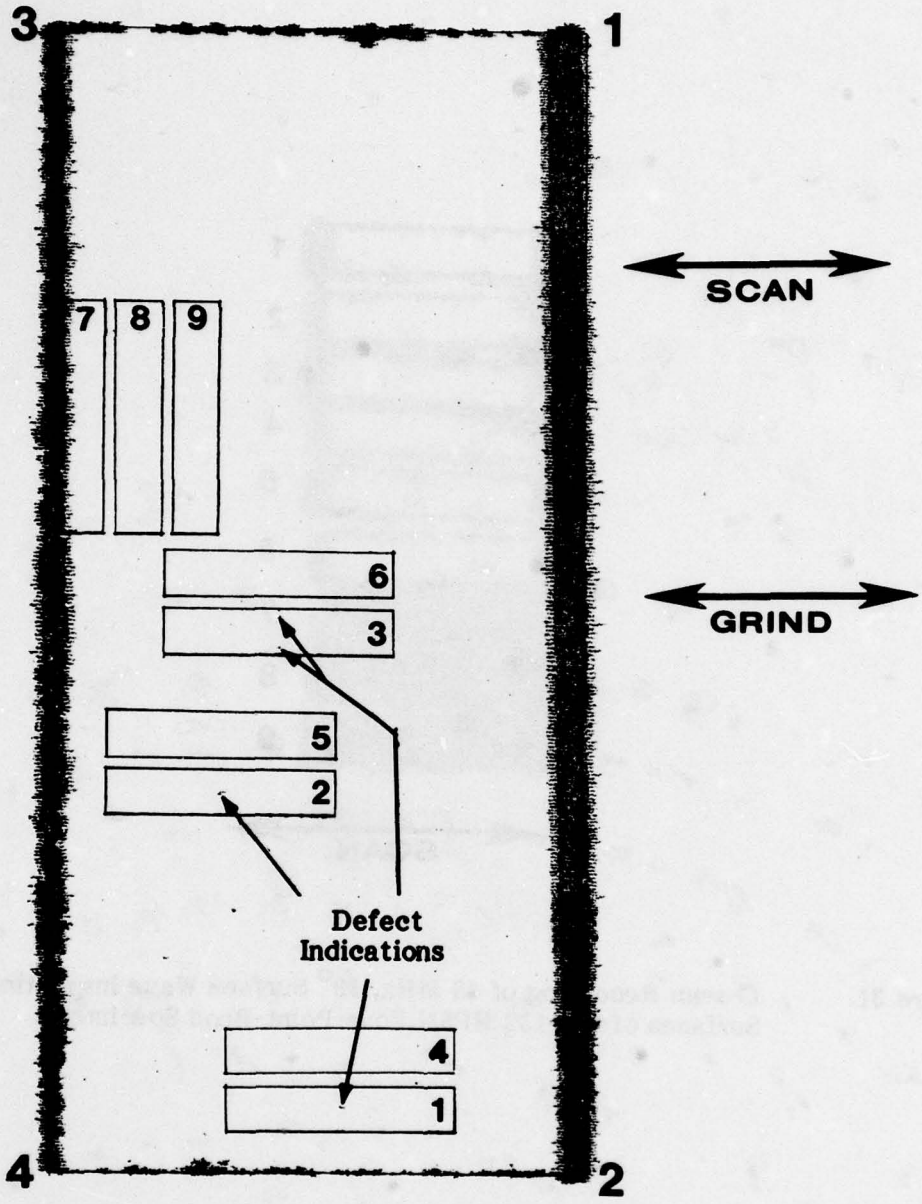

Figure 30. C-scan Recording of 45 MHz, 18° Surface Wave Inspection of Bottom Surface of Billet of NC-132 HPSN (Scan Perpendicular to Grinding Direction).

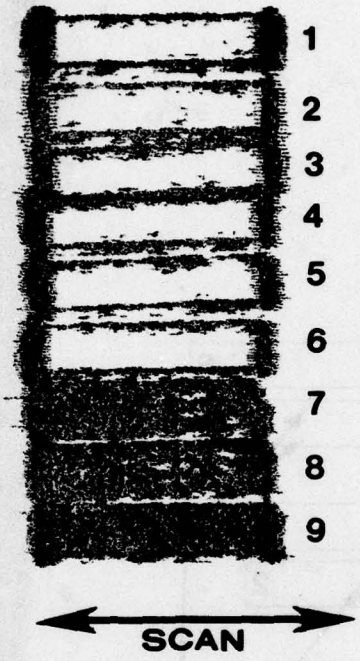

Figure 31. C-scan Recording of 45 MHz, 18° Surface Wave Inspection of Tensile Surfaces of NC-132 HPSN Four-Point-Bend Specimens.

Figure 32. C-scan Recording of 45 MHz, 11° Shear Wave Inspection of Billet of NC-350 Reaction Bonded Silicon Nitride (Notch on Top Side at 12 O'clock).

Figure 33. C-scan Recording of 45 MHz, 11° Shear Wave Inspection of Billet of NC-350 Reaction Bonded Silicon Nitride (Notch on Top Side at 3 O'clock).

Figure 34. C-scan Recording of 45 MHz, 11° Shear Wave Inspection of Billet of NC-350 Reaction Bonded Silicon Nitride (Notch on Bottom Side at 2 O'clock).

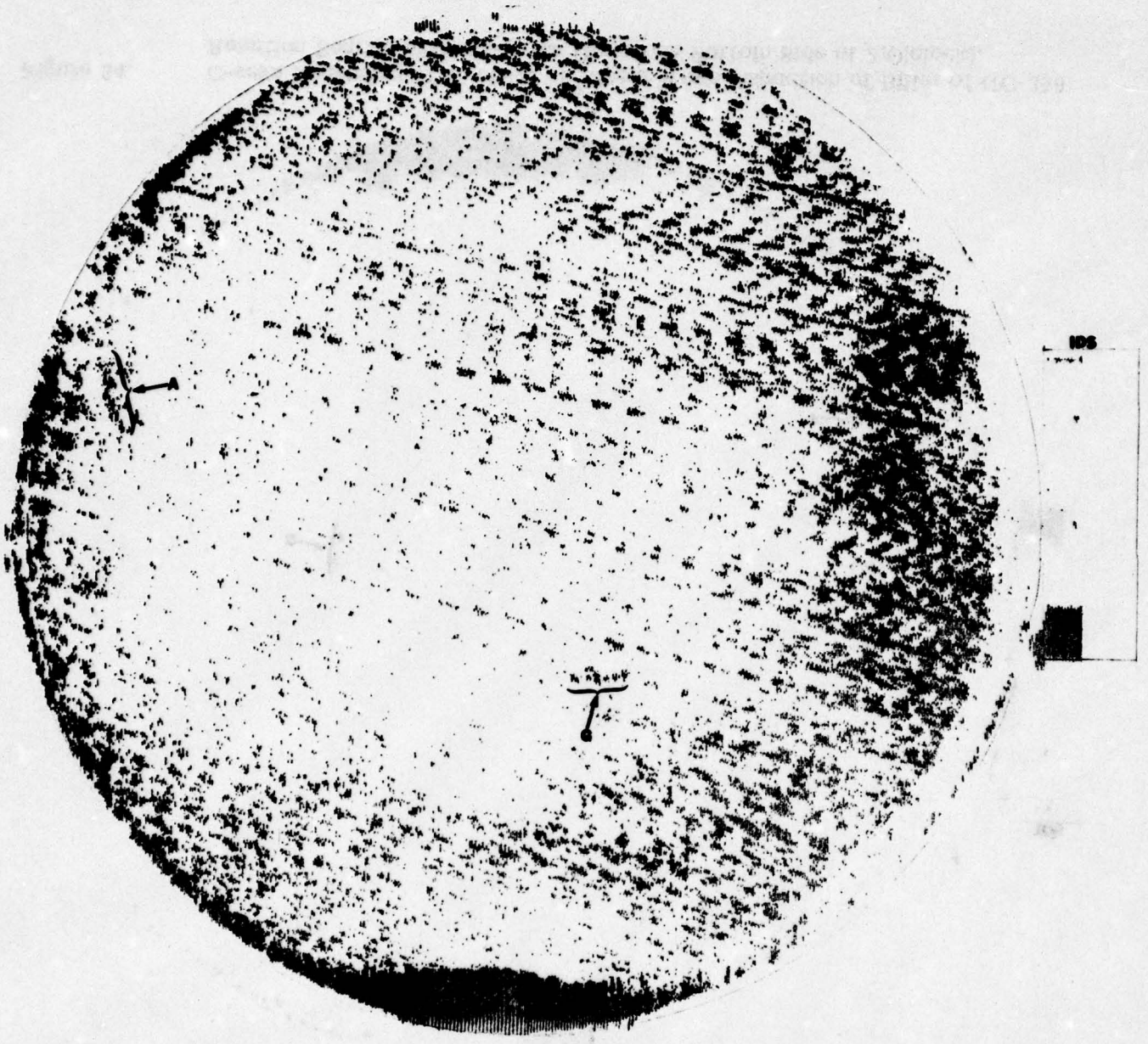

Figure 35. C-scan Recording of 45 MHz, 11° Shear Wave Inspection of Billet of NC-350 Reaction Bonded Silicon Nitride (Notch on Bottom Side at 11 O'clock).

part. These indications are extremely sensitive to beam orientation as can be seen by comparison with Figure 34, where the billet is rotated 90°. Visually, the billet shows three areas, approximately 2.5 cm square, near the edge where the material is lighter grey. These areas correspond to the groups of indications marked A, B and C on Figures 32 through 35. These are apparently areas of larger porosity since the defects associated with these areas are internal. The indications labeled E, F and G are associated with defects that are visible on the surface.

Figures 36 through 39 show C-scan recordings of the 45 MHz ultrasonic surface wave inspections of the billet of NC-350 RBSN. These correspond to the shear wave inspections shown in Figures 32 through 35, respectively. A shear wave inspection is performed with the surface to be inspected facing down, while a surface wave inspection is performed with the surface to be inspected facing up. To get the closest possible correlation, the surface wave inspection was done after rotating the billet around the direction of scan so that the ultrasonic beam strikes the defects from the same direction.

The most obvious conclusion that can be drawn from a comparison with the shear wave inspections is that the surface wave inspection is much more sensitive to the surface texture of the billet, which shows up as background indications in three of the four surface wave C-scans and in only one of the shear wave C-scans. These background indications are caused by a pattern of fine tightly spaced parallel lines that run across both sides of the billet as can be seen by the linear patterns in Figures 36 and 39. According to the manufacturer, these lines are created prior to nitriding, when the green billet is cut out of a much longer billet. They occur across the entire part, at a regular spacing of about 2 mm (0.080").

Because of the background indications from these lines, it is difficult to make a detailed comparison between the shear and surface wave C-scans. However, the visible surface defects, such as E in Figure 32 and F and G in Figure 34, show up clearly in the surface wave C-scans and are labeled with the same letters. In addition, there are a number of other linear indications, particularly in Figure 37, which cannot be associated with any readily visible surface defects, but which suggest the presence of surface cracks. A number of these indications have been labeled with the letter C in Figures 37 and 39.

Figure 40 is a reproduction of Figure 37 showing the bottom view of the billet overlayed with the locations of three 1.3 x7.6 cm (1/2 x 3-inch) burner rig specimens. Burner rig specimen #2 contains indication E, and one of the crack-like indications labeled C. Figure 41 shows the top view of the billet. In this C-scan recording the scan direction is rotated slightly from that of Figure 40, in order to eliminate the background of linear indications from the surface lines and to allow a better definition of the crack-like indication. In addition to showing the three burner rig specimens, this view shows an area where the surface lines were machined off (shaded area). This area contains indication F and half of the crack-like indication. The surface lines were removed by grinding off 15 μm (0.0006 inches) using a 320 grit diamond wheel to achieve a surface finish of about 20 microinches. The grinding was carried out perpendicular to the straight edge left by cutting out the burner rig specimens.

Figures 42, 43, and 44 are C-scan recordings of 45 MHz, 18° surface wave inspections of the top side of the segment of the billet containing the machined area. The arrows in these figures illustrate the relationship between the scan direction, the

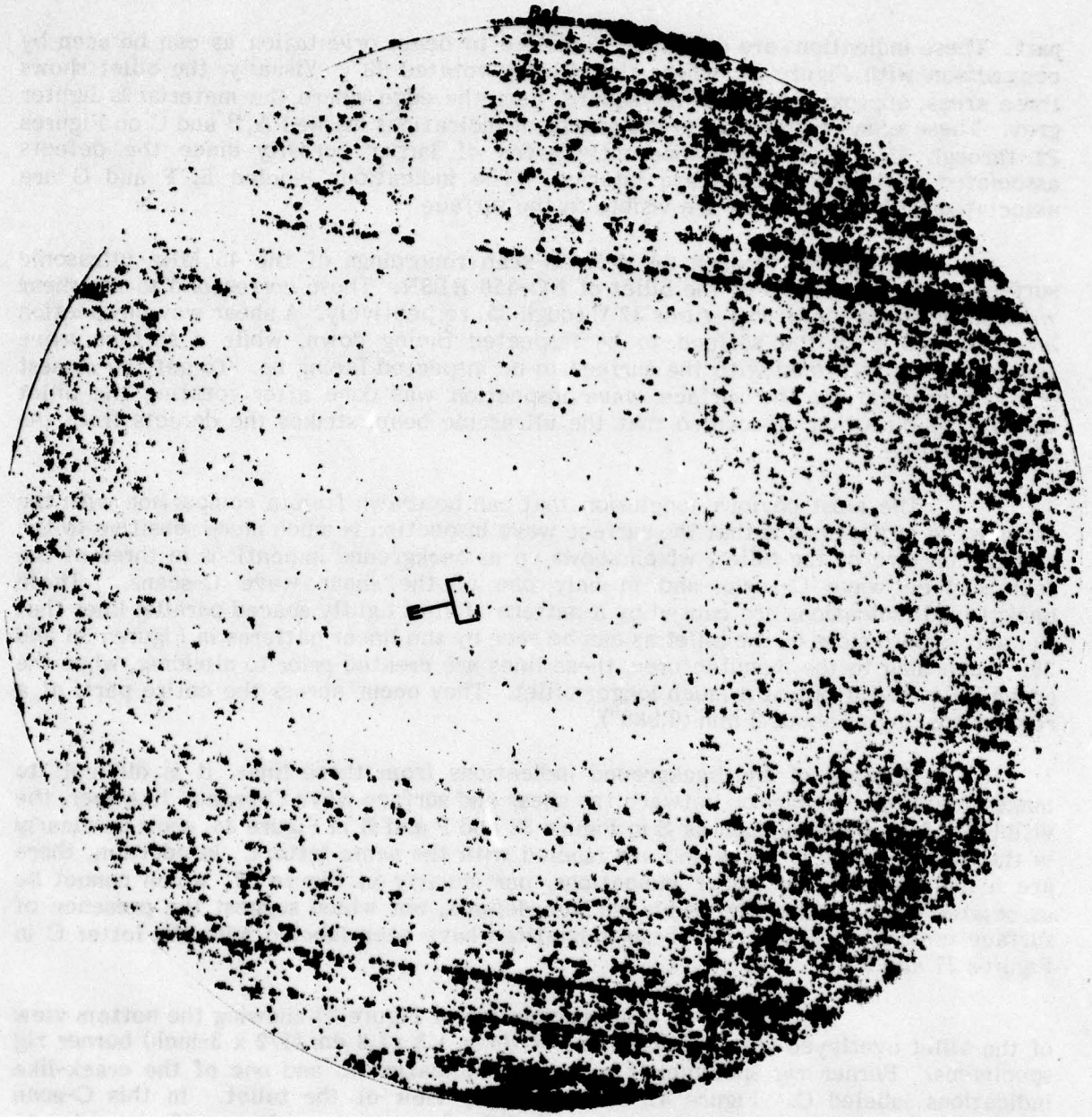

Figure 36. **C-scan Recording of 45 MHz, 18° Surface Wave Inspection of Billet of NC-350 Reaction Bonded Silicon Nitride (Notch on Bottom Side at 12 O'clock).**

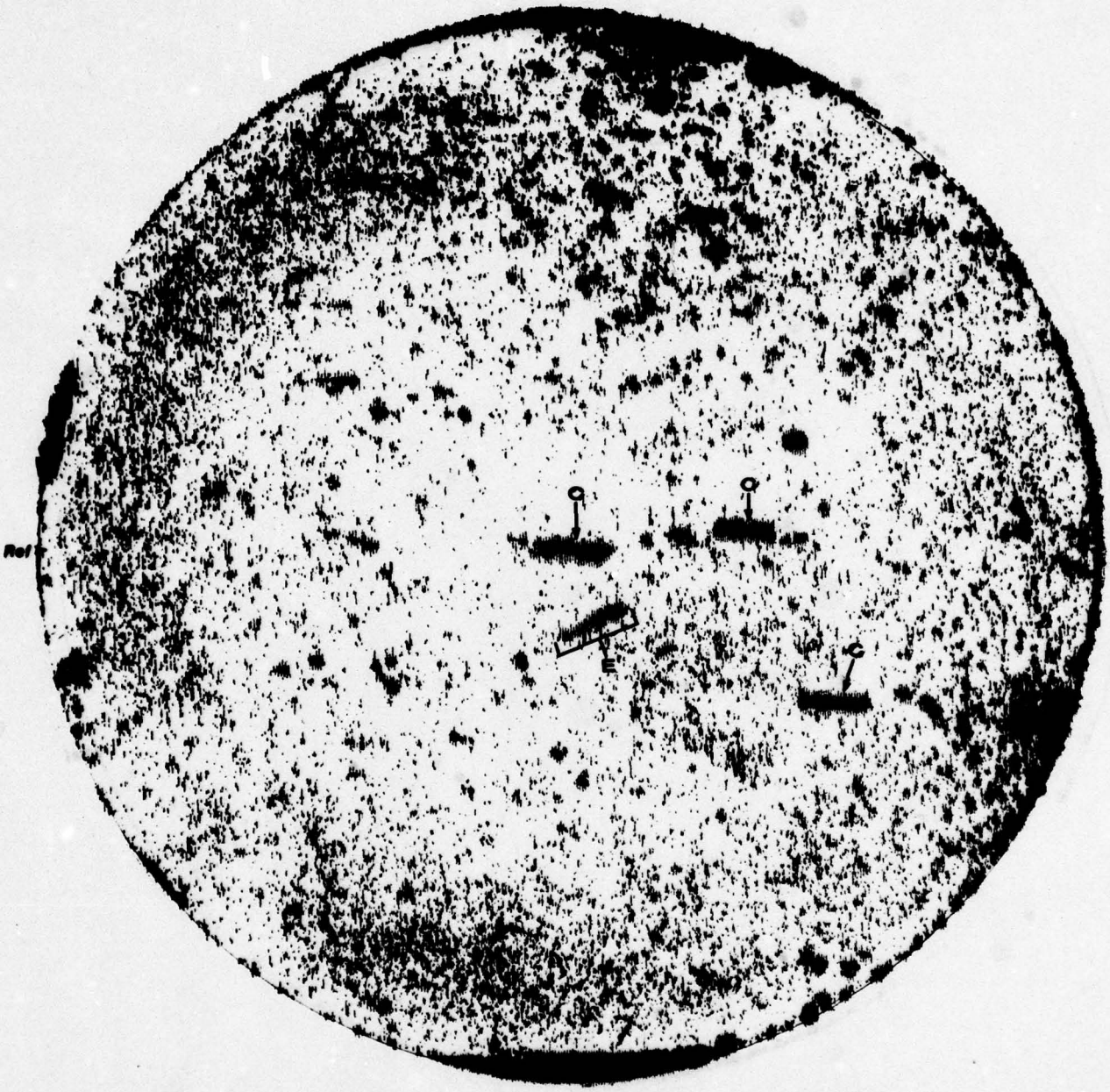

Figure 37. **C-scan Recording of 45 MHz, 18° Surface Wave Inspection of Billet of NC-350 Reaction Bonded Silicon Nitride (Notch on Bottom Side at 9 O'clock).**

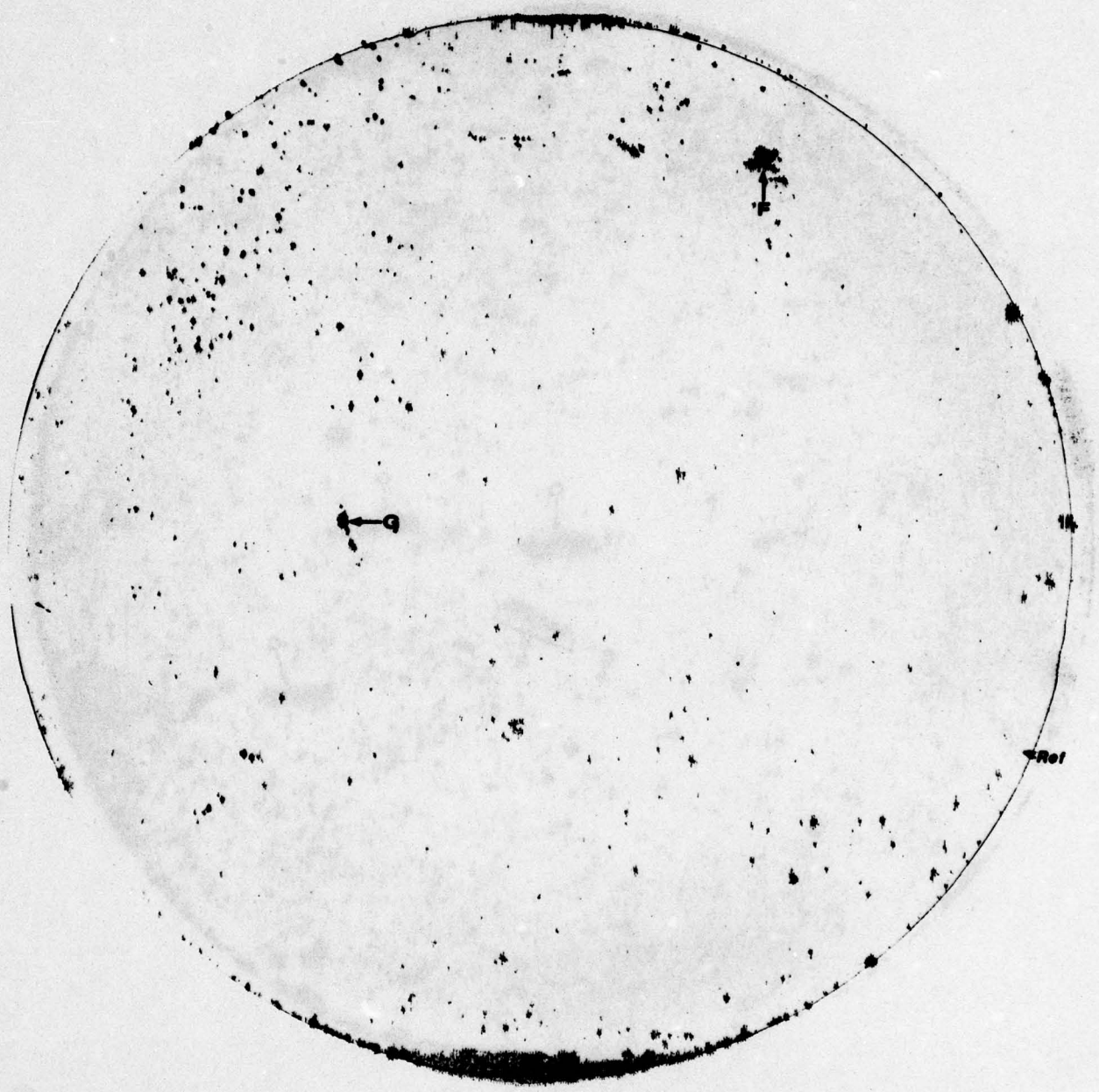

Figure 38. C-scan Recording of 45 MHz, 18° Surface Wave Inspection of Billet of NC-350 Reaction Bonded Silicon Nitride (Notch on Top Side at 4 O'clock).

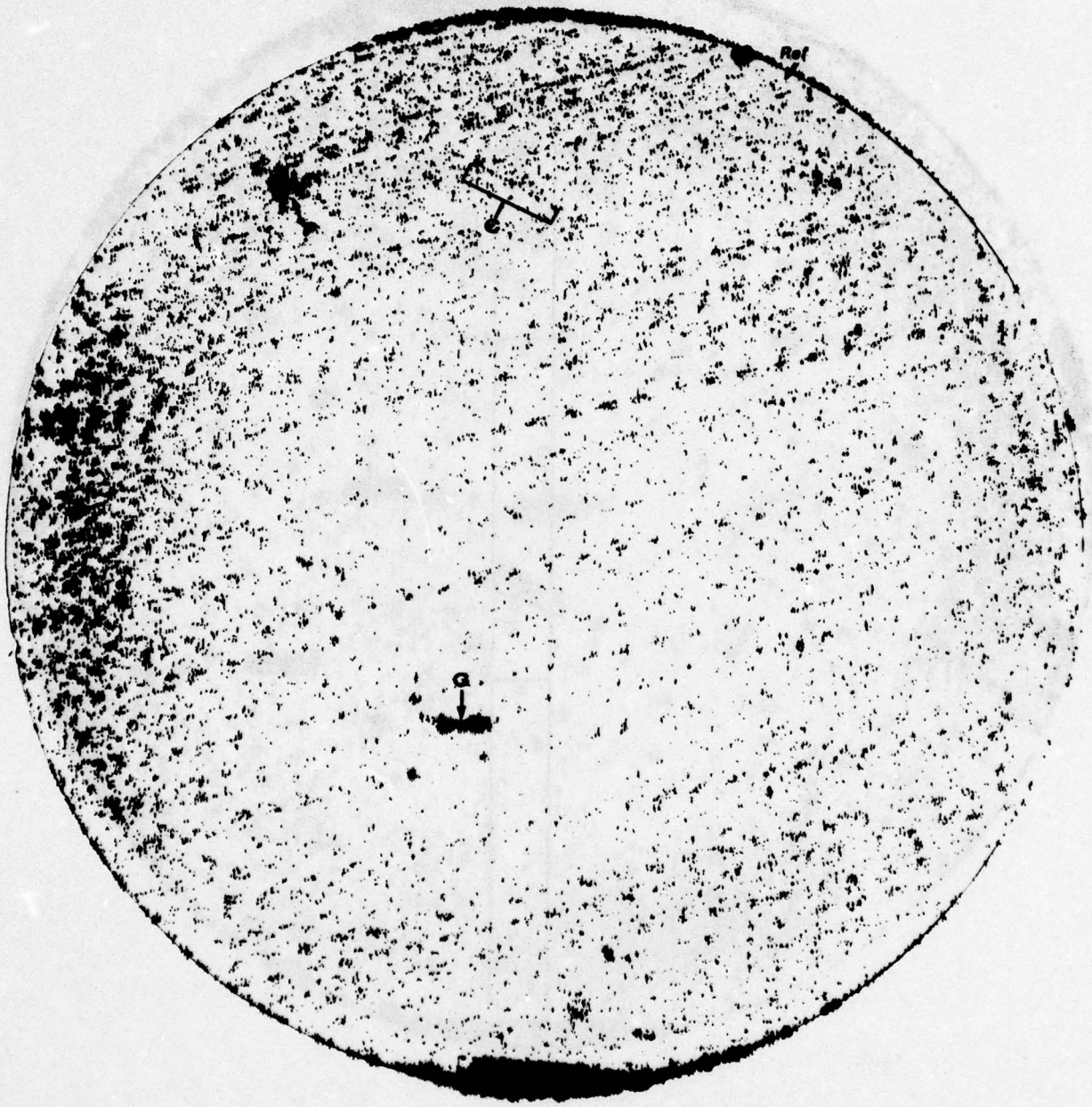

Figure 39. **C-scan Recording of 45 MHz, 18° Surface Wave Inspection of Billet of NC-350 Reaction Bonded Silicon Nitride (Notch on Top Side at 1 O'clock).**

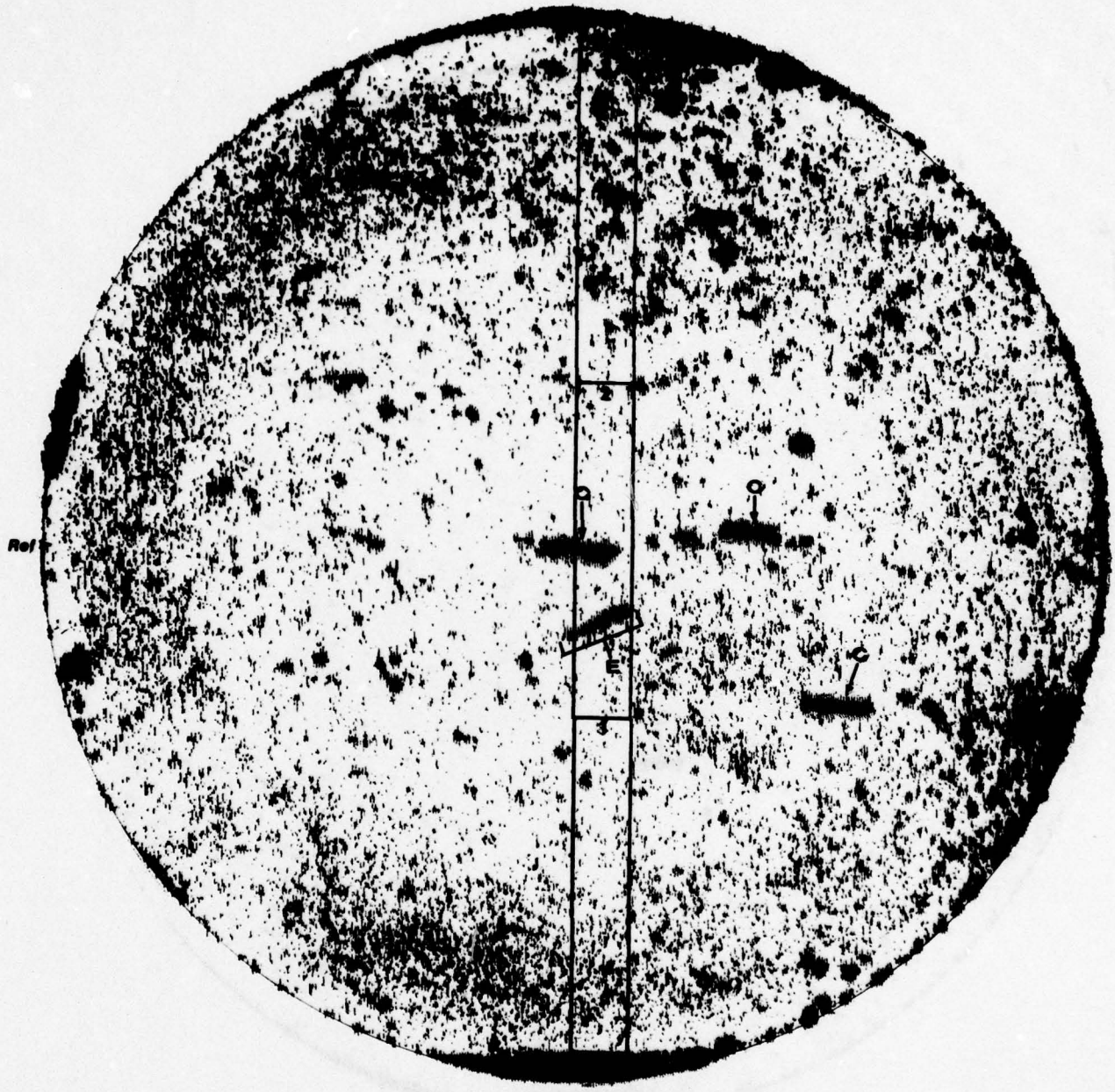

Figure 40. Location of Burner Rig Specimens Overlayed on C-scan Recording of 45 MHz, 18° Surface Wave Inspection of Bottom Surface of Billet of NC-350 RBSN.

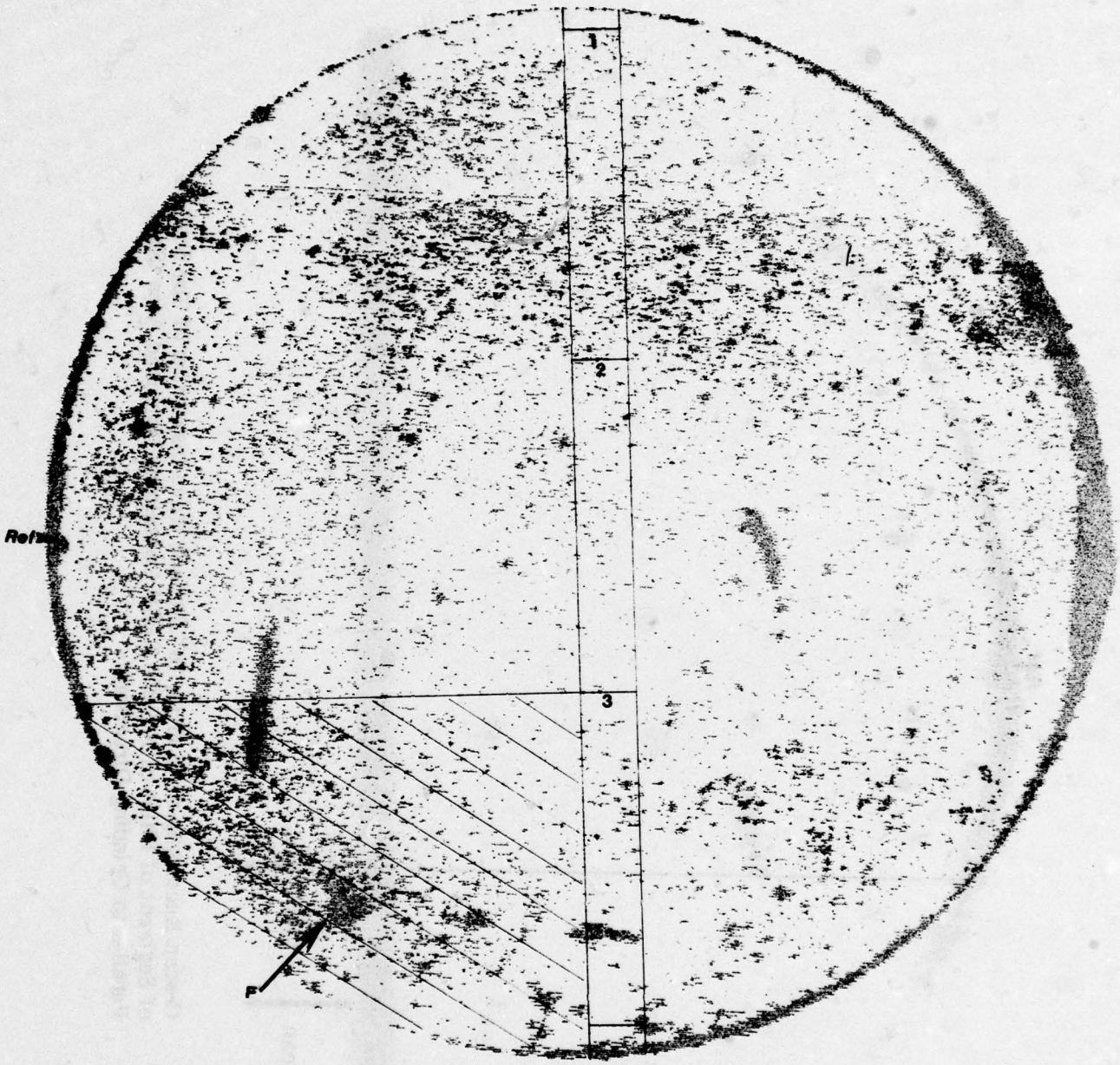

Figure 41. Location of Burner Rig Specimens and Machined (Shaded) Area Overlayed on C-scan Recording of 45 MHz, 18° Surface Wave Inspection of Top Surface of Billet of NC-350 RBSN.

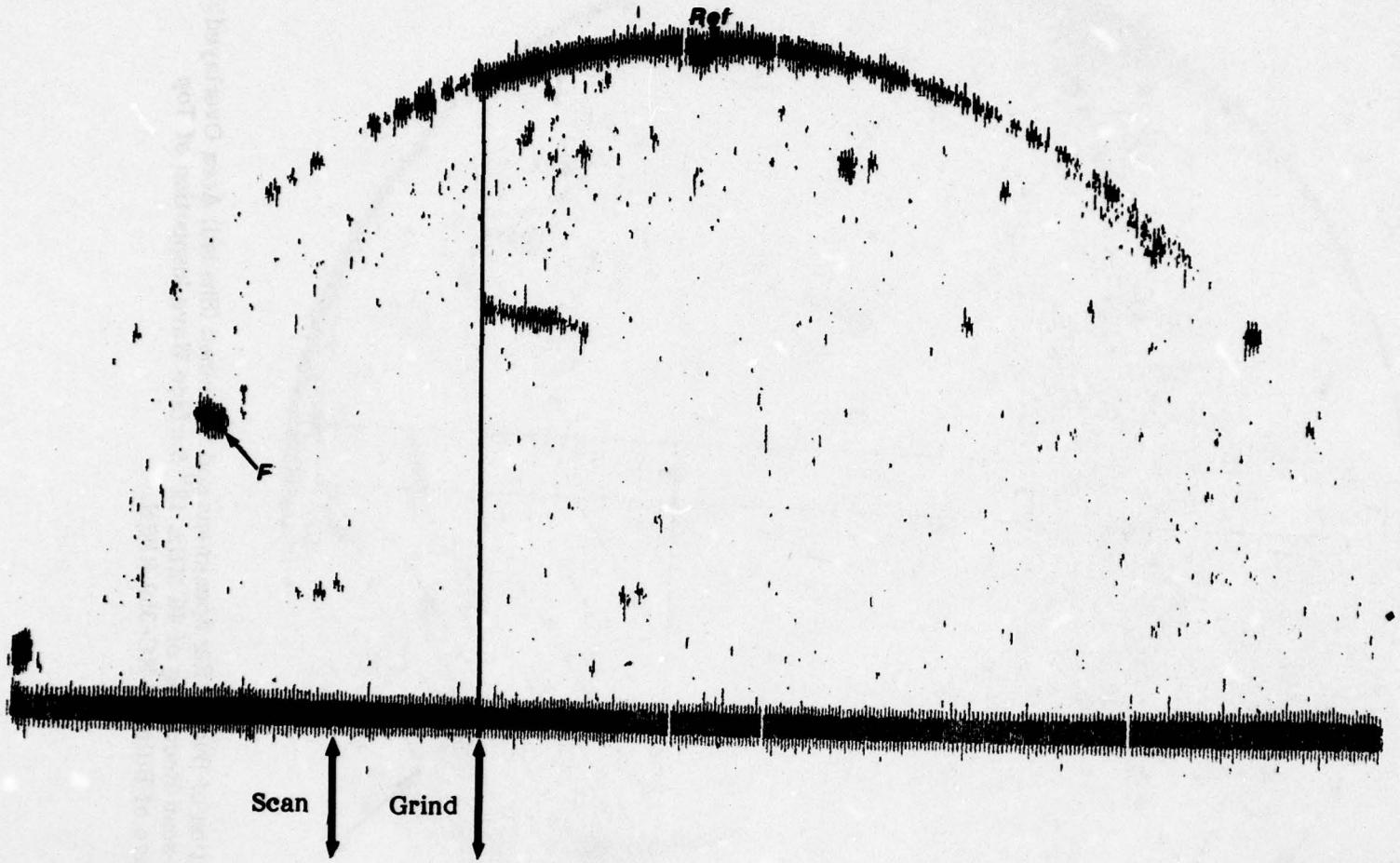

Figure 42. C-scan Recording of 45 MHz, 18° Surface Wave Inspection of Top Surface of Segment of Billet of NC-350 RBSN Containing Machined Area (Scan Parallel to Grinding Direction).

Figure 43. C-scan Recording of 45 MHz, 18° Surface Wave Inspection of Top Surface of Segment of Billet of NC-350 RBSN Containing Machined Area (Scan Perpendicular to Grind).

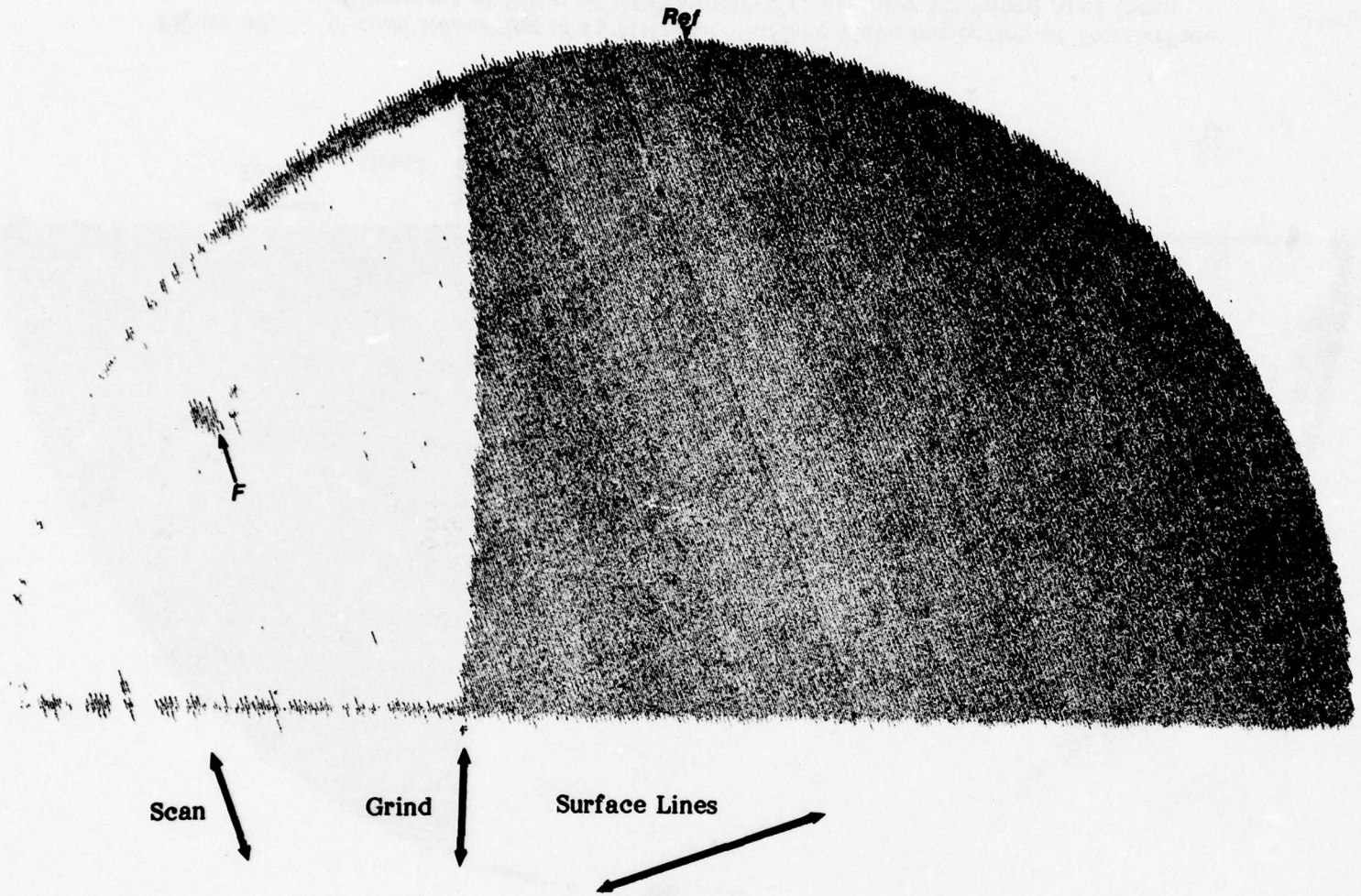

Figure 44. C-Scan Recording of 45 MHz, 18° Surface Wave Inspection of Top Surface of Segment of Billet of NC-350 RBSN Containing Machined Area (Scan Perpendicular to Surface Lines).

grinding direction and the surface lines in the unmachined portion of the billet. In Figure 42, ultrasonic scanning was performed parallel to the grinding direction. Indication F still appears in the machined area and the crack-like indication still appears in the unmachined area. Apparently the defect associated with this indication is less than 15 μm (0.0006 inches) deep.

In Figure 43, the scanning direction is perpendicular to the grinding direction. In this orientation the entire machined area shows up as defective. Apparently the damage caused by grinding is as severe as the defects detected from other orientations. It should also be noted that the crack-like indication cannot be detected from this orientation. In Figure 44, the scanning direction is perpendicular to the surface lines in the unmachined portion of the specimen. This is a rotation of about 20^{o} from Figure 43. In this case the entire unmachined area appears defective and indication F is again evident against a clean background in the machined area.

The following conclusions can be drawn from the inspections of this segment of the billet:

1. the surface wave inspection technique is capable of detecting defects at least as shallow as 15 μm (0.0006 inches) in depth;

2. detection of certain types of defects including grinding damage, is extremely sensitive to the acoustic beam orientation; and

3. the technique is sensitive enough to detect the surface texture of the part.

Figures 45 and 46 show the layout of four-point-bend specimens on the two halves of the billet. Specimens #1, 2 and 3 contain the remains of the crack-like indication that was partially machined away. Specimen #4 is in a defect-free area and #5 contains a small surface indication. Specimens #6, 7, 8 and 9 contain other small crack-like indications. Specimens #10, 11 and 12 run approximately perpendicular to the surface lines and specimens #13, 14 and 15 run approximately parallel to the surface lines. Figure 47 shows the C-scan recording of the 45 MHz ultrasonic surface wave inspections of the four-point-bend specimens prior to final machining.

5.4 Hot Pressed Silicon Carbide

5.4.1 Ceralloy 146

A 1.2 x 7.6 cm (1/2" x 3") burner rig specimen was cut out of the edge of the original billet. Figures 48 through 51 show the C-scan recordings of the 45 MHz ultrasonic surface wave inspections of the remaining 12 x 14 cm (4-3/4 x 5-1/2") portion. Since there were only a few very small defects detected in the billet, four-point-bend specimens were selected to evaluate the effect of machining damage only. The location of the three specimens cut parallel to the grinding direction (Nos. 4, 5, and 6) and the three specimens cut perpendicular to the grinding direction (Nos. 1, 2 and 3) are shown in Figures 48 and 49. Figure 52 shows the C-scan recording of the 45 MHz ultrasonic surface wave inspection of the tensile surfaces of the specimens prior to final machining to thickness.

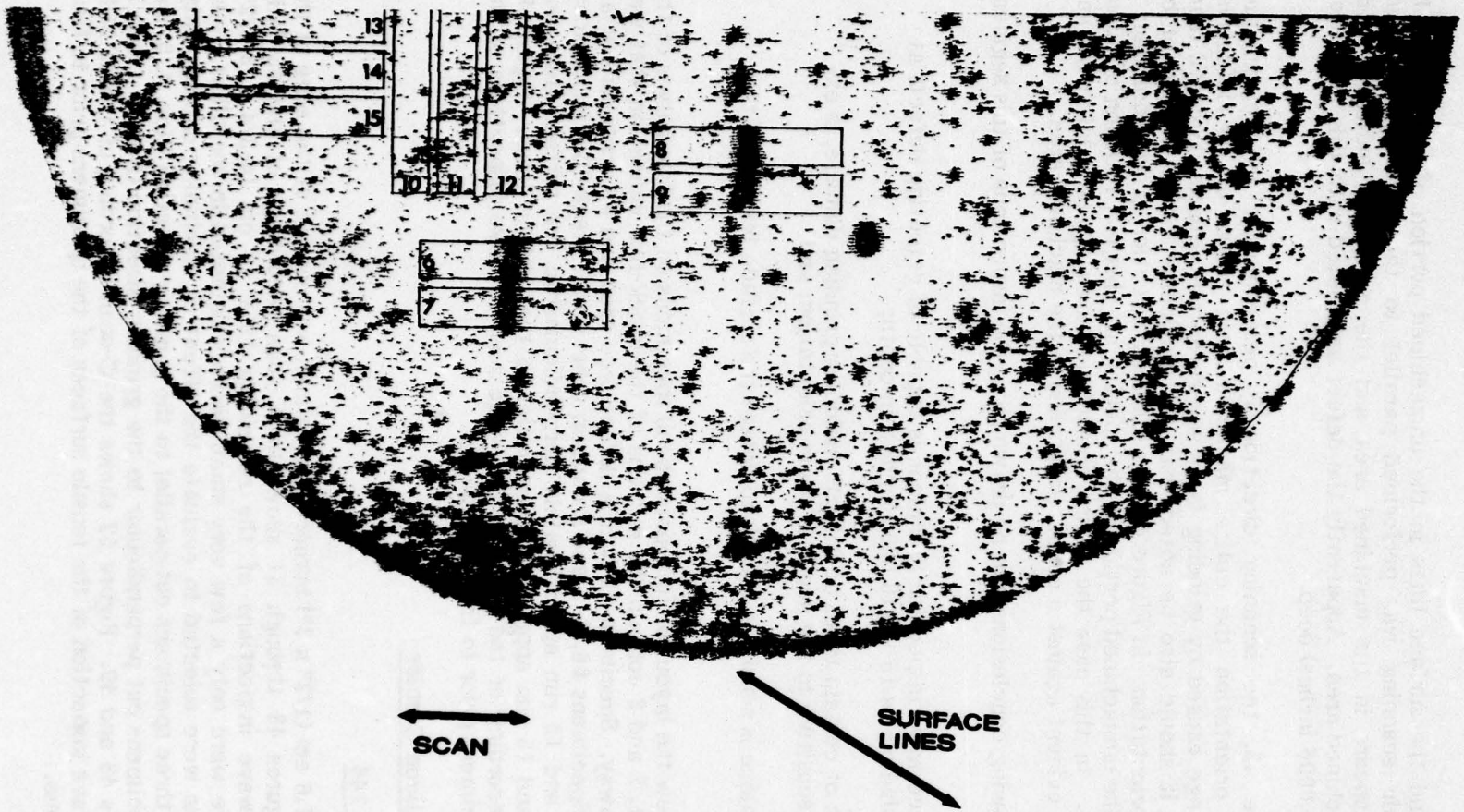

Figure 45. Layout of Four-Point-Bend Specimens on Bottom Surface of Unmachined Segment of Billet of NC-350 RBSN.

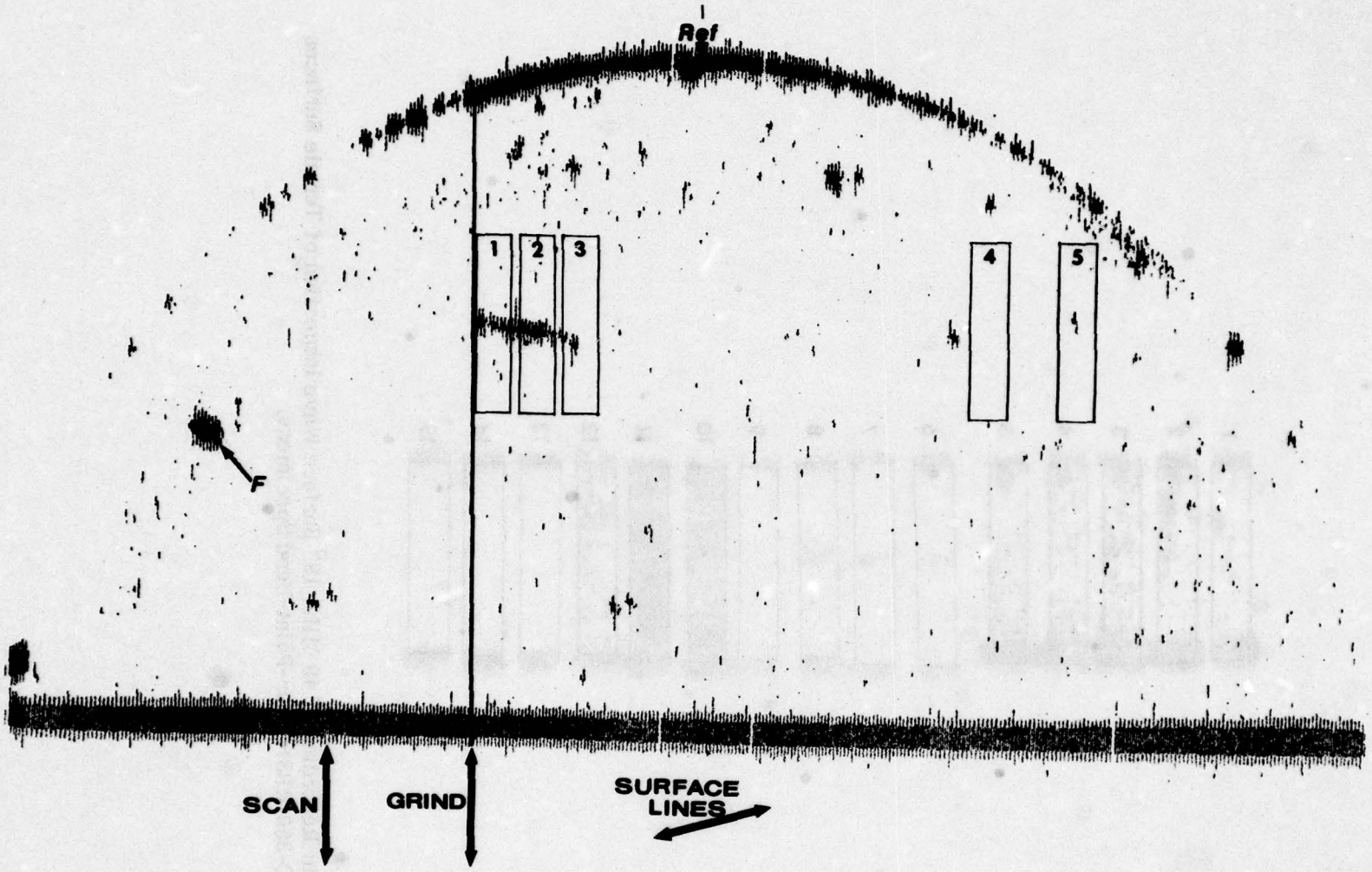

Figure 46. Layout of Four-Point-Bend Specimens of Top Surface of Partially Machined Segment of Billet of NC-350 RBSN.

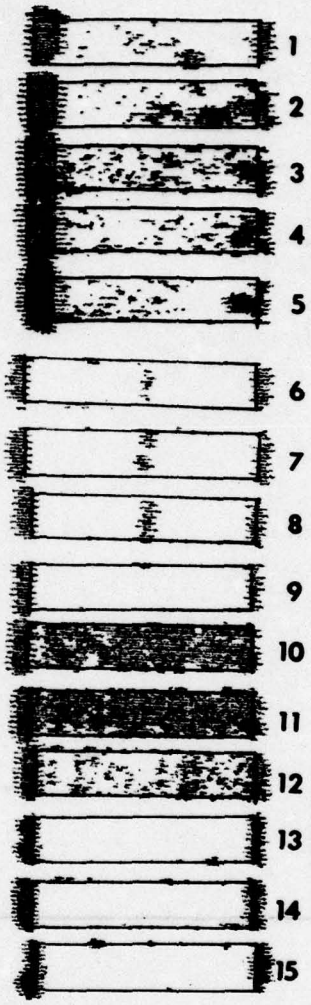

Figure 47. C-scan Recording of 45 MHz, 18° Surface Wave Inspection of Tensile Surfaces of NC-350 RBSN Four-Point-Bend Specimens.

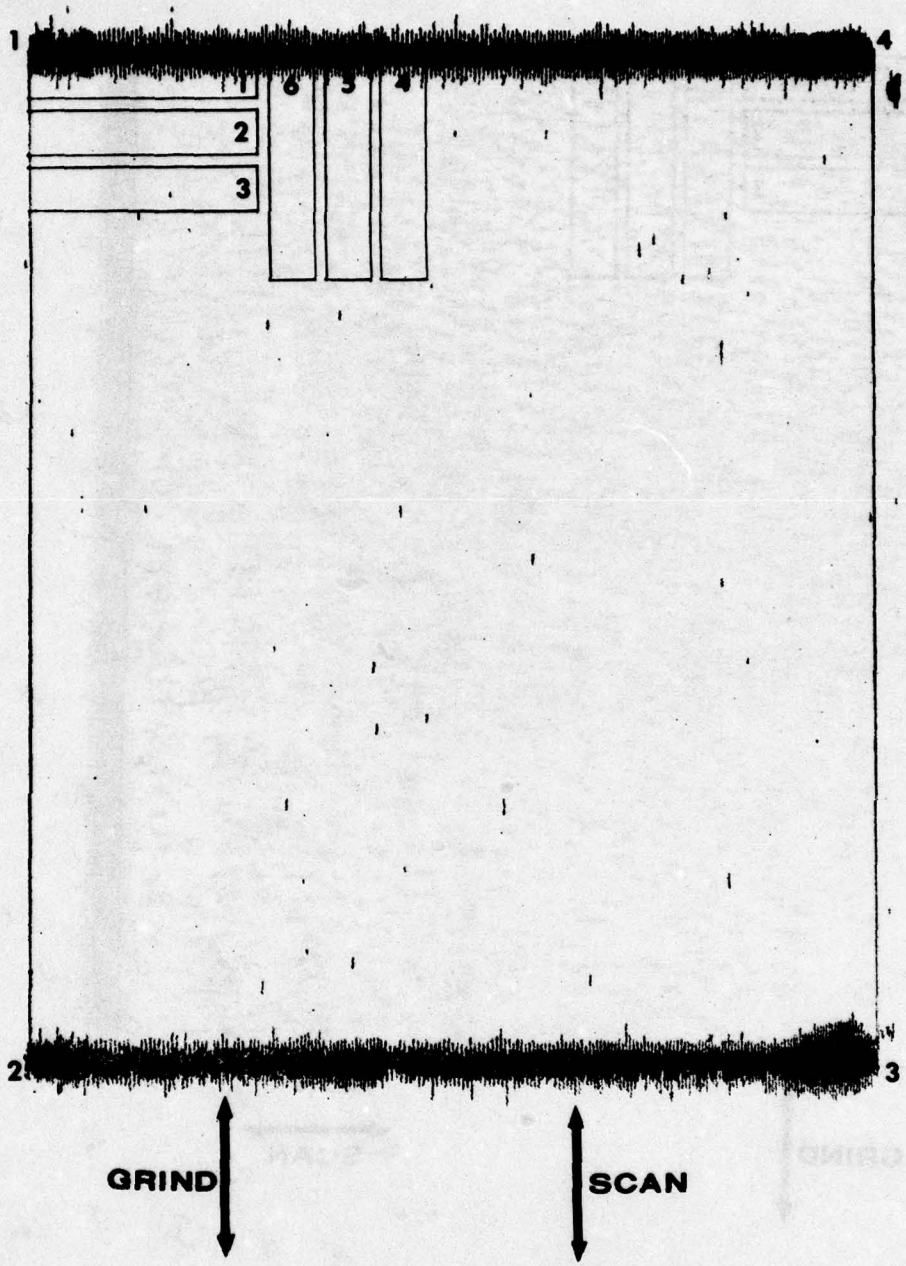

Figure 48. C-scan Recording of 45 MHz, 18° Surface Wave Inspection of Top Surface of Billet of Ceralloy 146 HPSiC (Scan Parallel to Grinding Direction).

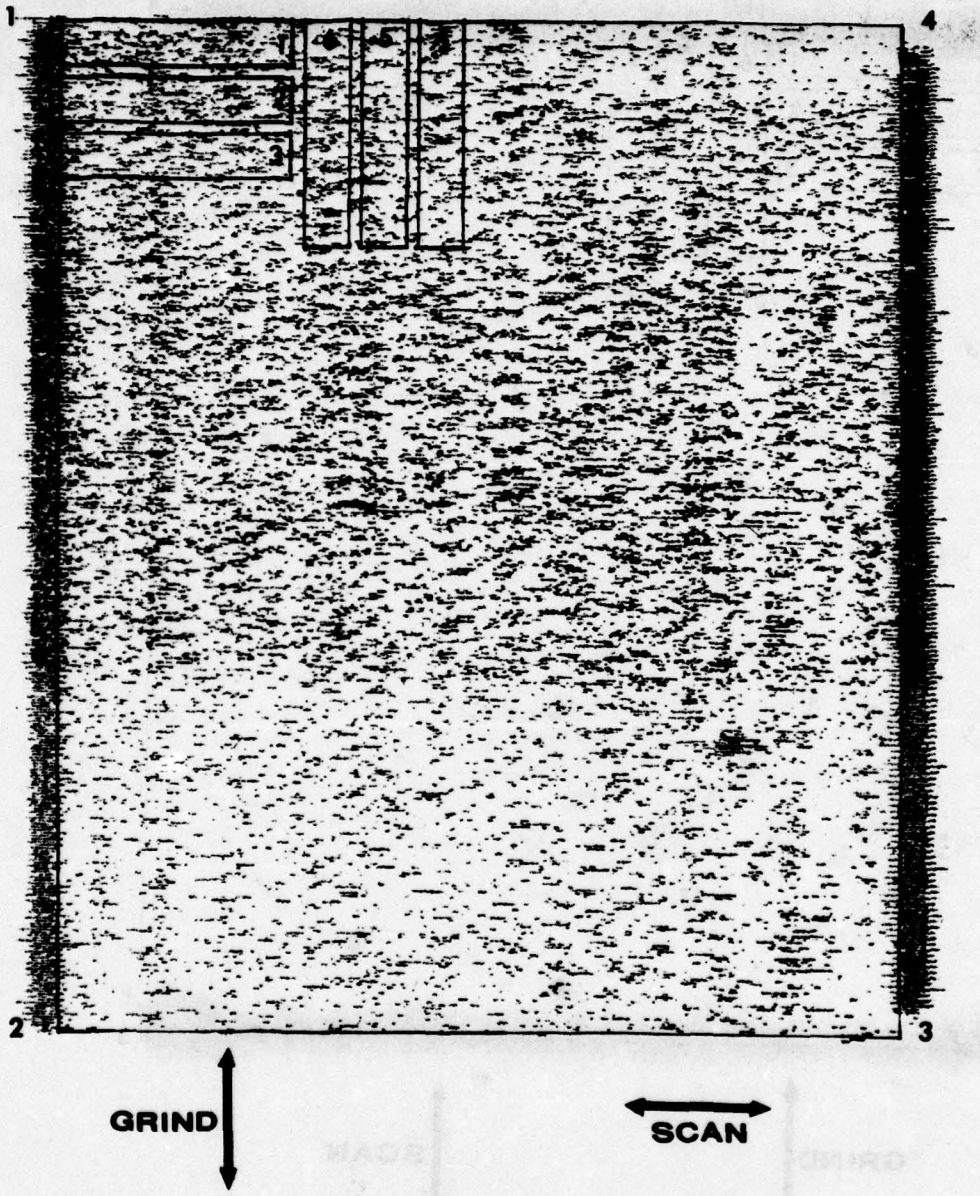

Figure 49. C-scan Recording of 45 MHz, 18° Surface Wave Inspection of Top Surface of Billet of Ceralloy 146 HPSiC (Scan Perpendicular to Grinding Direction).

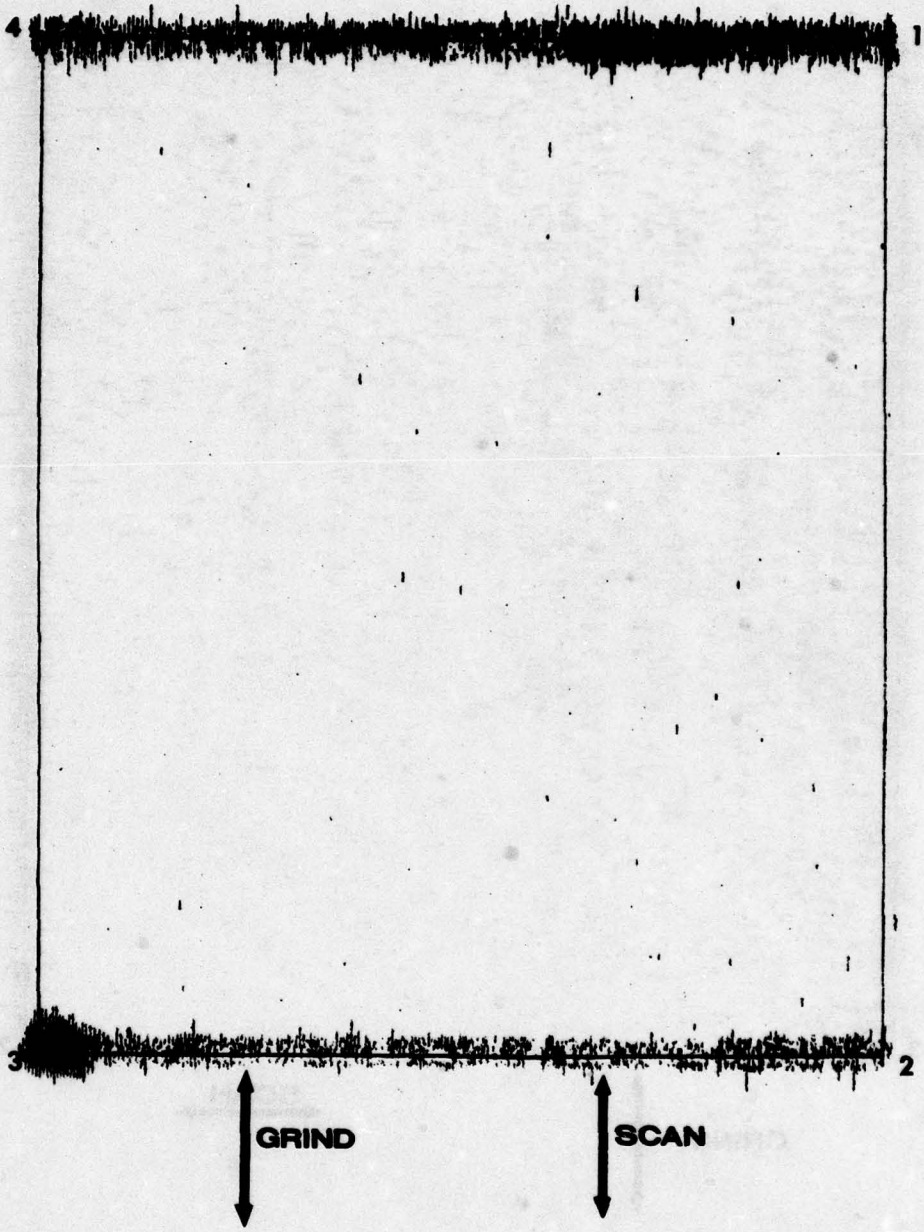

Figure 50. C-scan Recording of 45 MHz, 18° Surface Wave Inspection of Bottom Surface of Billet of Ceralloy 146 HPSiC (Scan Parallel to Grinding Direction).

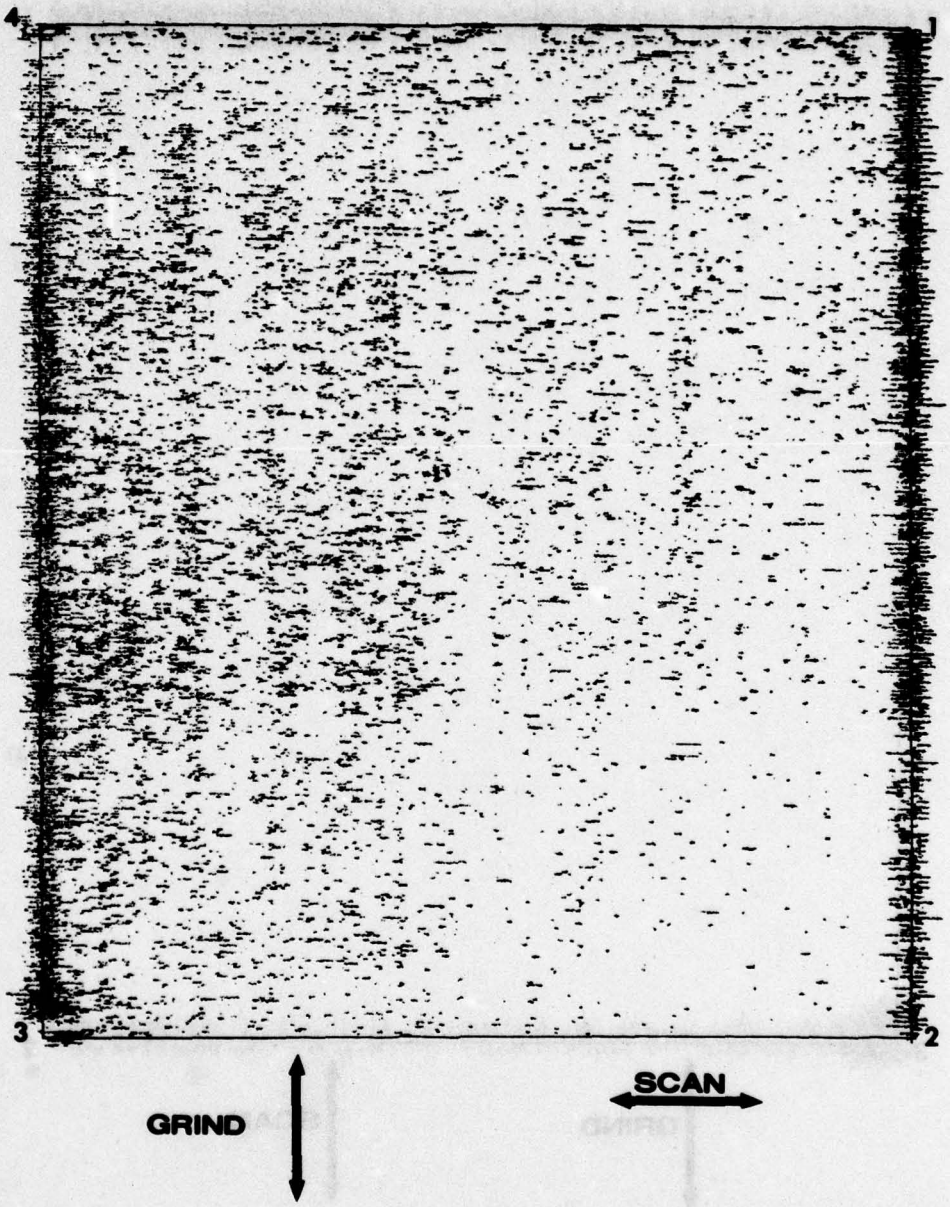

Figure 51. C-scan Recording of 45 MHz, 18° Surface Wave Inspection of Bottom Surface of Billet of Ceralloy 146 HPSiC (Scan Perpendicular to Grinding Direction).

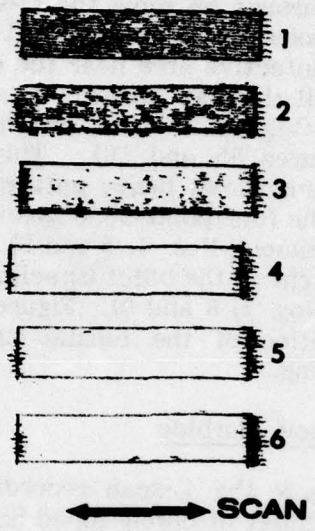

Figure 52. **C-scan Recording of 45 MHz, 18° Surface Wave Inspection of Tensile Surfaces of Ceralloy 146 HPSiC Four-Point-Bend Specimens.**

5.4.2 NC-203A

A 1.2 x 7.6 cm (1/2 x 3-inch) burner rig specimen was cut out of the edge of the original billet. Figures 53 through 56 show the C-scan recordings of the 45 MHz ultrasonic surface wave inspections of the remaining 14 x 16 cm (5-1/2 x 6-1/4-inch) portion. This billet has a large defective area near the center that was shown by shear wave inspection (Ref. 2) to go all the way through the part. This shows up as a heavy indication on the top surface (Figures 53 and 54) and as a cluster of scattered indications on the bottom (Figures 55 and 56). This billet had extremely smooth surfaces so that none of the scans shows heavy patterns of indications from grinding marks. As shown in Figure 54, the four-point-bend specimens were selected to compare an area free of indications (specimens Nos. 4, 5 and 6) with an area showing the only apparent machining damage present in the billet (specimen Nos. 1, 2 and 3) and with the large defective area (specimen Nos. 7, 8 and 9). Figure 57 is a C-scan of the 45 MHz ultrasonic surface wave inspection of the tensile surfaces of the four-point-bend specimens prior to finish machining.

5.5 Boron-Doped Sintered Silicon Carbide

Figures 58 through 61 show the C-scan recordings of the 45 MHz ultrasonic surface wave inspections of the billet of boron-doped SSiC. These inspections detected a number of small defects, particularly on the bottom surface, in the scans made parallel to the grinding direction. They also detected a number of lines of grinding damage running across the billet in the scans made perpendicular to the grinding direction. Since this billet was small, there was not enough material to make a burner rig specimen or to make many four-point-bend specimens. Figure 59 shows the locations of the four-point-bend specimens that were made from this billet. Specimen No. 1 is centered around a 64 mm (1/4 inch) long indication caused by a defect which appears visually to be a shallow scratch. Specimen No. 2 is centered around one of the lines of grinding damage that runs across the top surface of the billet. Specimen Nos. 3 and 4 are parallel to specimen Nos. 1 and 2 in defect-free areas. Figure 62 shows the C-scan recording of the 45 MHz ultrasonic surface wave inspection of the tensile surfaces of the four-point-bend specimens from the billet of boron-doped SSiC. The grinding damage present in specimen No. 2, as seen in Figure 59, was not detected in this scan.

5.6 Discussion

The inspection results presented in this section show that the surface wave technique is applicable to a variety of ceramic materials. Defect indications have been correlated with internal defects detected by the shear wave technique prior to machining of a billet, with visible surface scratches and pits, and with the surface textures caused by cutting or grinding the material. Of course, many of the defect indications are also from unknown sources, presumably from defects which cannot be detected by other techniques. By machining away a surface to remove a defect, it was determined that a defect as shallow as 15 μm (0.0006 inches) in depth could be detected. This, of course, was a case where the defect was wider than the ultrasonic beam. The ultrasonic beam is believed to have a diameter at the focal point of about 580 μm (0.023 inches). Therefore, the effective area of a 16 μm deep surface flaw of the type detected is about 7500 μm^2 (1 x 2 x 10^6 in^2). This is equivalent to a 70 μm

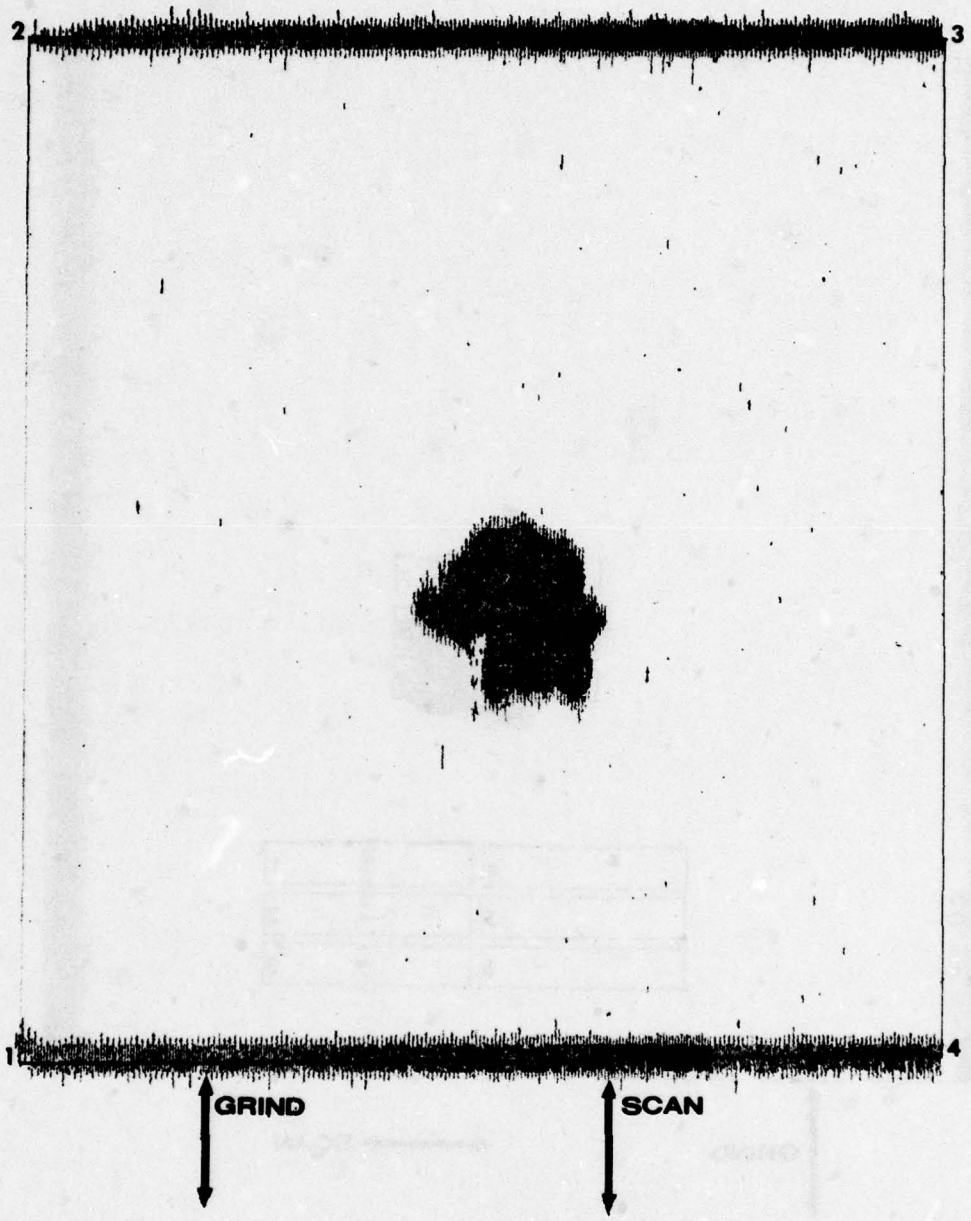

Figure 53. C-scan Recording of 45 MHz, 18° Surface Wave Inspection of Top Surface of Billet of NC-203A HPSiC (Scan Parallel to Grinding Direction).

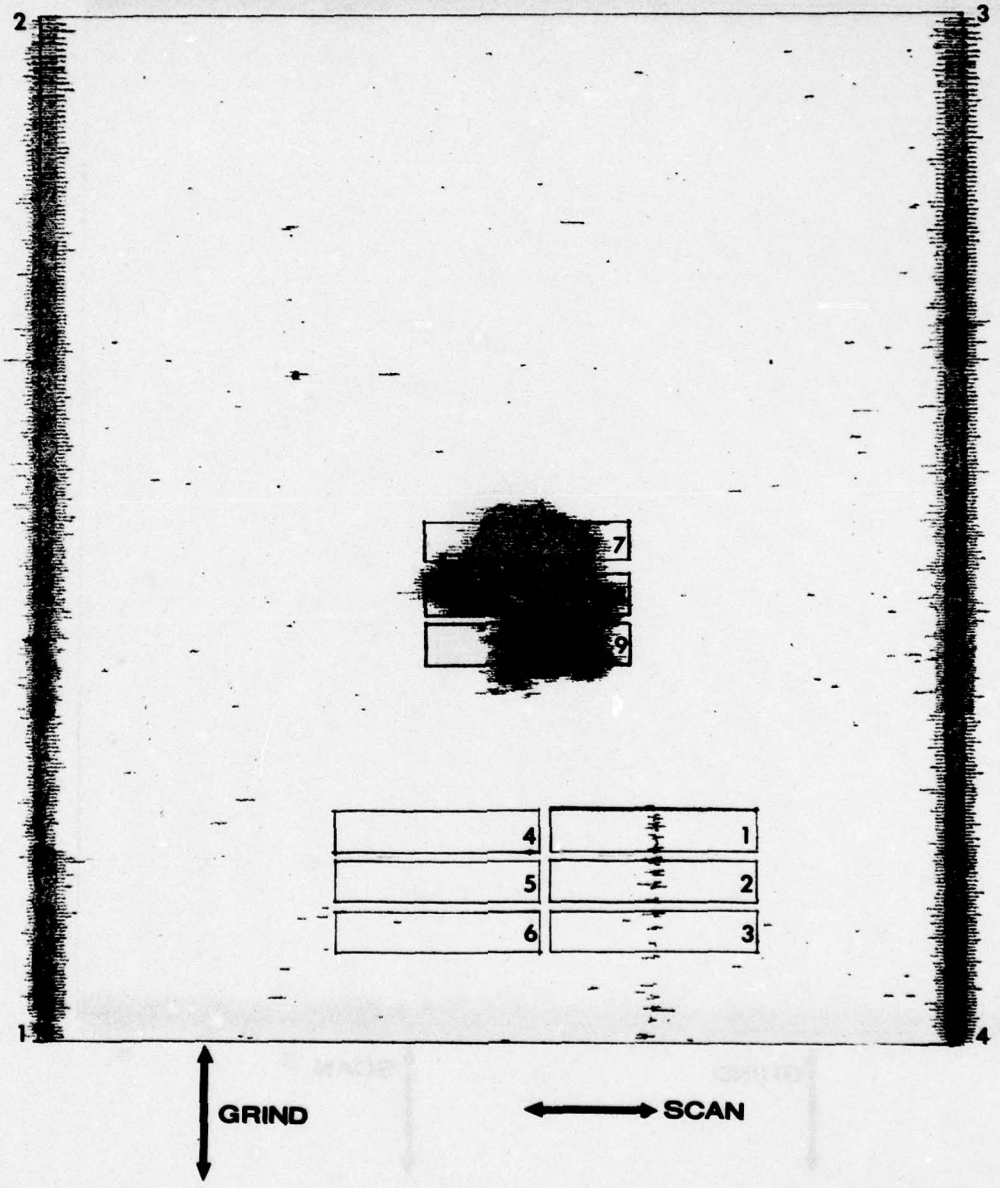

Figure 54. C-scan Recording of 45 MHz, 18° Surface Wave Inspection of Top Surface of Billet of NC-203A HPSiC (Scan Perpendicular to Grinding Direction).

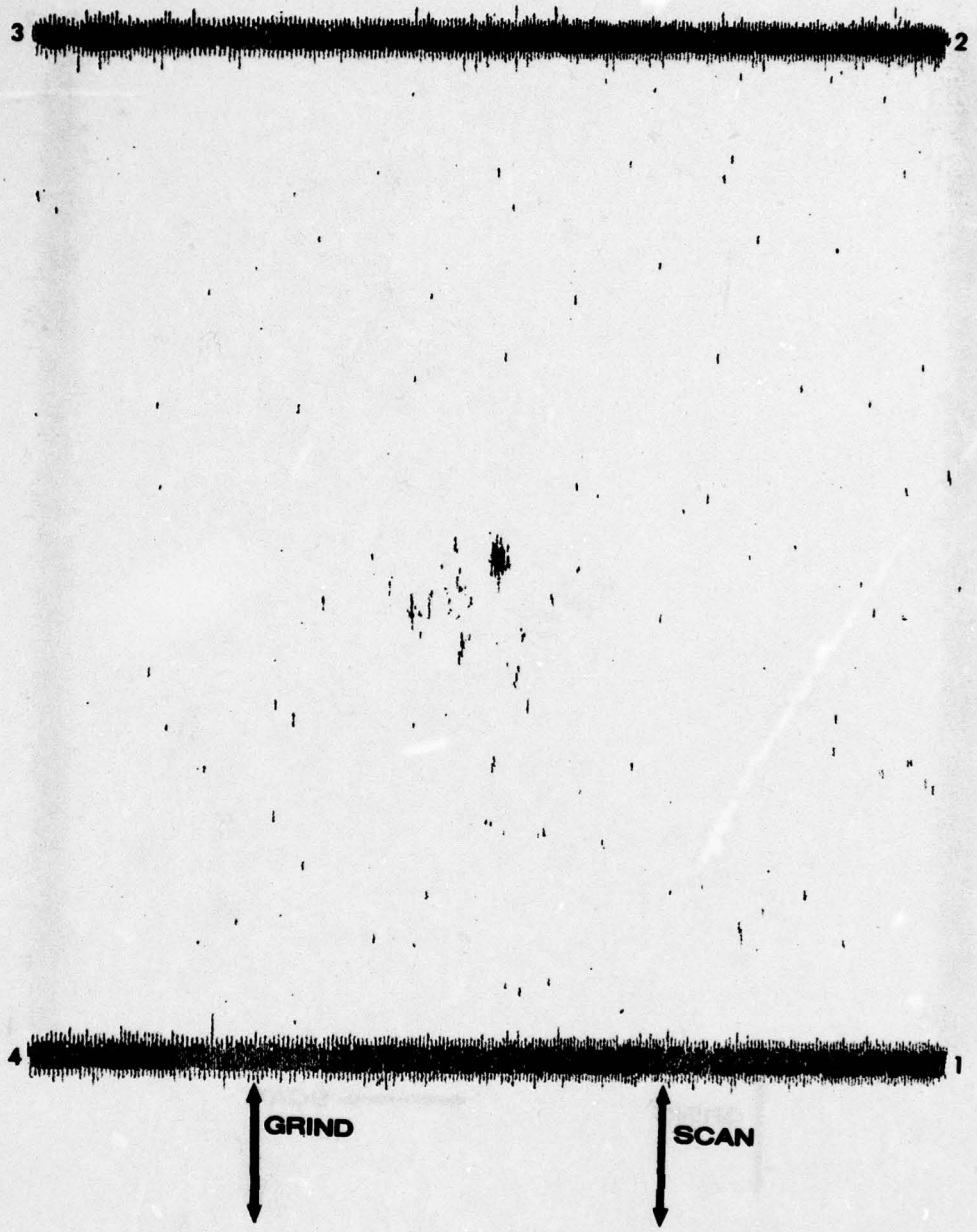

Figure 55. C-scan Recording of 45 MHz, 18° Surface Wave Inspection of Bottom Surface of Billet of NC-203A HPSiC (Scan Parallel to Grinding Direction).

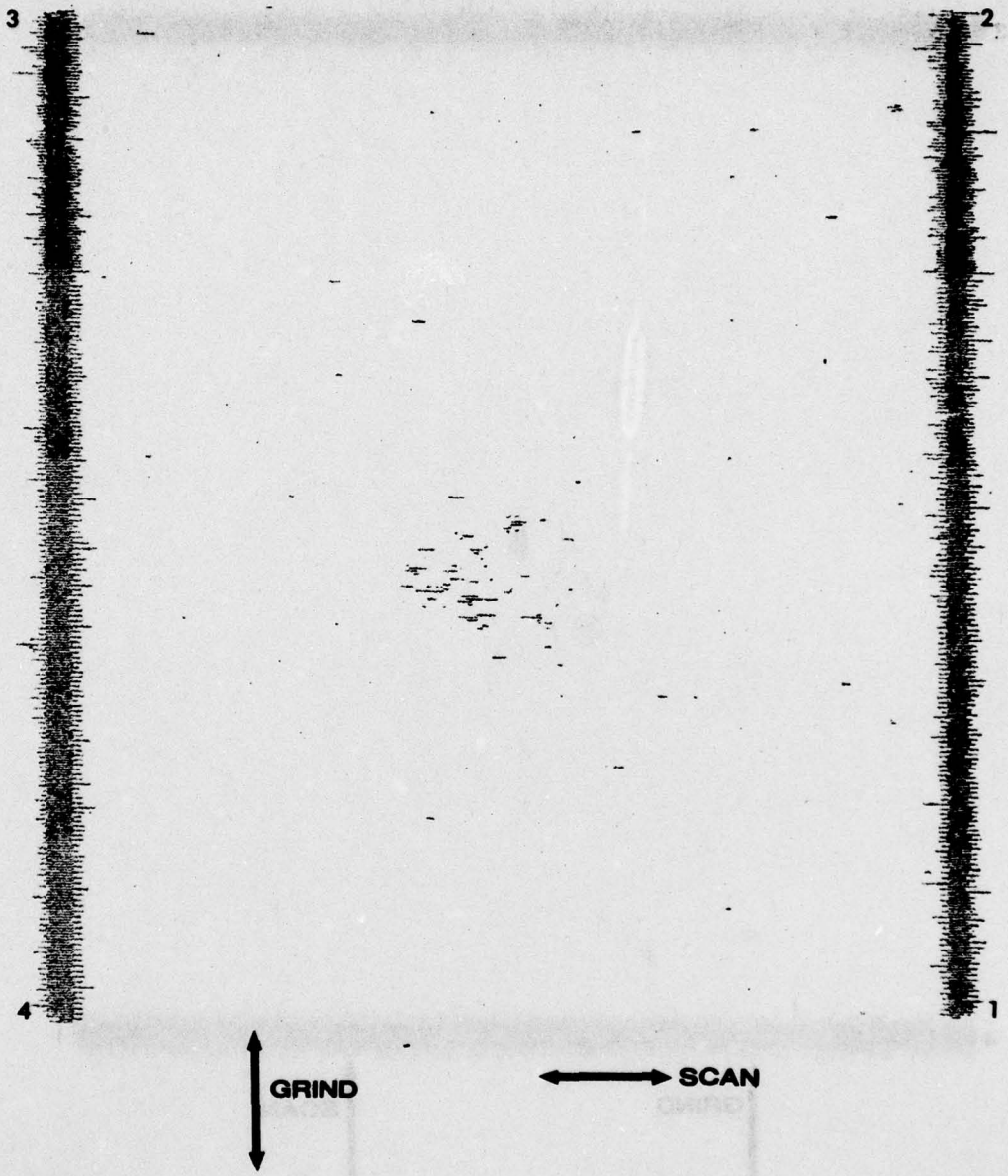

Figure 56. C-scan Recording of 45 MHz, 18° Surface Wave Inspection of Bottom Surface of Billet of NC-203A HPSiC (Scan Perpendicular to Grinding Direction).

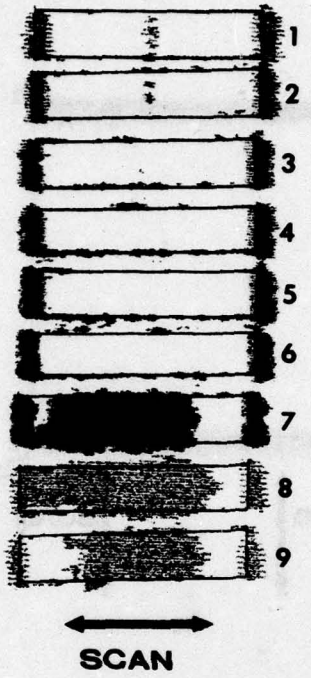

Figure 57. C-scan Recording of 45 MHz, 18° Surface Wave Inspection of Tensile Surfaces of NC-203A HPSiC Four-Point-Bend Specimens.

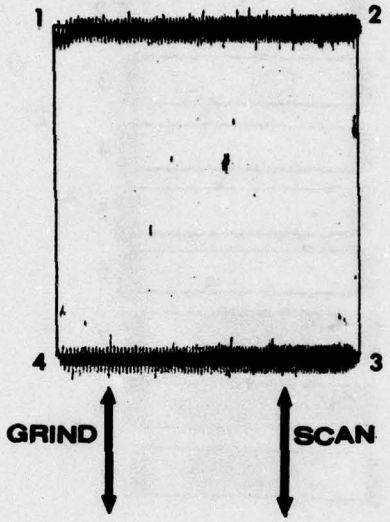

Figure 58. C-scan Recording of 45 MHz, 18° Surface Wave Inspection of Top Surface of Billet of Boron Doped SSiC (Scan Parallel to Grinding Direction).

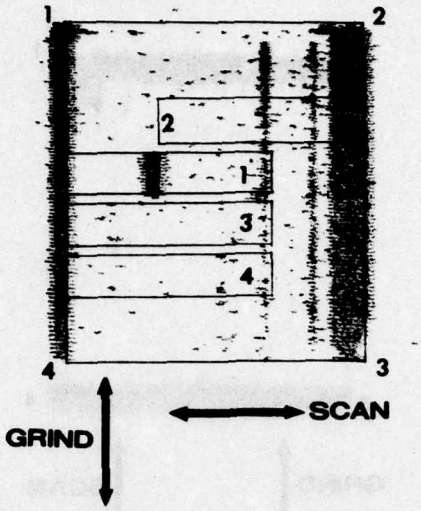

Figure 59. C-scan Recording of 45 MHz, 18° Surface Wave Inspection of Top Surface of Billet of Boron Doped SSiC (Scan Perpendicular to Grinding Direction).

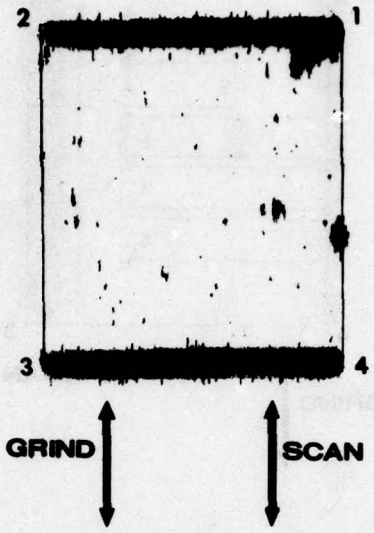

Figure 60. C-scan Recording of 45 MHz, 18° Surface Wave Inspection of Bottom Surface of Billet of Boron Doped SSiC (Scan Parallel to Grinding Direction).

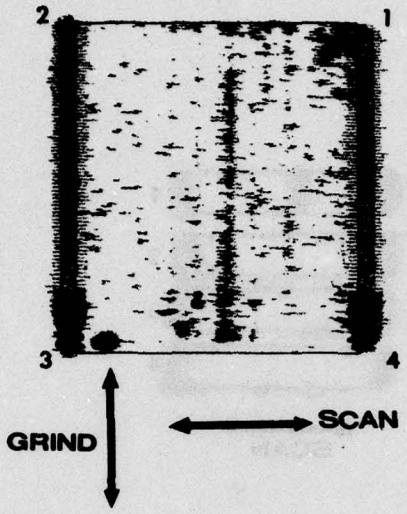

Figure 61. C-scan Recording of 45 MHz, 18° Surface Wave Inspection of Bottom Surface of Billet of Boron Doped SSiC (Scan Perpendicular to Grinding Direction).

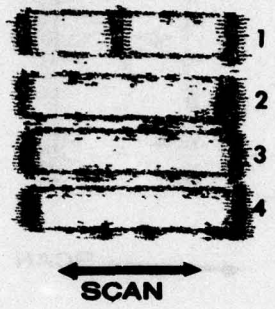

Figure 62. C-scan Recording of 45 MHz, 18° Surface Wave Inspection of Tensile Surfaces of Boron Doped SSiC Four-Point-Bend Specimens.

(0.0028 inch) deep semi-circular crack. Such a crack would only have a two-to-one signal-to-noise ratio with respect to the background signal from the surface texture. To have a three-to-one signal-to-noise ratio, which is believed the minimum required from reliable detection, requires a 100 μm (0.0040 inch) deep semicircular crack. Since detection of the surface texture is highly sensitive to orientation, this limitation is only applicable when scanning perpendicular to the grinding or cutting direction. It has been shown (See Figures 42 and 44) that rotation of the scan direction by as little as 20° significantly reduces the background signal from such surface texture. The other solution to this problem, of course, would be a reduced ultrasonic beam diameter. A beam diameter of 125 μm (0.005 inch) would allow 50 μm (0.0020 inch) deep semicircular cracks to be detected.

In directions not affected by the texture, the smallest defect that can be detected is limited by the sensitivity of the ultrasonic system. While determination of the minimum detectable defect requires an effort that is far beyond the scope of the program, one of the purposes of the four-point-bend testing described in the next section was to provide some data on the size defects that could be detected. The other purpose, of course, was to determine the effect of these defects on material strength.

6.0 METALLURGICAL EVALUATIONS

The metallurgical evaluations were made by performing flexural strength tests on selected specimens from each billet and examining the fracture origins using a scanning electron microscope (SEM). Measurements were made of the fracture origin locations with respect to both the length and width of the specimens, in order to determine whether or not the specimens had failed through ultrasonically detected defects. The purpose of these tests was both to expose defects detected by the surface wave inspection technique for SEM fractography in order to determine their nature and size, and to determine what correlation exists between defect indications and flexural strength. Standard four-point-bend testing was used with specimens machined to locate defects near the center of the tensile surfaces. Selected specimens containing only grinding line indications were given 1 kg or 50 kg Vicker's indentations in order to determine the size and effect on flexural strength of Vicker's indentations.

6.1 Test Procedures

Standard bend tests were performed at room temperature using a tensile loading bend test jig with universal-joint coupling to ensure load alignment. Specimens with a two-to-one width-to-thickness ratio were tested at a constant crosshead speed of 0.51 mm/min (0.02 inches/min) with load pins having an inner span of 6.4 mm (1/4 inch) and an outer span of 19.1 mm (3/4 inch) to provide a "third point" load span. Moment and stress distributions during testing are shown schematically in Figures 63 and 64 with relevant dimensions and formulae. In Figure 64, the simple tensile stress, at some location above the neutral axis and between the inner loading pins, is indicated. If Y represents the location of a particular defect, and if a suitable stress concentration factor can be assigned to this defect, then a simple calculation would provide an estimate of the effective stress at this point from which it should be possible to predict the fracture strength of the specimen. Conversely, knowing the location of the defect and the fracture stress, a value for the stress intensity factor can be calculated.

All of the specimens tested were 6.4 x 3.2 x 32 mm (1/4 x 1/8 x 1-1/4 inches) with the tensile surface during testing being a 0.4 x 32 mm (1/4 x 1-1/4 inch) area of the inspected surfaces. Since the defects of interest were on the tensile surface, this surface was not machined. The sides and the compression surface were finish machined parallel to the major axis with a 320 grit diamond wheel and the edges were chamfered 125 μm (0.005 inches) at 45°.

6.2 Flexural Strength

6.2.1 HPSN

The results of the four-point-bend tests on HPSN are listed in Table I. The table lists the strength, the failure location along the length as an offset from the center, the fracture origin across the width as an offset from the center, the condition of the tensile surface as determined ultrasonically, and the fracture origin as determined from SEM fractography. Specimens 1 through 5 of Ceralloy 147A contained defects which were verified by the inspection results on the specimens (see Figure 25). Specimens 1 and 5 did not fail through recognizable defects, nor do the locations of the fracture origins correlate with the ultrasonic results. Specimens 2, 3 and 4, however, show well defined defects at fracture origins whose positions correlate very well with the ultrasonic results in Figure 25.

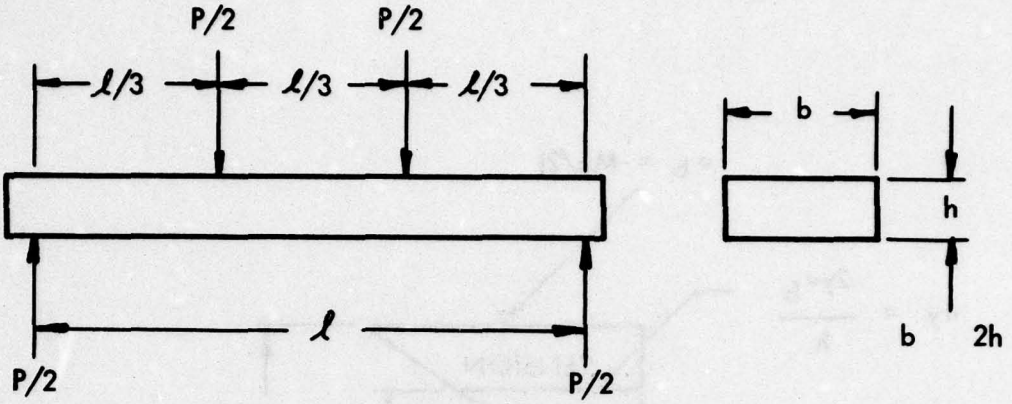

THIRD-POINT LOADING BEND TEST

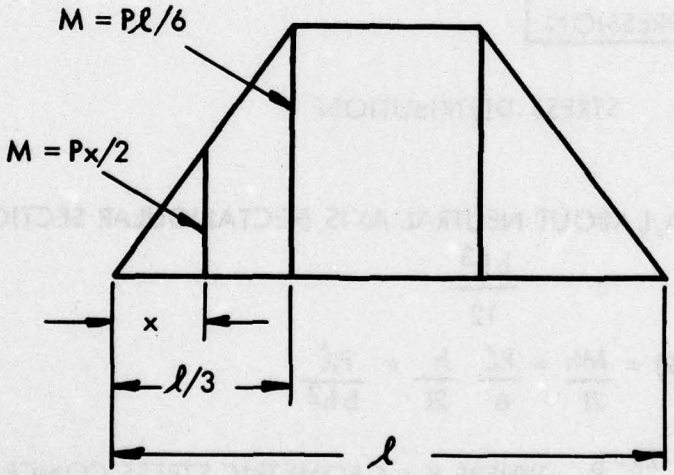

MOMENT DISTRIBUTION

Figure 63. Test Conditions for Flexural Strength Determinations.

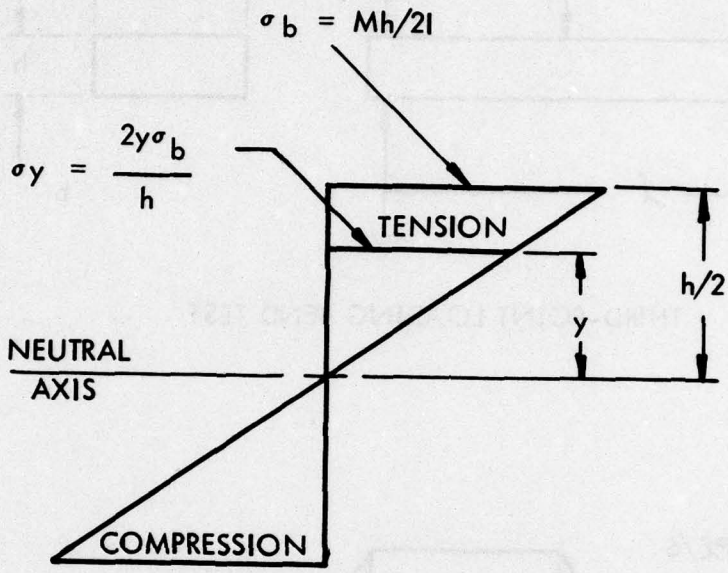

STRESS DISTRIBUTION

MOMENT OF INERTIA, I, ABOUT NEUTRAL AXIS (RECTANGULAR SECTION) = $\frac{bh^3}{12}$

σ_b (OUTER FIBER) = $\frac{Mh}{2I} = \frac{P\ell}{6}\frac{h}{2I} = \frac{P\ell}{bh^2}$

σ_y (FLAW) = K $\frac{2y\sigma_b}{h}$, WHERE K = GEOMETRIC STRESS CONCENTRATION FACTOR

Figure 64. Stress Distribution and Equations for Rectangular Bar Specimens.

TABLE I

Flexural Strength of HPSN

1. Ceralloy 147A

Specimen No.	Flexural Strength MN/m^2	ksi	Fracture Location mm from Center Length	Width	Condition	Fracture Origin
1	522	75.8	2.25	0.55	surf. def.	See Note 1
2	447	64.8	0.25	0.70	surf. def.	180 x 75 μm deep pit
3	341	49.4	0.75	0.75	def. E	500 x 300 μm area of large grains
4	329	47.7	0.25	1.00	def. A	400 x 50 μm flaw; 100 μm deep
5	492	71.4	0.75	1.40	def. G	See Note 1
6	487	70.6	0.75	0.10	1 kg Vicker's	60 μm deep crack
7	577	83.7	3.50	0.75	with grinding	See Note 1
8	621	90.1	3.25	1.05	" "	10 μm crystal; 35 μm deep
9	109	15.8	0.25	0.15	50 kg Vicker's	160 μm x 60 μm indent; 520 μm deep crack
10	477	69.2	1.50	1.10	against grinding	See Note 1
11	471	68.3	2.25	0.75	" "	See Note 1

2. NC-132

1	617	89.5	1.50	0.15	surf. def.	16 x 20 μm area of large grains at surface
2	580	84.1	3.50	0.70	surf. def.	cluster of 10 to 20 μm grains at surface
3	748	108.5	0.50	0.25	2 surf. def. near edges	See Note 1
4	813	117.9	2.50	1.20	with grinding	See Note 1
5	-	-	damaged during finish machining - not tested			
6	-	-	-	"	" " "	"
7	118	17.1	1.00	0.15	50 kg Vicker's	200 x 70 μm indent; 600 μm deep crack
8	579	84.0	3.50	1.10	against grinding	See Note 1
9	558	80.9	1.00	1.30	" "	See Note 1

Notes:

1. Surface fracture origin; flaw undefined

The fracture origin in specimen No. 2 can be seen in Figure 65 to be a surface pit, 180 μm (0.007 inches) wide by 75 μm (0.003 inches) deep. The fracture origin in specimen No. 3 can be seen in Figure 66 to be an area of large crystals extending down from the surface. It is about 500 μm (0.020 inches) across and 350 μm (0.014 inches) deep. This is defect E in Figures 23 and 24. The fracture origin in specimen No. 4 can be seen in Figure 67 to be a flake-like inclusion oriented parallel to the specimen surface. It is about 400 μm (0.016 inches) long, 50 μm (0.002 inches) wide and located about 100 μm (0.004 inches) below the surface. This is defect A in Figures 21 and 22. In comparing the defects that have been examined in specimen Nos. 2, 3 and 4 with the other indications in Figures 21 through 24, it can be seen that these are among the largest defects that were detected.

Ceralloy 147A specimen Nos. 6 through 8 were machined parallel to the grinding marks and specimen Nos. 9 through 11 were machined perpendicular to the grinding marks, in order to determine if there is a strength difference corresponding to the difference in inspection results evident in Figure 25. A Vicker's indentation of 1 kg was placed in specimen No. 6 and a Vicker's indentation of 50 kg was placed in specimen No. 9 in order to obtain an estimate of the size defects created by the Vicker's indentations. This leaves two specimens in each direction to compare. The average strength for specimens No. 7 and 8 is 599 ± 22 MN/m^2 (86.9 ± 3.2 ksi) compared to 474 ± 3 MN/m^2 (68.8 ± 0.5 ksi) for specimens No. 10 and 11. This difference of 125 MN/m^2 (18.1 ksi) is significant at the 90% confidence level.

Figure 68 shows the fracture surfaces of specimen No. 6. The Vicker's indentation cannot be identified by a pit on the surface, although it is possible that it was lost due to shattering of the specimen. The fracture origin is a crack about 60 μm (0.0024 inches) deep which is assumed to be the result of the indentation. Figure 69 shows the fracture surface of specimen No. 9. The indentation consists of a 140 μm (0.0056 inch) wide x 40 μm (0.0016 inch) deep pit with a crack extending about 530 μm (0.0212 inches) deep. This specimen was the weakest of the group with a strength of only 109 MN/m^2 (15.8 ksi). Even specimen No. 3, which had an inclusion almost as large, had a strength of 341 MN/m^2 (49.4 ksi). Specimen No. 6, on the other hand, had a strength of 486 MN/m^2 (70.6 ksi) which is slightly higher than the strength of specimens No. 10 and 11, which were machined perpendicular to the grinding marks. This indicates that a 1 kg Vicker's indentation probably would not have been a fracture origin, i.e., a strength limiting defect, in a specimen machined perpendicular to the grinding direction.

The specimens of NC-132 HPSN were divided into the same three categories as those of Ceralloy 147A. Specimens Nos. 1, 2 and 3 contained very tiny defects (see Figure 29). Specimens 4, 5, and 6 were machined parallel to the grinding damage, while specimens 7, 8, and 9 were machined perpendicular to the grinding damage (see Figure 30). However, based on the ultrasonic inspection results after machining (Figure 31), only specimen No. 2 from among the defective ones looks significantly worse than the nondefective ones (specimens No. 4, 5 and 6). Specimens 5 and 6 were damaged during finish machining and could not be tested. Therefore, no specimens were tested containing a 1 kg Vicker's indentation. Specimen No. 7 was given a 50 kg Vicker's indentation.

AD-A076 023 TRW INC CLEVELAND OHIO F/G 11/2
ULTRASONIC DETECTION OF SURFACE FLAWS IN GAS TURBINE CERAMICS.(U)
AUG 79 T DERKACS , I M MATAY N62269-77-C-0136
UNCLASSIFIED TRW-ER-7980-F NADC-76369-30 NL

2 OF 2
AD
A076023

END
DATE
FILMED
11 -79
DDC

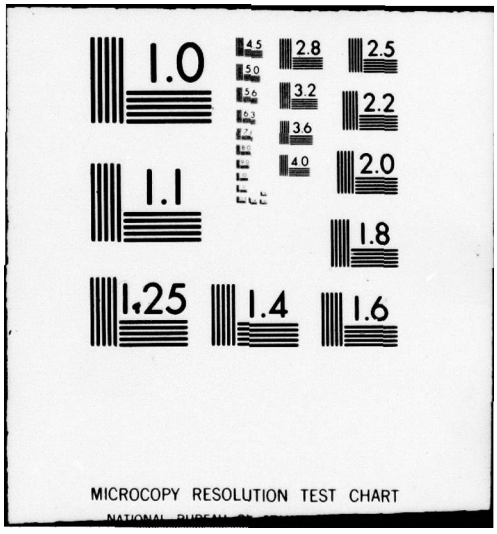
1.0
1.1
1.25
1.4
1.6
1.8
2.0
2.2
2.5
2.8
3.2
3.6
4.0
4.5
5.0
5.6
6.3
7.1
8.0
9.0
MICROCOPY RESOLUTION TEST CHART

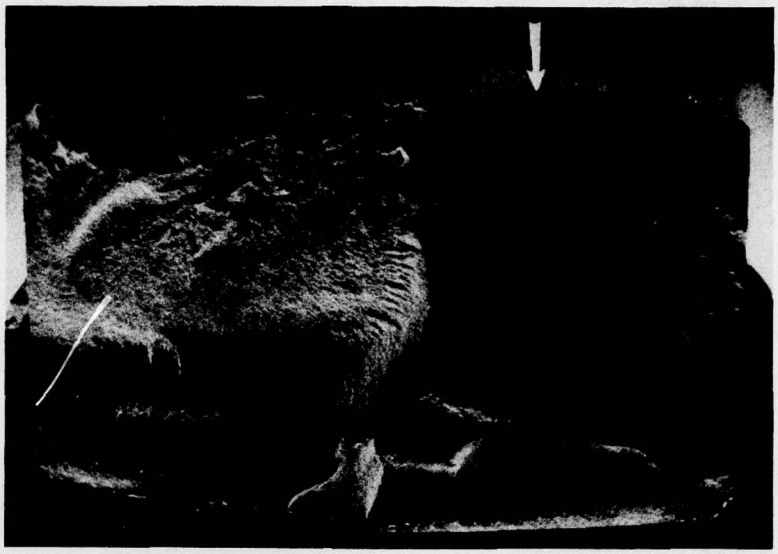

16X

100X

Figure 65. Fracture Surface of Ceralloy 147A HPSN Specimen No. 2 Showing Ultrasonically Detected Defect at Fracture Origin.

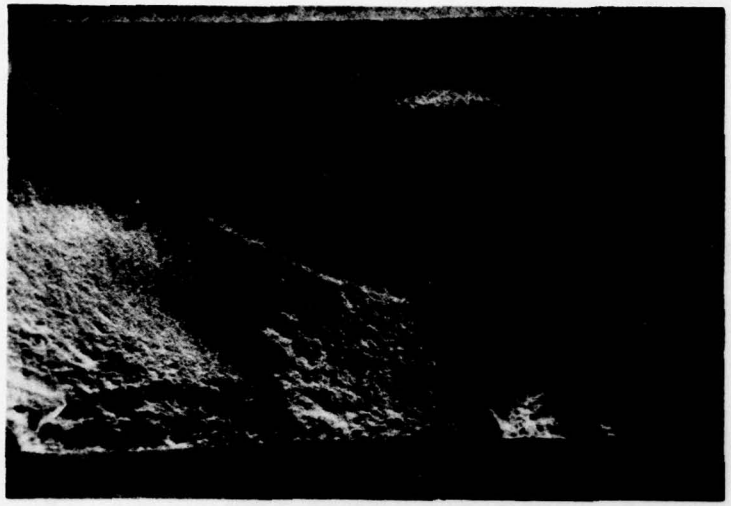

16X

1000X

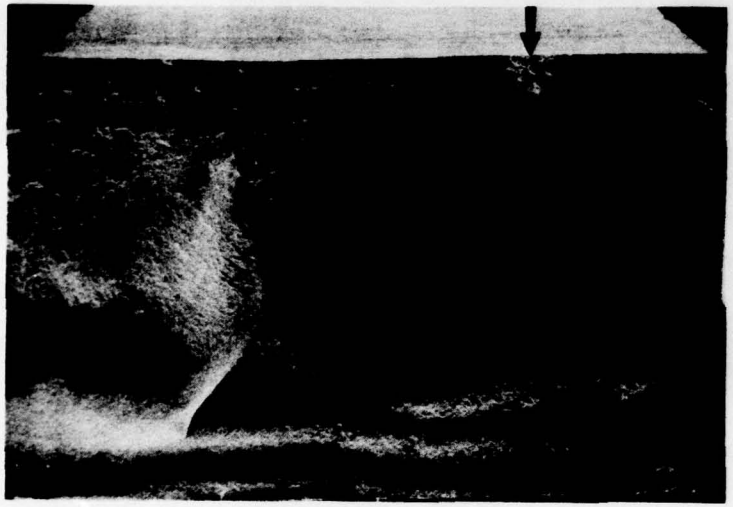

16X

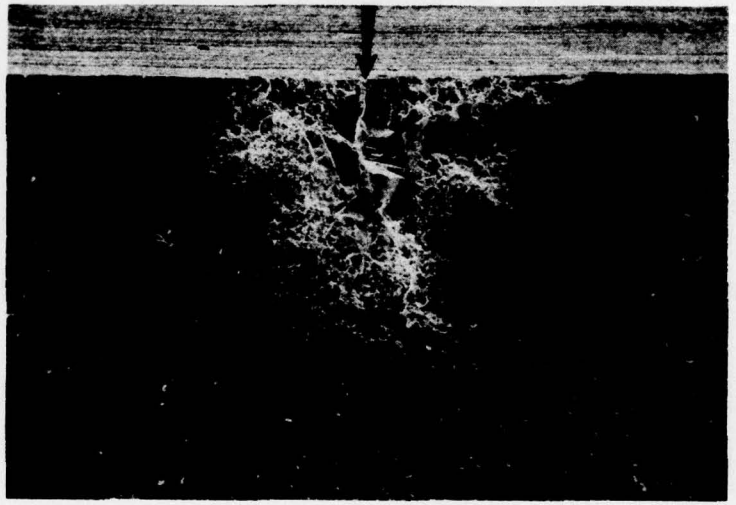

100X

Figure 66. Fracture Surfaces of Ceralloy 147A HPSN Specimen No. 3, Showing Ultrasonically Detected Defect at Fracture Origin.

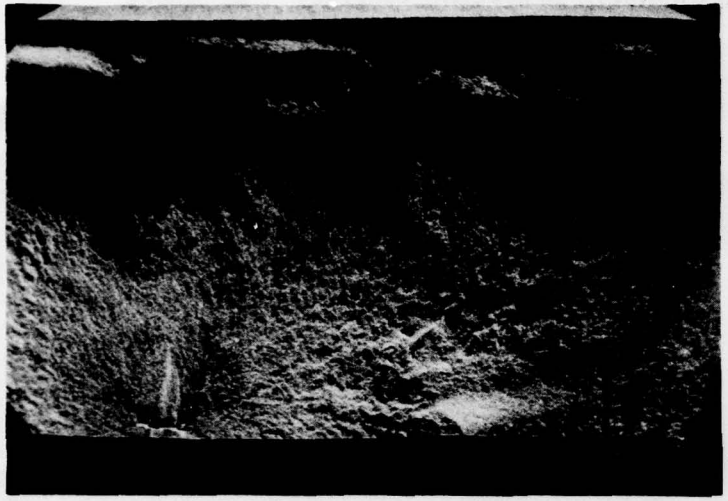

16X

500X

16X

100X

Figure 67. Fracture Surfaces of Ceralloy 147A HPSN Specimen No. 4, Showing Ultrasonically Detected Defect at Fracture Origin.

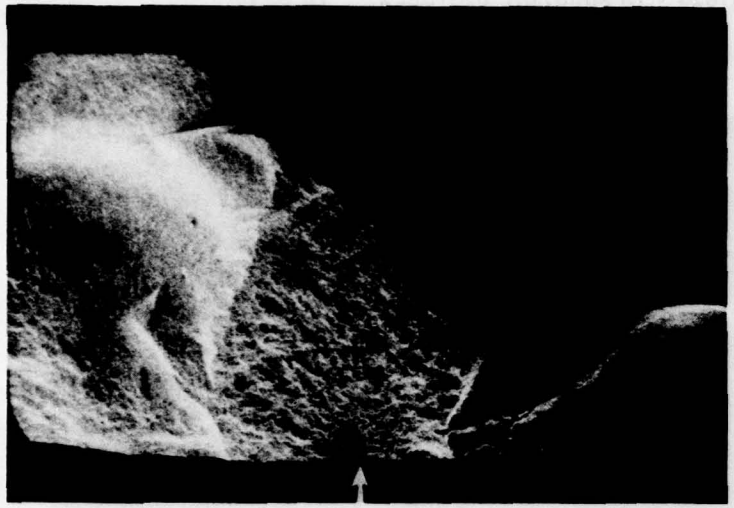

16X

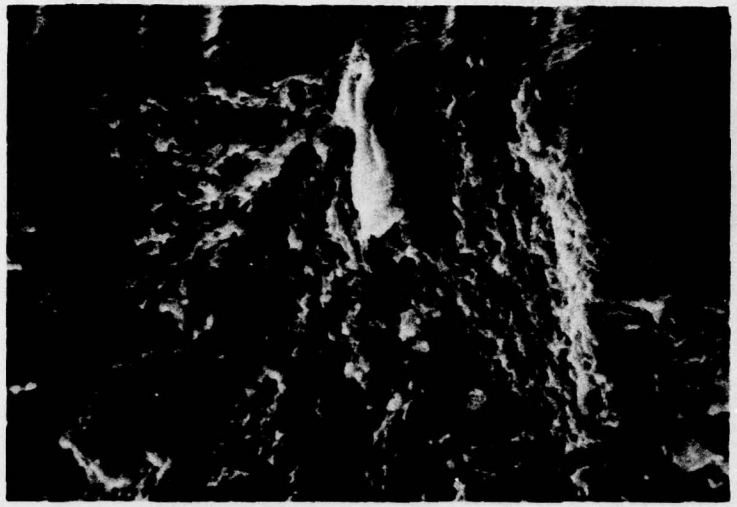

1000X

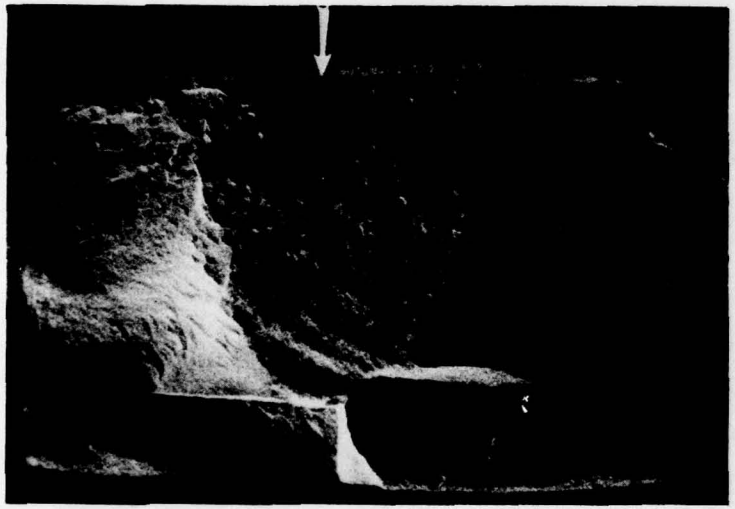

16X

100X

Figure 68. Fracture Surfaces of Ceralloy 147A HPSN Specimen No. 6, Showing 1kg Vicker's Indentation at Fracture Origin.

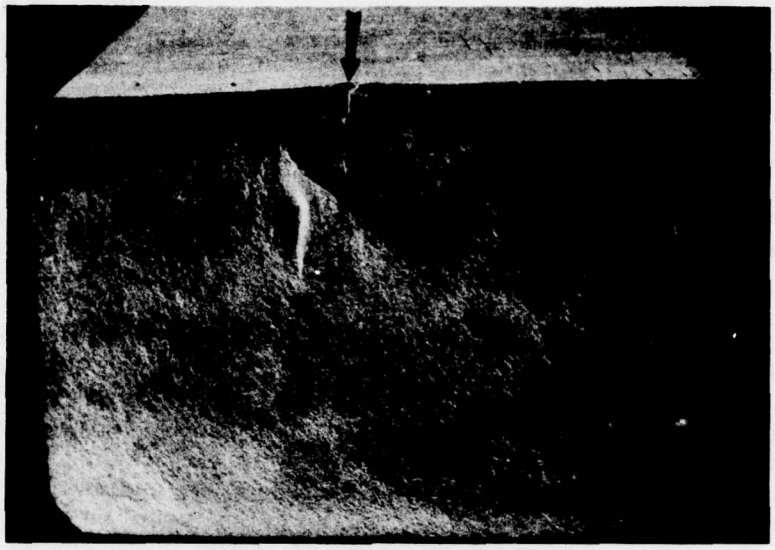

16X

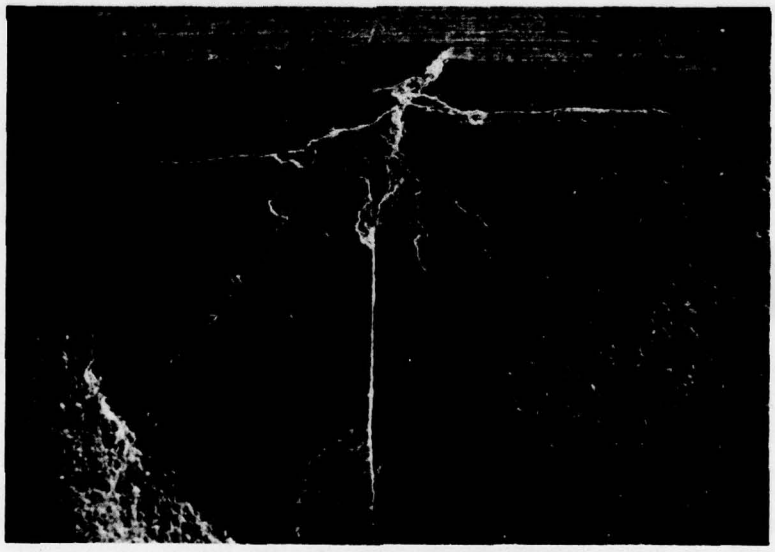

100X

Figure 69. Fracture Surface of Ceralloy 147A HPSN Specimen No. 9, Showing 50 kg Vicker's Indentation at Fracture Origin.

Figure 70 shows the fracture surfaces of specimen No. 1 of NC-132 HPSN. The fracture origin is seen to be an area of large grains 16 μm (0.0006 inches) wide by 20 μm (0.0008 inches) deep. The location of the defect as well as its size correlate well with the indication in Figure 29. The fact that the same indication was not seen in Figure 31 cast some doubt on the correlation. However, with such a small defect, this may simply be normal statistical variation in sensitivity. Specimens No. 2 and No. 3 do not appear to have fractured through the ultrasonically detected defects. Specimen No. 2 broke from a fracture origin at the surface (see Figure 71) associated with several 10 to 20 μm (0.0004 to 0.0008 inch) grains. Specimen No. 3 broke through a fracture origin at the surface in which no defect could be identified.

The loss of specimens No. 5 and No. 6 makes it impossible to make a statistically valid conclusion about the difference in the two directions with respect to grinding. The large difference in the strengths however (813 MN/m^2 (117.9 ksi) for specimen No. 4 compared to an average 569 MN/m^2 (82.5 ksi) for specimens 9 and 10) tends to indicate that grinding damage perpendicular to the grinding direction was the strength limiting defect. All three of these specimens are similar to No. 3 in that a definite fracture origin could be identified, but no defect could be seen at the origin. Another useful comparison is between specimen No. 1 and specimens No. 8 and No. 9. The strength of specimen No. 1, which was machined parallel to the grinding marks and which contains a small, but detectable defect, was greater (617 MN/m^2 (89.5 ksi), than that of either No. 8 or No. 9, which were machined perpendicular to the grinding marks. Figure 72 shows the fracture surfaces of specimen No. 7, which contained the 50 kg Vicker's indentation. It can be seen that the damage is a pit 200 μm (0.008 inches) wide by 70 μm (0.024 inches) deep and a crack extending about 600 μm (0.024 inches) deep.

6.2.2 RBSN

The results of the four-point-bend tests on RBSN are listed in Table II. Specimens No. 1, 2, 3, 6, 7, 8 and 9 contained portions of the cracklike defects detected in numerous locations in this billet. Only one of these, No. 3, broke in the area of ultrasonic indication, and the fracture origin was a large grain, 25 x 15 μm (0.001 x 0.0006 inches) with an associated 60 μm deep crack. The cracklike indications are apparently not strength limiting defects. The average strength of these specimens, 219.1 $\pm$ 35.8 MN/m^2 (31.8 $\pm$ 5.2 ksi) is not significantly different from that of the other specimens, 224.5 $\pm$ 45.3 MN/m^2 (32.6 $\pm$ 6.6 ksi), excluding the one containing the Vicker's indentation. Most of the specimens failed either from the corner or from 10 to 20 μm (0.0004 to 0.0008 inch) grains at the surface. A comparison of these two modes of failure shows that the strength associated with large grain failures, 224.2 $\pm$ 27.3 MN/m^2 (32.5 $\pm$ 4.0 ksi), is not significantly different from that for corner failures, 217.8 $\pm$ 46.6 MN/m^2 (31.6 $\pm$ 6.8 ksi). For a comparison of the effect of the cutting lines in the surface specimens No. 10 and 11 were machined perpendicular to the lines and specimens 13 and 14 were machined parallel to the lines. Since the other effects studied were not found to be significant, the other specimens were included in this comparison. Specimens 1 through 5 were combined with 10 and 11 and specimens 6 through 9 were combined with 13 and 14.

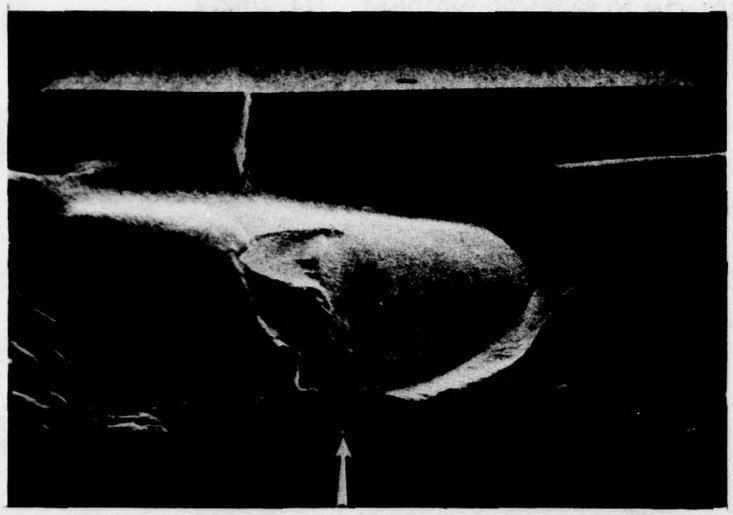

16X

1000X

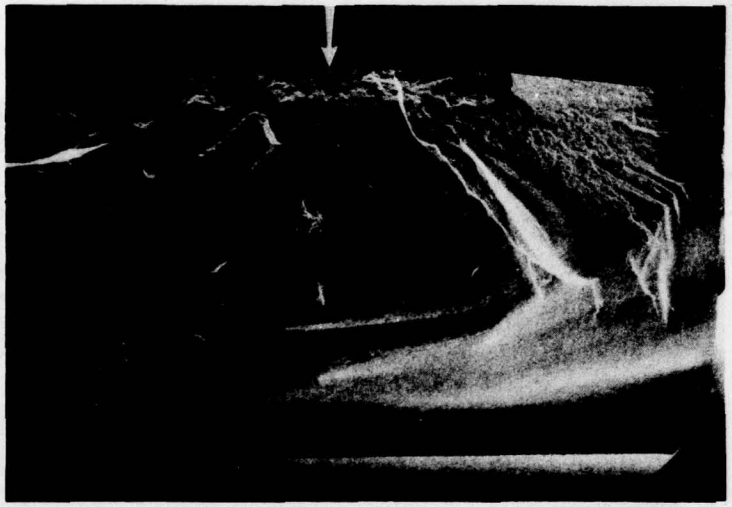

16X

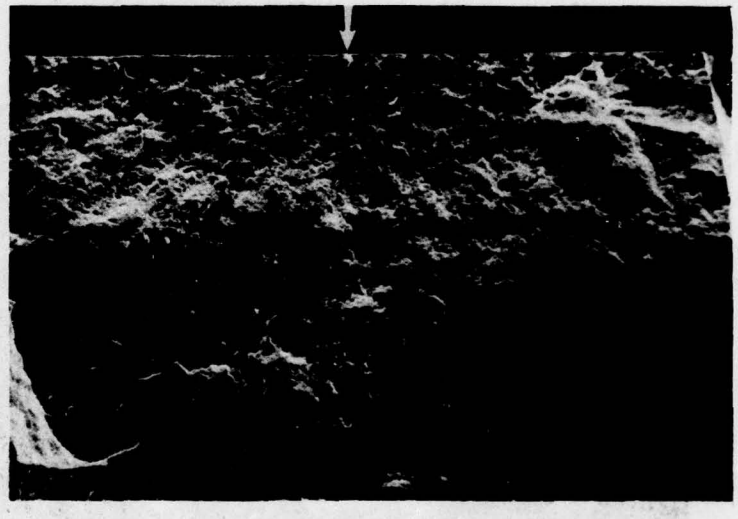

100X

Figure 70. Fracture Surfaces of NC-132 HPSN Specimen No. 1, Showing Ultrasonically Detected Defect at Fracture Origin.

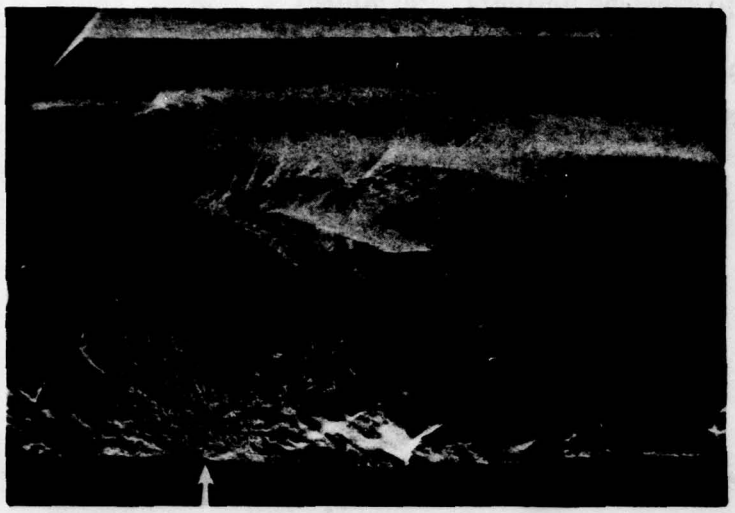

16X

1000X

16X

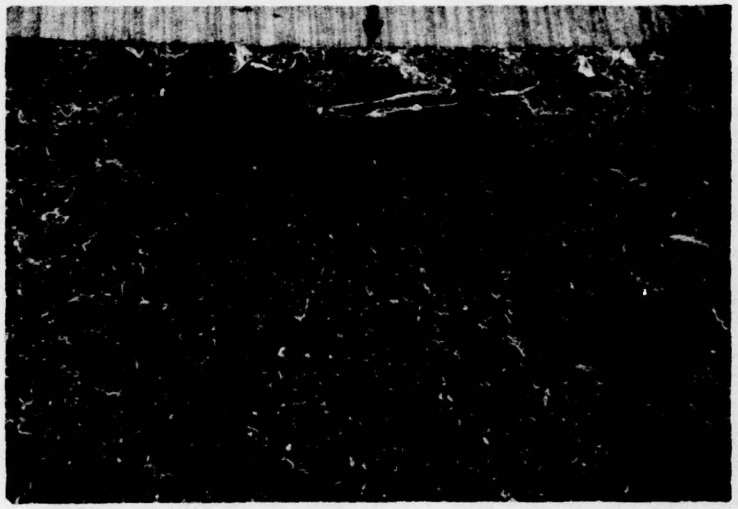

100X

Figure 71. Fracture Surfaces of NC-132 HPSN Specimen No. 2, Showing Fracture Origin.

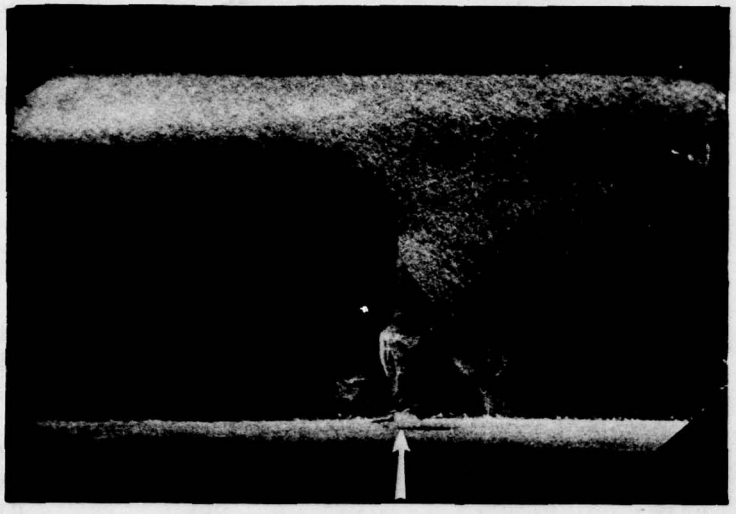

16X

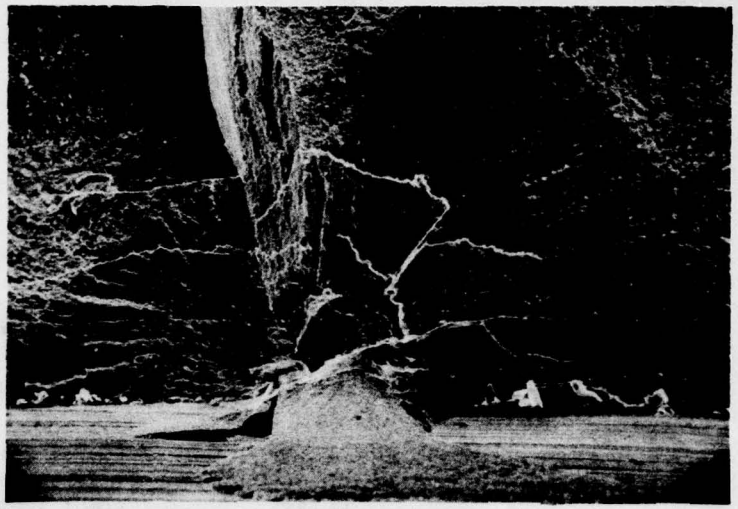

100X

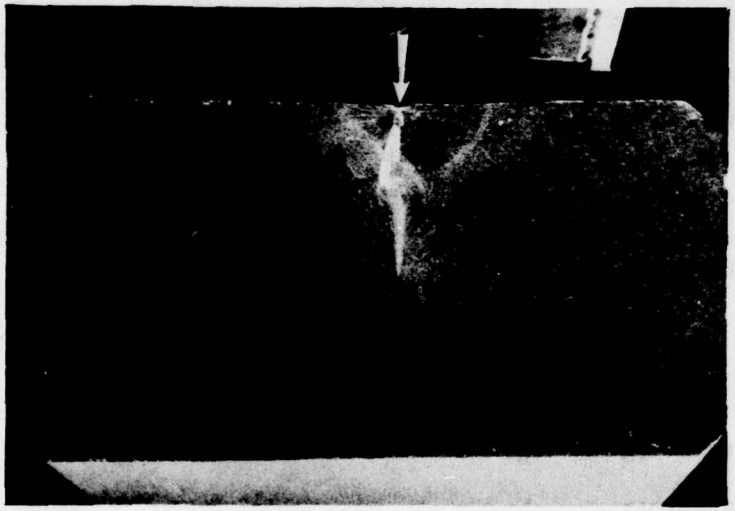

16X

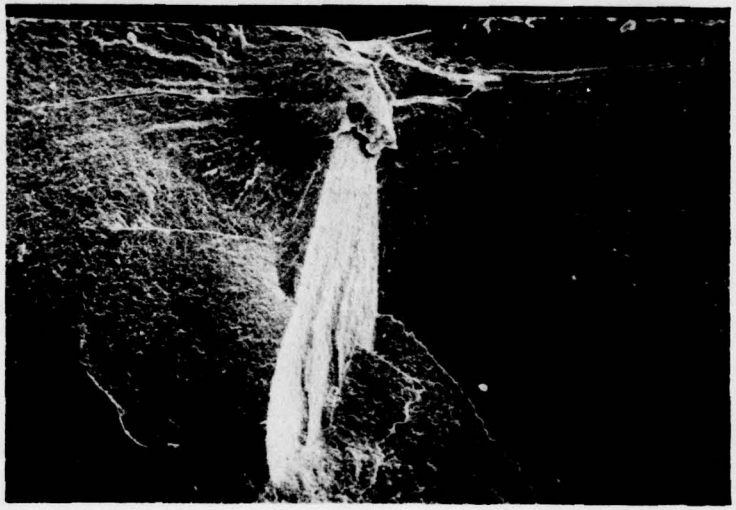

100X

Figure 72. Fracture Surfaces of NC-132 HPSN Specimen No. 7, Showing 50 kg Vicker's Indentation at Fracture Origin.

TABLE II

Flexural Strength of RBSN

NC-350

Specimen No.	Flexural Strength MN/m^2	ksi	Fracture Location mm from Center Length	Width	Condition	Fracture Origin
1	227	32.9	2.50	1.60	crack-like indic.	20 μm grain at surface
2	276	40.0	2.50	-	" " "	multiple origins
3	179	25.9	0.25	0.96	" " "	25 x 15 μm grain
4	239	34.6	2.75	3.20	" " "	corner
5	247	35.8	2.75	3.20	small surf. defect	corner
6	232	33.6	1.00	-	crack-like ind.	corner
7	213	30.9	2.50	1.30	" " "	20 μm grain
8	171	24.8	4.50	0.00	" " "	surface
9	236	34.3	2.50	3.20	" " "	corner
10	135	19.6	0.75	3.20	against lines	corner
11	234	34.0	1.00	0.90	" "	20 μm grain
12	-	-	-	-	50 kg Vicker's	600 x 200 μm pit; 3150 μm deep crack
13	262	38.0	0.25	0.00	with lines	10 μm grain
14	230	33.4	3.00	0.00	" "	20 x 15 μm grains
15	121	17.6	3.50	0.60	1 kg Vicker's	70 μm deep crack

The average flexural strength perpendicular to the lines, 219.6 ± 47.2 MN/m^2 (31.9 ± 6.8 ksi), was not significantly different from that parallel to the lines, 224.0 ± 30.4 MN/m^2 (32.5 ± 4.4 ksi). In summary, the various conditions that were delineated by the ultrasonic surface wave technique did not have a significant effect on material strength.

Specimen No. 12, which contained a 50 kg Vicker's indentation, broke in two along a diagonal when the indentation was made. Figure 73 shows one side of the fracture surface. The pit is about 600 μm (0.026 inches) across and 200 μm (0.0079 inches) deep and the crack extends all the way through the 3150 μm (0.124 inch) thickness of the specimen. Specimen 15, which contained a 1 kg Vicker's indentation, broke at a low strength and shattered so that it was not possible to determine if it fractured from the indentation or not.

6.2.3 HPSiC

The results of the four-point-bend tests on HPSiC are listed in Table III. Specimens 1 and 4 of Ceralloy 146 contained the 50 kg and 1 kg Vicker's, respectively. The fracture surfaces of these specimens are shown in Figures 74 and 75. In Figure 74 it can be seen that the 50 kg Vicker's indentation consisted of a pit 200 μm (0.008 inches) wide by 160 μm (0.0064 inches) deep with a crack extending 605 μm (0.0242 inches) deep. The 1 kg Vicker's indentation shown in Figure 75 consists of a pit 20 μm (0.0008 inches) wide by 2 μm (0.00008 inches) deep with a crack extending about 25 μm (0.0010 inches) deep. Specimens 2 and 3 of Ceralloy 146, which were machined perpendicular to the grinding damage, had an average strength of 429 ± 16 MN/m^2 (62.3 ± 2.3 ksi) compared to 509 ± 61 MN/m^2 (73.8 ± 8.8 ksi) for specimens 5 and 6 which were machined parallel to the grinding direction. While this difference is large, there is too much scatter in the data and too few specimens to conclude that it is significant with a high degree of confidence. The specimen containing the 1 kg Vicker's was significantly weaker, 299 MN/m^2 (43.3 ksi) than those machined perpendicular to the grinding damage. Specimens 2, 3, 5 and 6 all failed through identifiable fracture origins in which no specific defect could be identified.

Specimens 1 and 4 of NC-230 also contain 50 kg and 1 kg Vicker's indentations, respectively. The fracture surfaces of these specimens are shown in Figures 76 and 77, respectively. In Figure 76 it can be seen that the 50 kg Vicker's indentation consists of a 200 μm (0.0008 inch) wide by 160 μm (0.0064 inch) deep pit with a 510 μm (0.0204 inch) deep crack. The 1 kg Vicker's indentation shown in Figure 77 consists of a 20 μm (0.0008 inch) wide by 5 μm (0.0002 inch) deep pit with a 35 μm (0.0014 inch) deep crack. Specimens 2 and 3 were machined in an area of heavier grinding damage while specimens 5 and 6 were machined in an area of lighter grinding damage, but all specimens were machined perpendicular to the damage. Specimen 2 was damaged during finish machining and was not tested. Specimen 3 had a strength of 412 MN/m^2 (59.8 ksi) compared to 504 ± 13 MN/m^2 (73.1 ± 1.9 ksi) for specimens 5 and 6. Here again there is a considerable difference in strengths which corresponds with the ultrasonic results, but the data is insufficient to draw a statistically valid conclusion. Specimens 7, 8 and 9 were from an area that showed extensive ultrasonic indications, not only by the surface wave technique, but also by shear and longitudinal wave techniques. The average strength of these specimens was 187 ± 21 MN/m^2 (27.2 ± 3.1 ksi). This is significantly lower than the average of specimens 3, 5 and 6, 473 ± 54

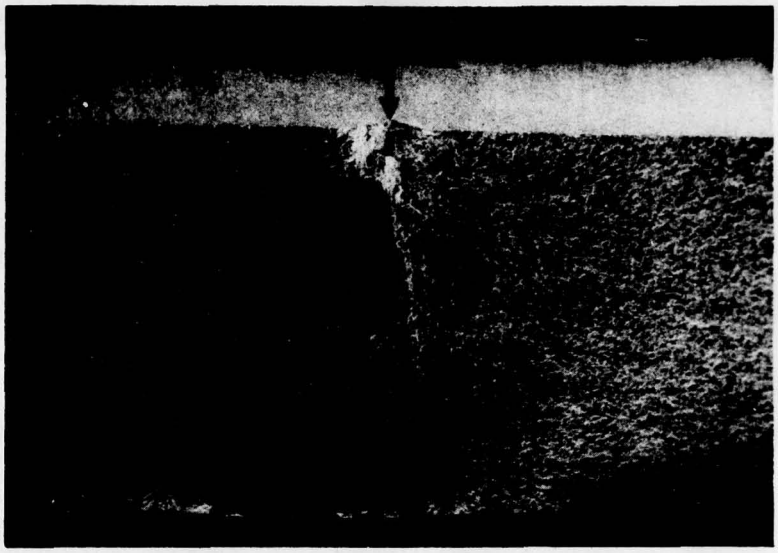

16X

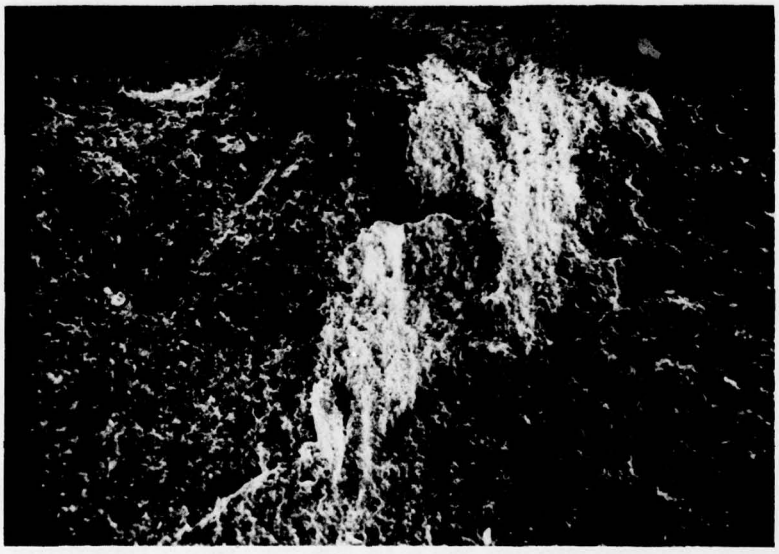

100X

Figure 73. Fracture Surfaces of NC-350 RBSN Specimen No. 12, Showing 50 kg Vicker's Indentation at Fracture Origin.

TABLE III

Flexural Strength of HPSiC

1. Ceralloy 146

Specimen No.	Flexural Strength MN/m^2	ksi	Fracture Location mm from Center Length	Width	Condition	Fracture Origin
1	119.9	17.4	0.00	0.32	50 kg Vicker's	200 x 160 μm pit; 605 μm crack
2	412.9	59.9	2.50	2.24	against grinding	See Note 1
3	445.3	64.6	0.25	0.00	" "	See Note 1
4	298.5	43.3	0.00	0.26	1 kg Vicker's	20 μm x 2 pit; 25 μm crack
5	465.3	67.5	2.25	0.51	with grinding	See Note 1
6	552.1	80.1	1.50	2.56	" "	See Note 1
2. NC-230						
1	122.0	17.7	0.00	0.51	50 kg Vicker's	200 x 140 μm pit; 510 μm crack
2	-	-	-	-	Heavy grind damage	Not tested
3	412.2	59.8	2.50	1.60	" " "	
4	379.8	55.1	0.25	0.06	1 kg Vicker's	20 x 5 μm pit; 35 μm crack
5	512.8	74.4	0.25	1.60	light grind damage	See Note 1
6	494.2	71.7	3.75	1.22	" " "	See Note 1
7	163.4	23.7	2.25	1.34	Defective area	See Note 1
8	195.5	28.5	1.75	3.20	" "	corner
9	202.7	29.4	4.25	1.92	" "	See Note 1

Notes:

1. Surface fracture origin; flaw undefined.

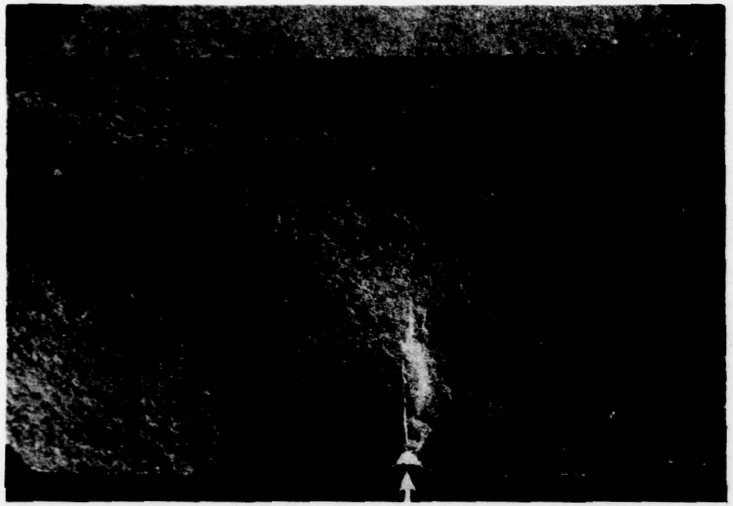

16X

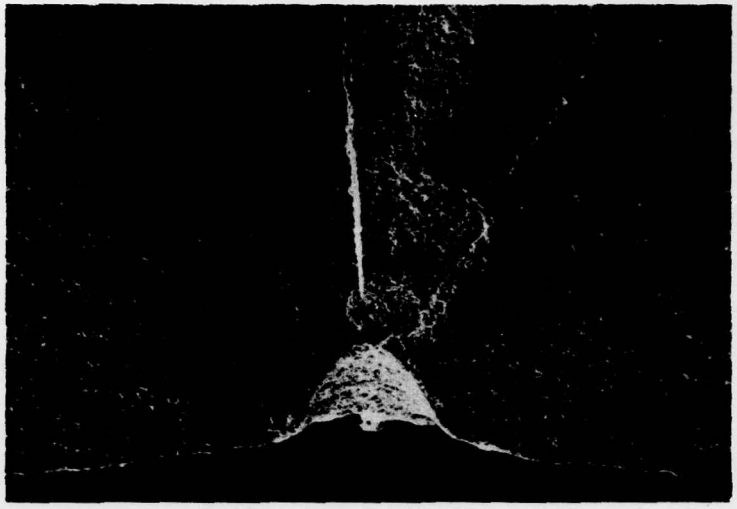

100X

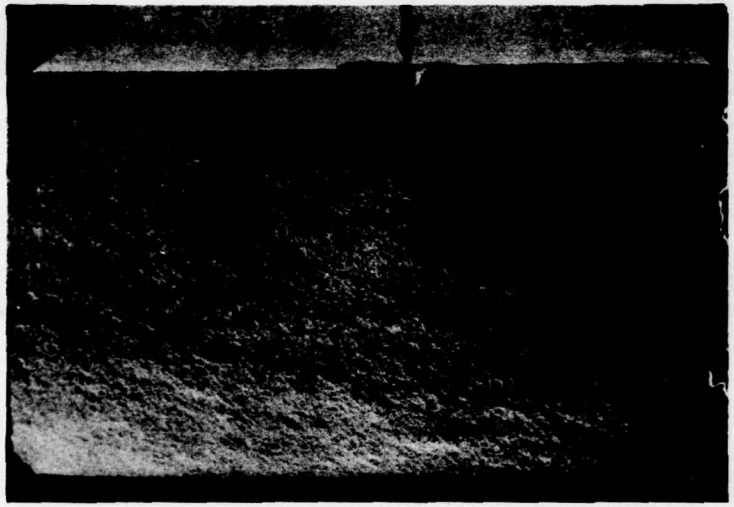

16X

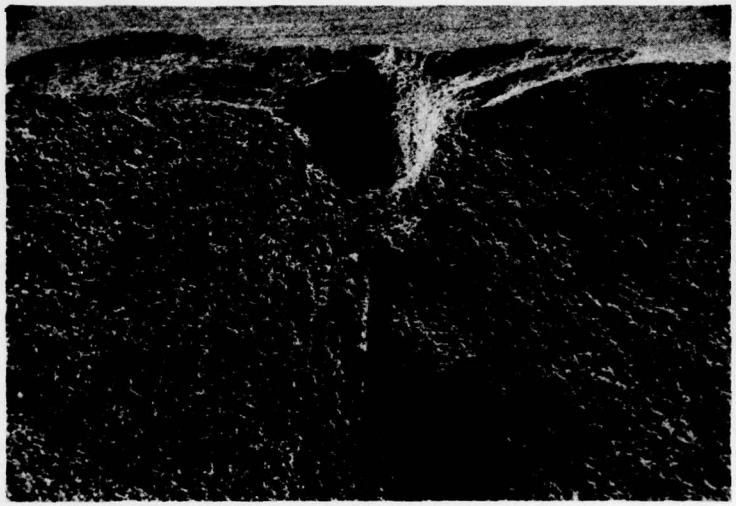

100X

Figure 74. Fracture Surfaces of Ceralloy 146A HPSiC Specimen No. 1, Showing 50 kg Vicker's Indentation at Fracture Origin.

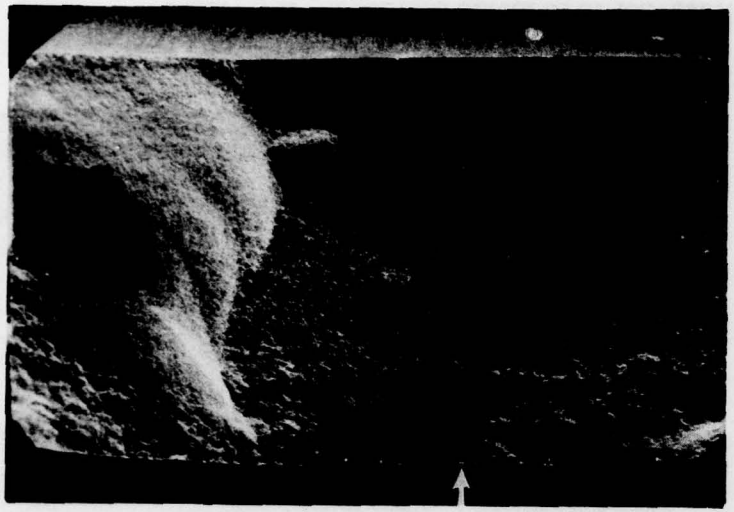

16X

1000X

16X

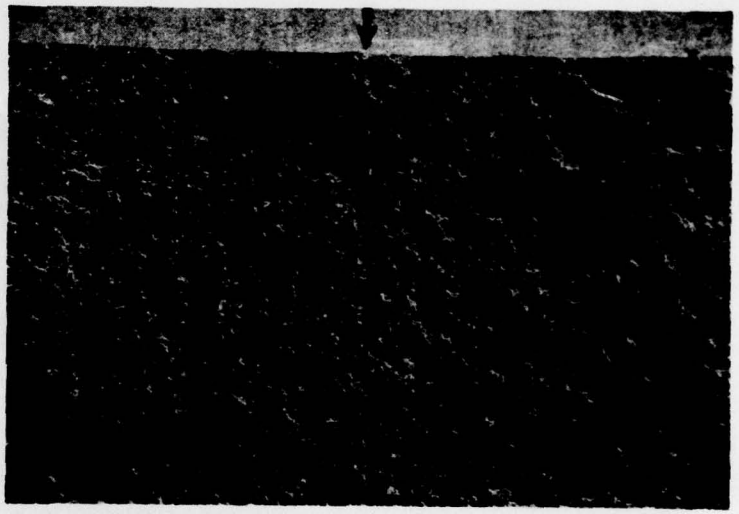

100X

Figure 75. Fracture Surfaces of Ceralloy 146A HPSiC Specimen No. 4, Showing 1 kg Vicker's Indentation at Fracture Origin.

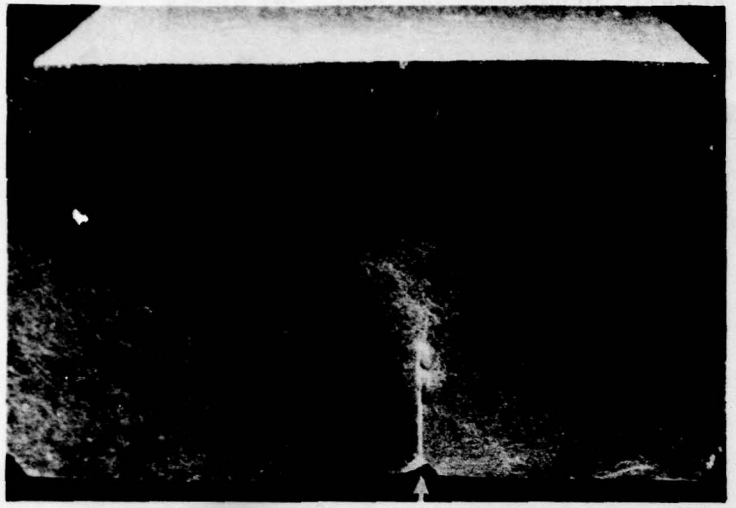

16X

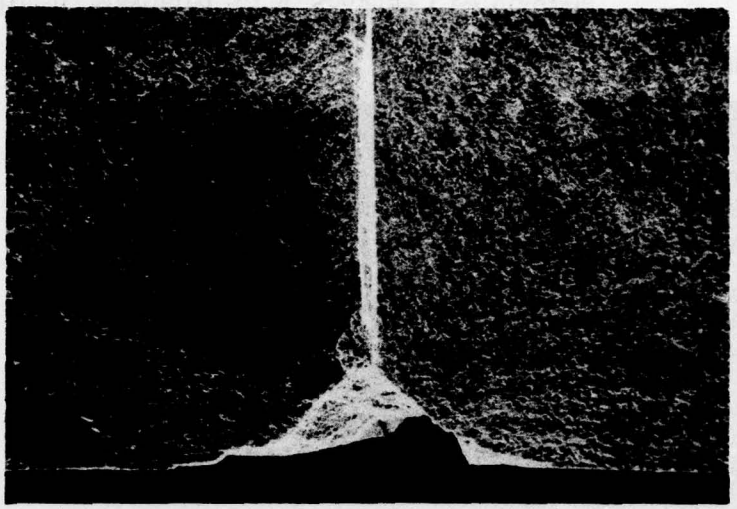

100X

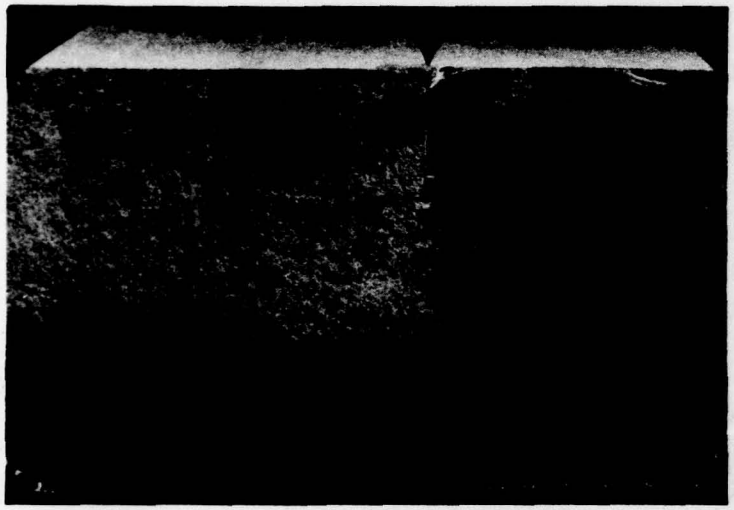

16X

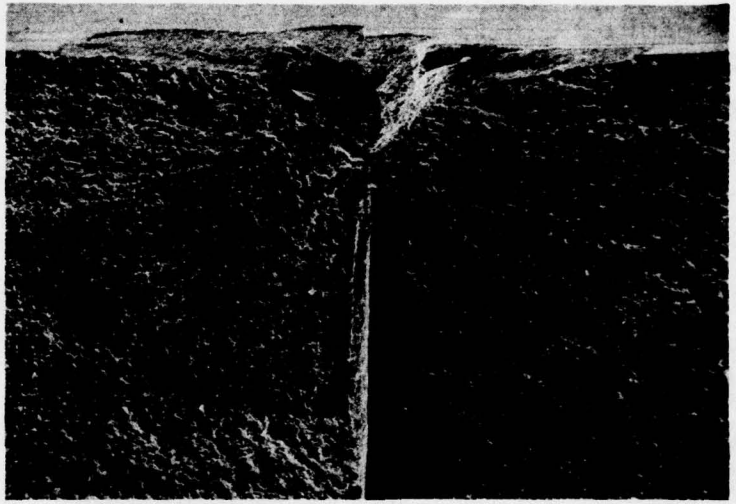

100X

Figure 76. Fracture Surfaces of NC-230A HPSiC Specimen No. 1, Showing 50 kg Vicker's Indentation at Fracture Origin.

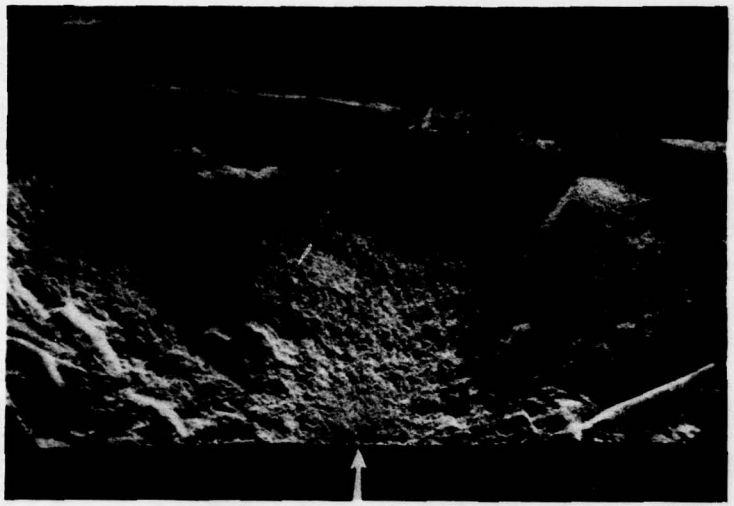

16X

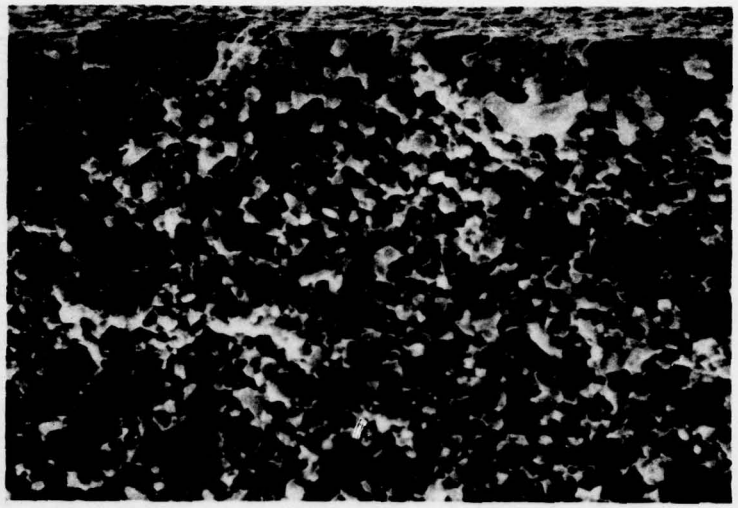

1000X

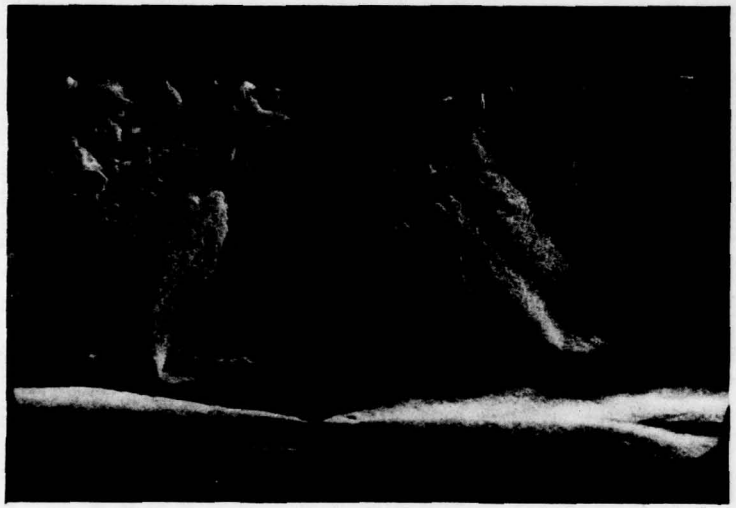

16X

100X

Figure 77. Fracture Surfaces of NC-230A HPSiC Specimen No. 4, Showing 1 kg Vicker's at Fracture Origin.

MN/m^2 (68.6 ± 7.8 ksi). The specimen containing the 1 kg Vicker's indentation was weaker at 380 MN/m^2 (55.1 ksi) than specimen 3, but stronger than specimens 7, 8 and 9. The specimens not containing Vicker's indentations all failed from fracture origins on the surface except for specimen 8 which failed from a corner. Only specimen 6 showed a well defined defect at the fracture origin. In Figure 78, which shows the fracture surfaces of specimen 6, it can be seen that the fracture origin is at an area of missing material at the surface 20 μm (0.0008 inches) wide by 10 μm (0.0004 inches) deep which probably represents a pre-existing pit or crack. Figure 79 shows the fracture surfaces of specimen 7. Even in the 1000X view it is not clear what difference between this specimen and No. 6 accounts for the great difference in ultrasonic response by all techniques.

6.2.4 SSiC

The results of the four-point-bend tests on boron-doped SSiC are listed in Table IV. All the specimens were machined perpendicular to the grinding damage. As can be seen in Figure 59, specimen No. 1 contained a severe individual linear defect indication. It failed at the defect location at a strength of only 192 MN/m^2 (27.9 ksi). Specimen No. 2 contained machining damage less severe than the defect in specimen 1. It failed at the defect location at a strength of 358 MN/m^2 (51.9 ksi). Specimens 3 and 4 showed no machining damage at the sensitivity of inspection. Their average strength was 423 ± 27 MN/m^2 (61.4 ± 3.9 ksi). Figure 80 shows the fracture surfaces of specimen No. 1. While there is a well defined fracture origin at the surface near one corner, the failure appears to have propagated along a line of pre-existing surface damage over most of the width of the specimen. Figure 81 shows 100X views of this damage away from the fracture origin. The depth of the defective area is estimated to have been about 50 μm (0.0020 inches). Specimen No. 2 shows similar results, except that the defect depth is only about 15 μm (0.0006 inches). Specimens 3 and 4 shattered so badly that a fracture origin could not be identified.

6.3 Discussion

Evaluation of the flexural strength test and SEM results in light of the ultrasonic results presented in Section 5 provides a basis for a qualitative, and to some extent, a quantitative evaluation of the ultrasonic technique. Qualitatively, for all the materials tested except RBSN, a direct correlation was observed between the intensity of ultrasonic indications and the weakness of the material. In the case of machining damage, specimens were found to be weaker in the direction in which the damage was detected ultrasonically. In the case of individual defects, while not all of the specimens containing such defects failed as a result of the defect, those that did showed considerably less strength than those that did not and also less strength than those in which no defect was detected. This shows that the ultrasonic technique is fairly reliable in providing a qualitative estimate of material strength. To put the results on a quantitative basis would require establishing a correlation between the defect signal amplitude (and/or other characteristics) and the material strength. This would require development of a suitable reference standard.

In the case of RBSN, the surface pattern is caused by cutting before nitriding, not by machining. It is possible that any damage associated with cutting is healed during nitriding. Also, both the cutting lines and the crack-like defects detected ultrasonically are quite shallow. Since the bulk strength of these materials is quite low, these defects

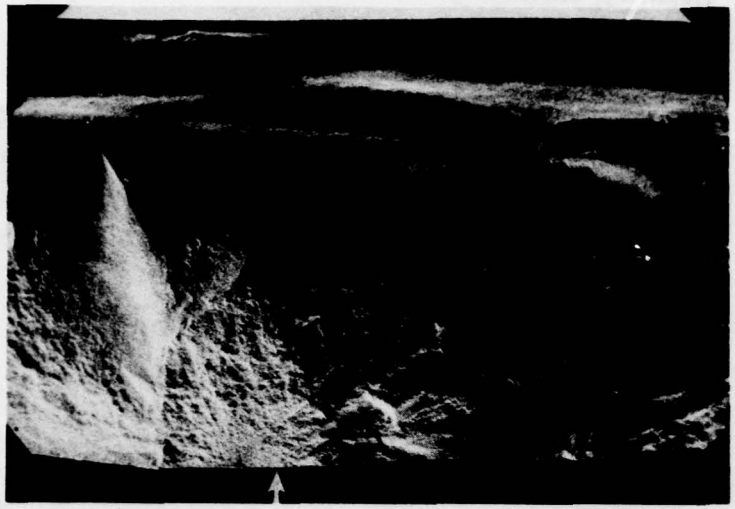

16X

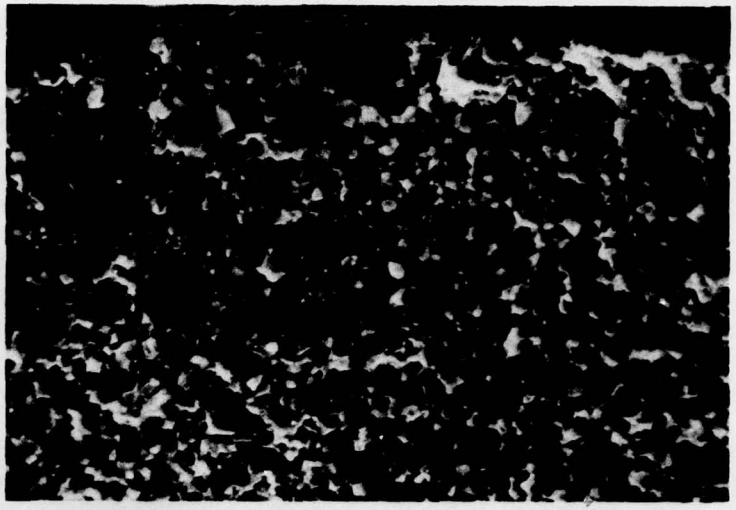

1000X

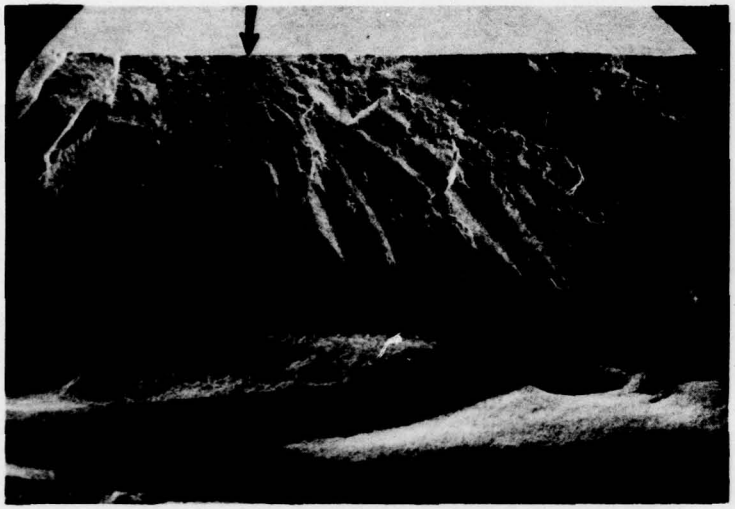

16X

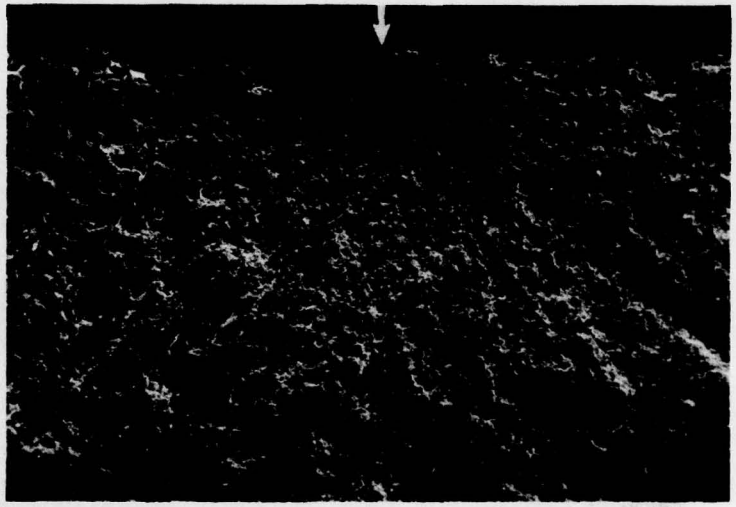

100X

Figure 78. Fracture Surfaces of NC-203A HPSiC Specimen No. 6 (Typical Sound Material With Light Grinding Damage).

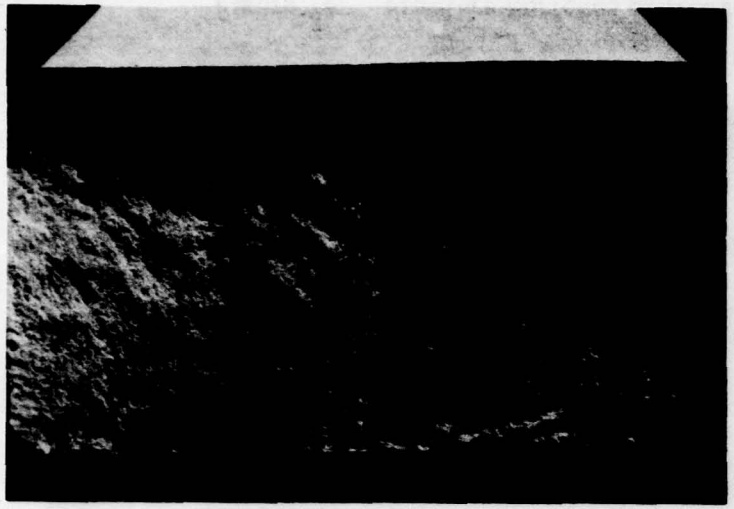

16X

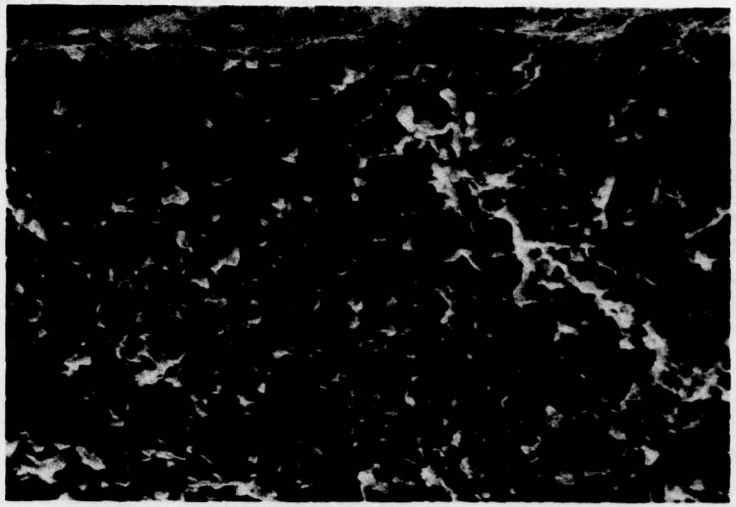

1000X

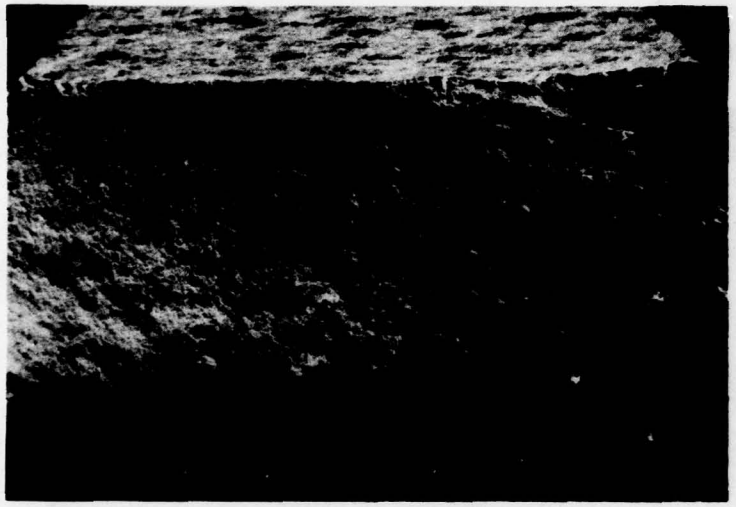

16X

100X

Figure 79. Fracture Surfaces of NC-203A HPSiC Specimen No. 7 (Typical Defective Material).

TABLE IV

Flexural Strength of Boron-Doped SSiC

Specimen No.	Flexural Strength MN/m^2	Flexural Strength ksi	Fracture Location mm from Center Length	Fracture Location mm from Center Width	Condition	Fracture Origin
1	192	27.9	1.75	1.12	Heavy Lin. Ind.	Surface scratch, 50 μm deep
2	358	51.9	1.75	3.10	Light Lin. Ind.	Machining line, 15 μm deep
3	405	58.9	1.50	3.20	against grinding	See Note 1
4	440	63.9	0.50	-	against grinding	See Note 1

Notes:

1. Specimen shattered too badly to identify fracture origin.

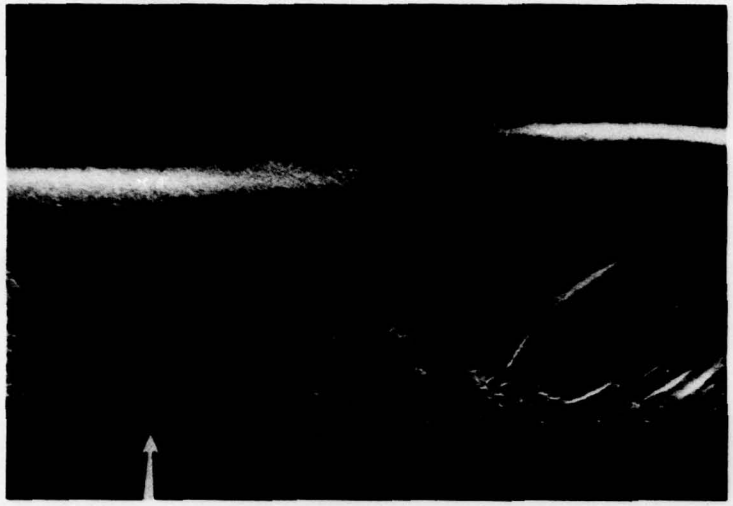

16X

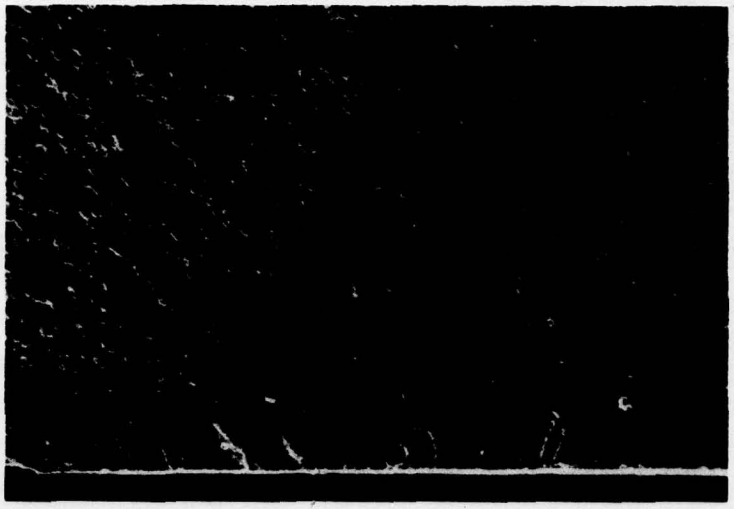

100X

16X

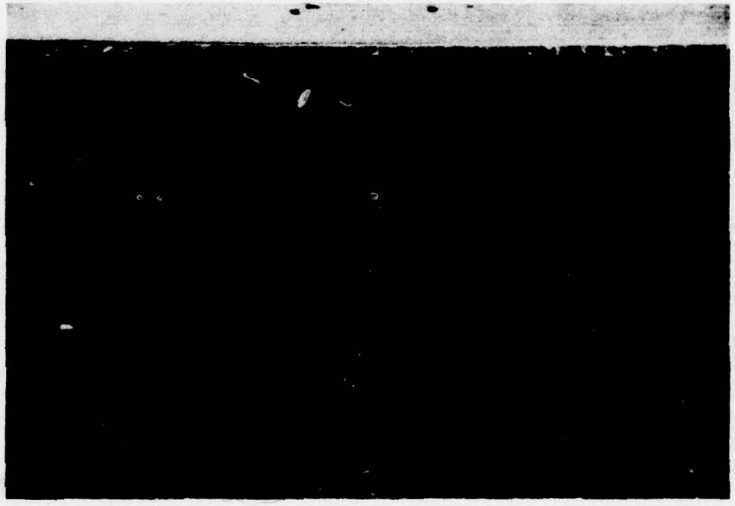

100X

Figure 80. Fracture Surfaces of Boron Doped SSiC Specimen No. 1, Showing Fracture Origin Along Ultrasonically Detected Linear Defect.

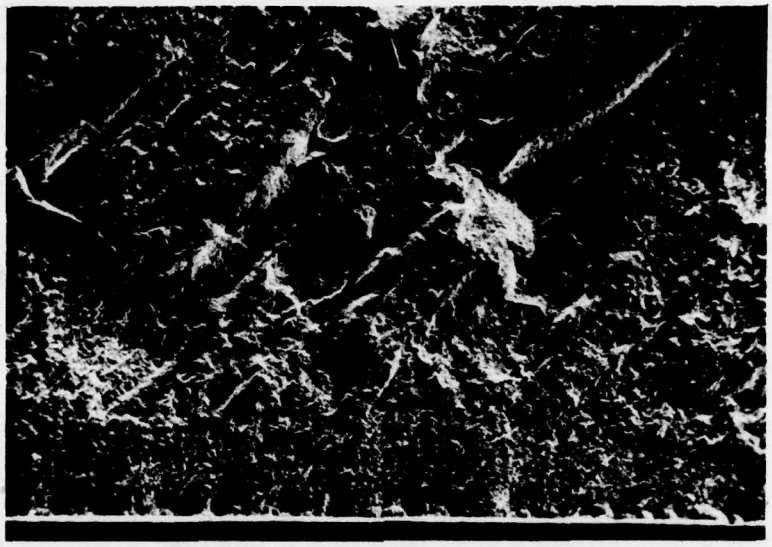

100X

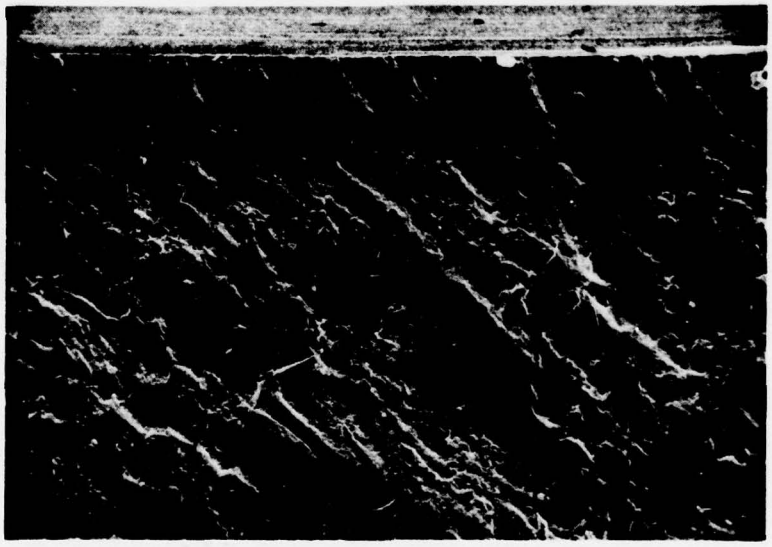

100X

Figure 81. Fracture Surfaces of Boron Doped SSiC Specimen No. 1, Showing Ultrasonically Detected Linear Defect in Area Away From Fracture Origin.

may not be large enough to be strength controlling. This conclusion is supported by the fact that most of the failures in this material result either from large near-surface grains or from corner damage probably inflicted during machining. The consequence of this is that strength controlling defects can only be detected in a material with this surface condition when the defect is large compared with these background indications.

This same condition exists to a lesser extent in the other materials. The 1 kg Vicker's indentations generally produce strengths that are less than, or at best equal to, the strength perpendicular to the grinding direction. Since the 1 kg Vicker's probably cannot be detected against the background of indications from the machining damage, it is possible to miss a strength controlling defect. As mentioned in Section 5, this limitation is primarily a result of the focal spot size of the ultrasonic beam, and only exists in the direction of sensitivity to the surface texture.

The quantitative data provided by these results has to do with the detectable defect size. The smallest defect correlated with an ultrasonic indication had a cross-sectional area of 700 μm^2 (0.6×10^{-6} $inches^2$). On the other hand, defects as large as 375 μm^2 (1.1×10^{-6} $inches^2$) were missed. The sensitvity limit would appear to be somewhere in this range, although even here it is a function of surface quality. Even when scanning parallel to the surface damage, full sensitivity of the ultrasonic system could not be used because of background indications from the surface texture. The 1 kg Vicker's indentations were not considered in this analysis because the ones tested were not examined ultrasonically and the crack sizes were very difficult to measure accurately from the micrographs.

7.0 BURNER RIG TESTING

7.1 Procedure

One specimen of each of the materials except SSiC was made for burner rig testing. Although some of these specimens contained natural defects, each was also given a 50 kg Vicker's indentation as a reference defect. Normally, burner rig specimens are metal and are machined from a large enough piece so that they can have a 12.7 mm (1/2 inch) diameter base to fit in the specimen holder. In this case, 12.7 x 76.2 mm (1/2 x 3 inch) specimens were cut with the thickness of the original billet. These specimens were then cemented in metal bases that would fit in the specimen holder using a high temperature ceramic adhesive*. Although this adhesive deteriorated somewhat under the stress of thermal cycling during the burner rig test, it was adequate to keep the specimens in place.

The test run on these specimens was a standard hot corrosion test in which the burner uses jet fuel with the addition of 0.3 g/hr of salt (sodium chloride). Four specimens in a holder are rotated at 1750 RPM. They are heated over a period of 2 min. to 927°C (1700°F), held at that temperature for 3 min., heated over a period of 0.5 min. to 1063°C (1950°F), held at that temperature for 0.5 min. and then allowed to cool for 2 min. before repeating the cycle. The purpose of running this test was to determine what type of surface changes would take place and what effect these changes would have on ultrasonic inspectability of the material. In order to determine this the specimens were inspected before the test, part way through the test and at the end.

7.2 Results

Figures 82 through 86 show the results of the ultrasonic inspections of the burner rig specimens. Each figure shows the results before exposure and after two different periods of exposure. The exposure times vary somewhat from one specimen to the other because there were only four test positions and five specimens. Therefore, some cycling of specimens in and out of the rig was required to get exposure on all specimens. Nevertheless, the results are remarkably similar. The burner rig flame was aimed at about the center of the lower half of each specimen. The 50 kg Vicker's indentation was placed in the upper half. The sensitivity of the inspections made after exposure was adjusted to allow the Vicker's indentation to be distinguished from the background. As the test progressed the deterioration of the surface quality required the sensitivity of the inspection to be reduced resulting in progressively smaller indications from the Vicker's indentations. In spite of this reduction in sensitivity, the area exposed to the flame became progressively darker with indications. The net effect was to make the specimens uninspectable.

* Ceramacoat 516 Adhesive, Aremco Products, Inc., Ossinning, NY.

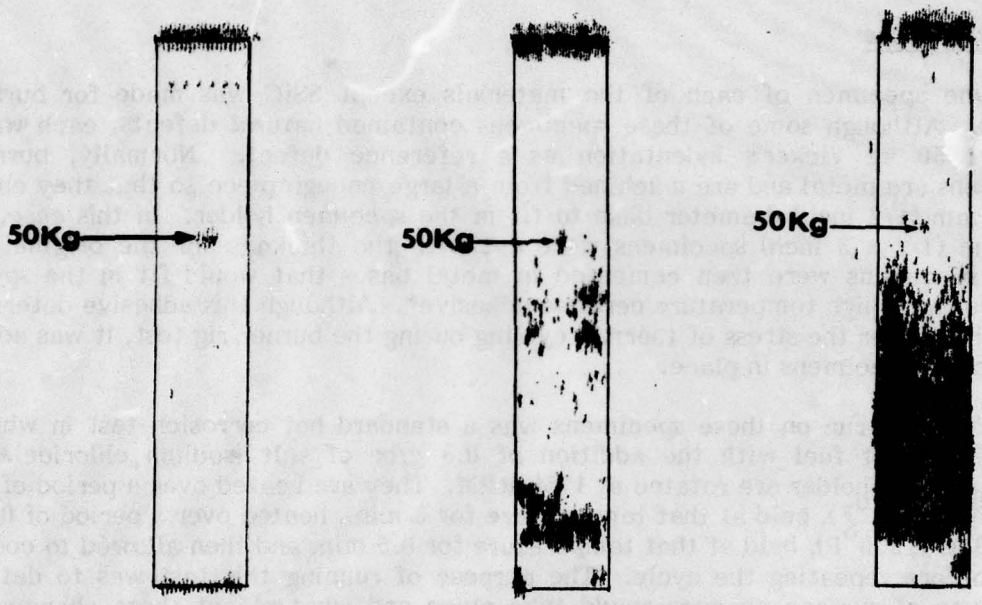

Figure 82. C-scan Recordings of 45 MHz, 18° Surface Wave Inspections of Specimen of Ceralloy 147A HPSN After 0, 22 and 28 Hours Exposure in Burner Rig.

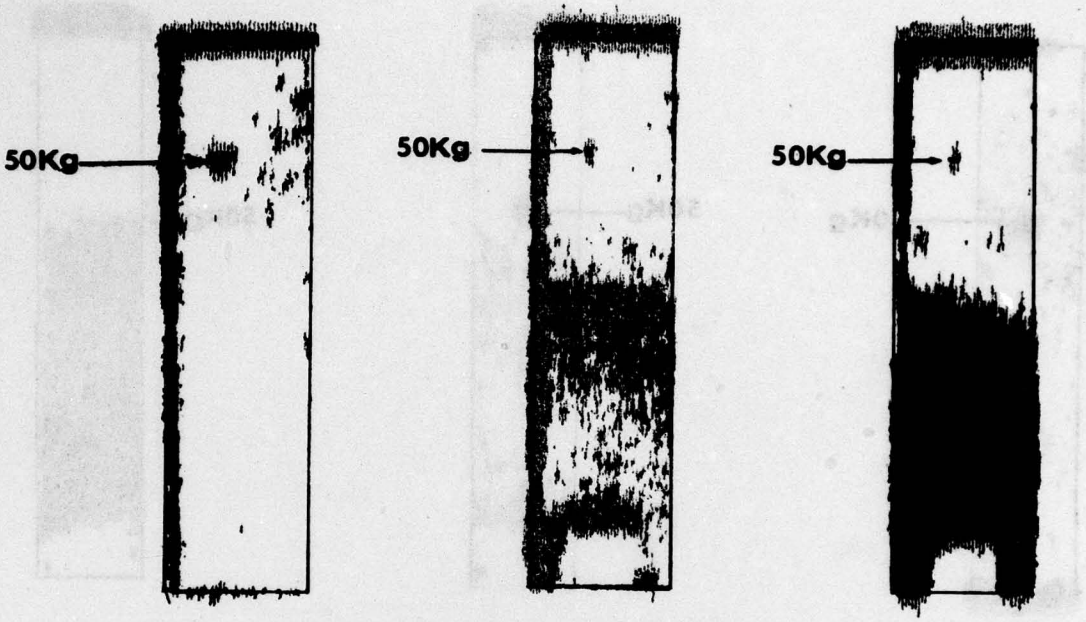

Figure 83. C-scan Recordings of 45 MHz, 18° Surface Wave Inspections of Specimen of NC-132 HPSN After 0, 13.5 and 19.5 Hours Exposure in the Burner Rig.

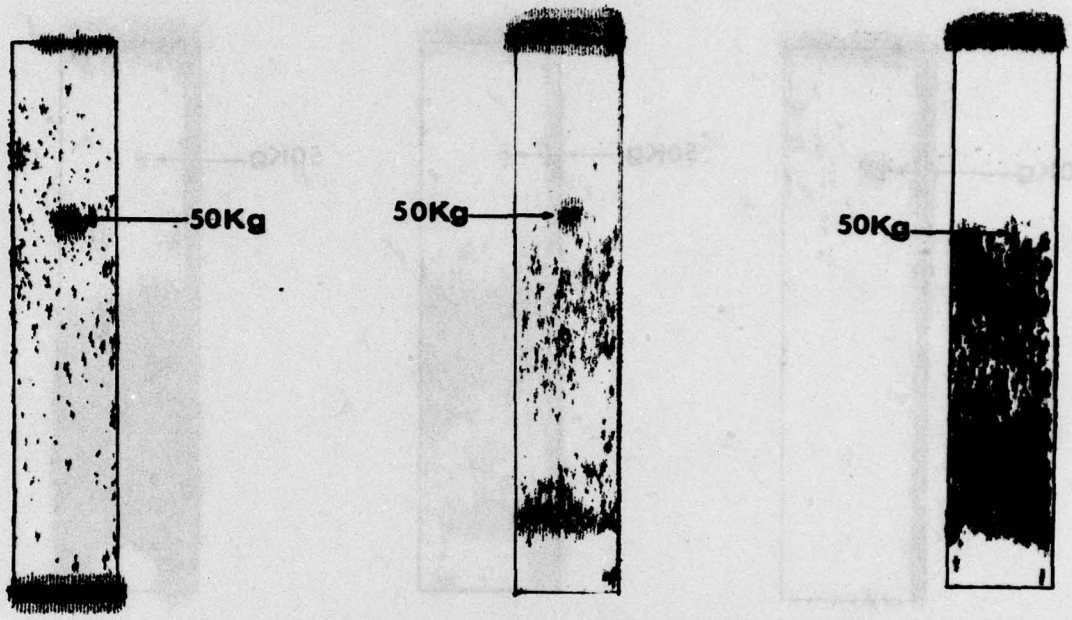

Figure 84. C-scan Recordings of 45 MHz, 18° Surface Wave Inspections of Specimen of NC-350 RBSN After 0, 22 and 28 Hours Exposure in the Burner Rig.

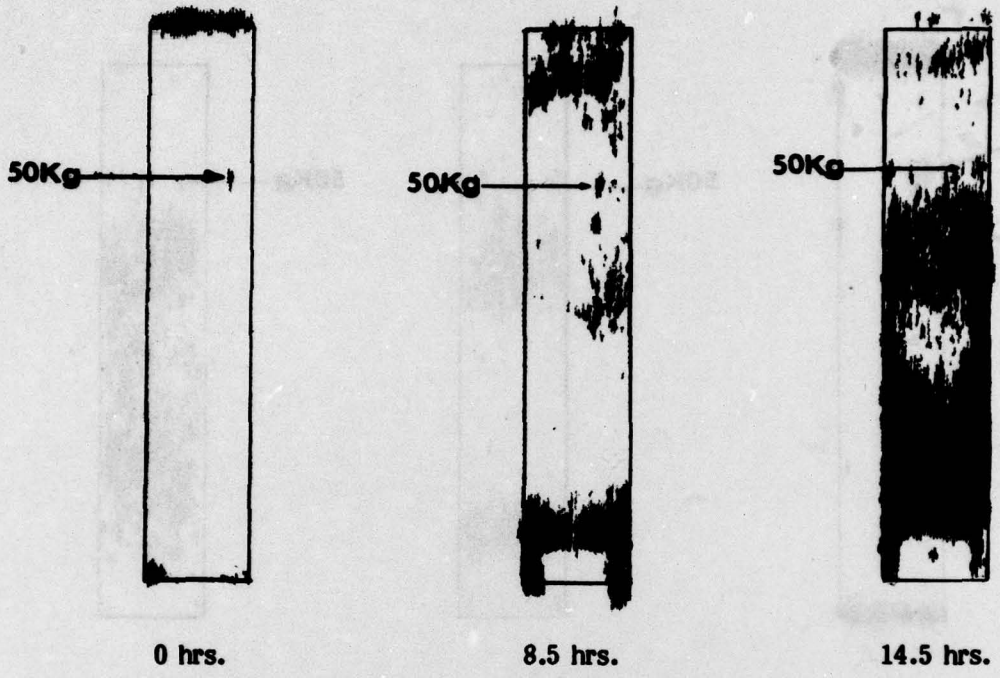

Figure 85. C-scan Recordings of 45 MHz, 18° Surface Wave Inspections of Specimen of Ceralloy 146 HPSiC After 0, 8.5 and 14.5 Hours Exposure in the Burner Rig.

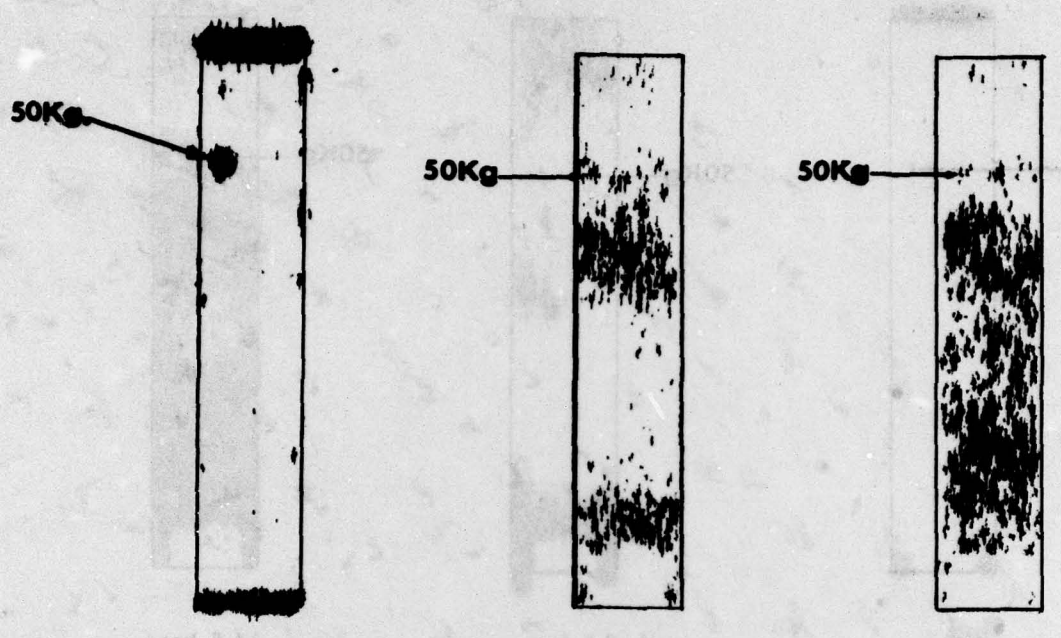

Figure 86. C-scan Recordings of 45 MHz, 18° Surface Wave Inspections of Specimen of NC-230A HPSiC After 0, 22 and 28 Hours Exposure in the Burner Rig.

The condition that made the specimens uninspectable is shown in Figure 87. The surface became covered with material that had the appearance of droplets of liquid that had solidified on the surface. These beads were transparent and varied in size, being smallest at the point where the center of the flame struck the specimen and getting larger with decreasing temperature. The largest beads were on the backsides of the specimens. Although each of the specimens had this condition, the distribution of sizes varied from one to the other. The possibility that the deposit was salt was considered. However, efforts to remove it using water or soap and water were unsuccessful.

Following final inspection of the specimens, electron microprobe analysis was run on the specimens to determine the nature of the surface deposits. The only elements found in large concentrations on the surface of the parts were silicon and oxygen. It was concluded that the surface condition was the result of fused silica beading up on the surface of the material.

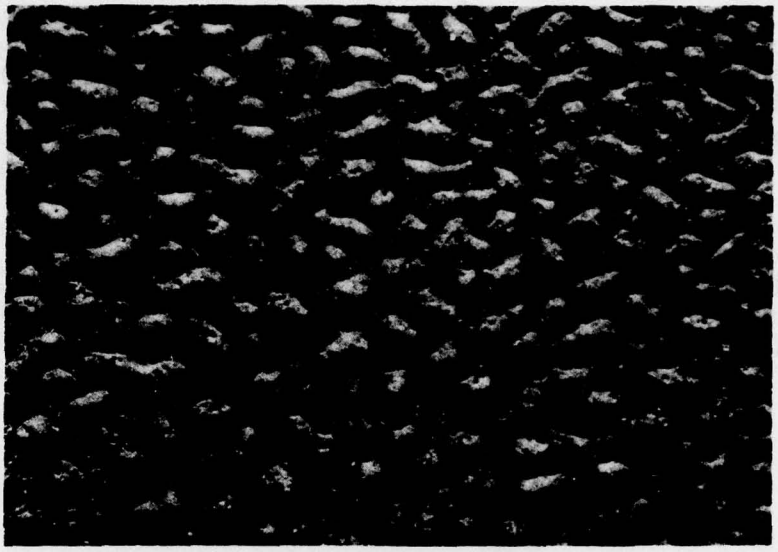

a. Back Side 5X

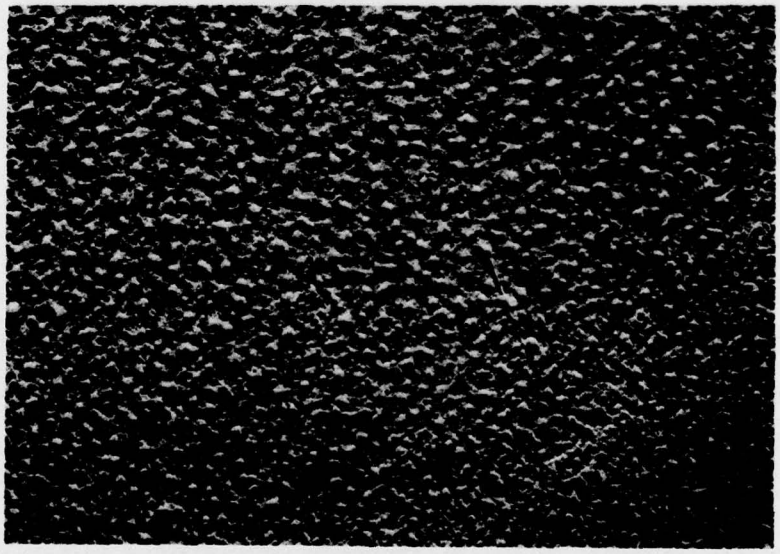

b. Flame Side 5X

Figure 87. Photomacrographs of Typical Burner Rig Specimen Surfaces After Testing, Showing Beads of Fused Silica.

8.0 CONCLUSIONS AND RECOMMENDATIONS

A 45 MHz ultrasonic immersion surface wave technique has been successfully developed for inspection of ceramic materials. This technique provides the unique capability to automatically scan a part with ultrasonic surface waves and record indications from small defects. The following specific conclusions were drawn concerning use of the technique on ceramic materials:

1. The technique is sensitive to the surface texture left by grinding damage, so that the ultrasonic inspection results can be correlated at least qualitatively, to the flexural strength of the material in the direction of propagation of the ultrasonic beam.

2. The size defect that can be detected is determined by the severity of the grinding damage and the focal spot size of the ultrasonic beam. Either a smoother surface finish or a smaller spot size will allow smaller defects to be detected.

3. On the machined surfaces tested, which were ground to approximately a 20 μin rms surface finish with a 320 grit diamond wheel and inspected with a transducer having a 580 μm (0.023 inch) diameter focal spot, a 1 kg Vicker's indentation is more severe than the grinding damage. However, it cannot be detected against the background of indications when scanning perpendicular to the grinding damage. This indicates the need for a smaller focal spot size.

4. Scanning parallel to the grinding damage to minimize the background indications, the smallest strength controlling defect, detected ultrasonically and verified metallurgically, had a cross-section of 700 μm^2 (1.2×10^{-6} in^2), which is equivalent to a 30 μm (0.0012 inch) deep semi-circular crack. The largest strength controlling defect found metallurgically but not detected ultrasonically had a cross-sectional area of 375 μm^2 (0.6×10^{-6} in^2), which is equivalent to a 15 μm (0.0006 inch) deep semi-circular crack.

5. Although Knoop and Vicker's indentations are potential reference defects, laser drilled holes seem more promising because their size can be more easily verified.

6. Specimens run in the burner rig became uninspectable because of fused silica beaded up on the surface.

Based on these conclusions, the following further activities are recommended:

1. Development of suitable reference standards for ultrasonic surface wave inspection of ceramics.

2. **Determination of the quantitative correlation between ultrasonic surface wave inspection and the flexural strength in the direction of beam propagation.**

3. **Use of ultrasonic surface wave inspection as a tool to evaluate surface damage in order to optimize grinding parameters for ceramic materials. This should include investigation of ultrasonics as an in-process method to provide feedback control for automated grinding.**

4. **Development and evaluation of a small focal spot size, high frequency ultrasonic transducer.**

9.0 REFERENCES

1. Derkacs, T., Matay, I.M. and Brentnall, W.D., "Nondestructive Evaluation of Ceramics," Final Report, Contract N00019-75-C-0238, Naval Air Systems Command, July 1976, TRW Internal Report No. ER-7798-F.

2. Derkacs, T., Matay, I.M. and Brentnall, W.D., "Ultrasonic Inspection of Ceramics Containing Small Flaws," Final Report, Contract N62269-76-C-0148, Naval Air Development Center for Naval Air Systems Command, August 1977, Internal Report No. ER-7867-F.

3. Private communication from J. A. Rubin, Technical Director, Ceradyne, Inc., January 13, 1977.

4. Private communication from C. A. Johnson, General Electric Co. Research and Development Center, May 18, 1976.

5. Schuldies, J.J. and Derkacs, T., "Ultrasonic NDE of Ceramic Components," Proceedings of the ARPA/NAVSEA Review of the Ceramic Gas Turbine Engine Demonstration Program, 21-2599(16), Aug. 1977.

6. Krautkramer, J. and Krautkramer, H., Ultrasonic Testing of Materials, 1969, p. 18, Springer-Verlag New York, Inc., New York.

7. Harrison, D.E., "Properties Important to the Design of Ceramic Stator Vanes for Industrial Gas Turbines," Proc. British Ceramic Soc., No. 22, 1973, pp. 391-408.

8. Fate, W.A., "High Temperature Shear Modulus of Si_3N_4 and SiC," J. AM. Ceram. Soc., Vol. 57, No. 1, Jan. 1974, pp. 49-50.

9. Rosinger, H.E., Ritchie, J.G., and Shillinglau, A.J., "A Systematic Study of the Room Temperature Elastic Moduli of Silicon Carbide," Materials Science and Engineering, 16, 1974, pp. 143-154.

10. Petrovic, J.J., et al, "Controlled Surface Flaws in Hot Pressed Si_3N_4," J. Am. Ceram. Soc., Vol. 58, Nos. 3 and 4, 1975, pp. 113-16.

11. Petrovic, J.J., and Jacobson, L.A., "Controlled Surface Flaws in Hot Pressed SiC," J. AM. Ceram. Soc., Vol. 59, No. 1-2, Jan-Feb, 1976, pp. 34-36.

12. Khuri-Yakub, B.T., et al, "Acoustic Surface Wave Scattering; The Detection of Surface Cracks in Ceramics," Technical Report, 11/01/76 to 11/30/77, Contract N00014-76-C-0624, Office of Naval Research, December 1977.

13. Derkacs, T., "Investigation of Ultrasonic Inspection Techniques for Defect Detection in Small, Complex Shaped Ceramic Turbine Blades," ER-8026, December, 1978.

DISTRIBUTION LIST

(one copy unless otherwise noted)

(3 copies plus balance after distribution)
U.S. Naval Air Systems Command
AIR-52031B
Department of the Navy
Washington, DC 20360

(7 copies, for internal distribution by AIR-954)
AIR-954 (2 copies), AIR-5361B1 (1 copy), AIR-330A (1 copy)
AIR-330B (1 copy), AIR-5361A (1 copy), AIR-5362A (1 copy)
U.S. Naval Air Systems Command
AIR-954
Department of the Navy
Washington, DC 20361

(2 copies)
Commander
Naval Air Development Center
Code 302A, A. Fletcher (1 copy),
Code 30232, E. Tankins (1 copy)
Warminster, Pennsylvania 18974

(2 copies)
U.S. Naval Air Turbine Test Station
Attn: E. Lister (AT-1P) (1 copy)
A. Martino (AT-1) (1 copy)
1440 Parkway Avenue
Trenton, New Jersey 08628

U.S. Naval Sea Systems Command
Code 035, Department of the Navy
Washington, DC 20362

Commander
Naval Weapons Center
Code 5516
China Lake, California 93555

Naval Ships Engineering Center
Code 6146
Center Bldg. Room 202
Prince Georges Center
Hyattsville, Maryland 20782

Naval Weapons Laboratory
Attn: W. Mannschreck
Dahlgren, Virginia 22448

U.S. Naval Ships Research & Development Center
Code 2812
Annapolis, Maryland 21402

Commander
Naval Surface Weapons Center
(Metallurgy Division)
White Oak
Silver Spring, Maryland 20910

(2 copies)
Director
Naval Research Laboratory
Code 6130 (1 copy)
Code 6360 (1 Copy)
Washington, D.C. 20375

Office of Naval Research
The Metallurgy Program, Code 471
Arlington, Virginia 22217

Director
Army Materials and Mechanics Research Center
(A. Gorum)
Watertown, Massachusetts 02172

Mr. George A. Darcy, Jr.
NDTIA Branch
Army Materials and Mechanics Research Center
Watertown, Massachusetts 02172

Commander
U.S. Army Material Command
Attn: AMCRD-TC
5001 Eisenhower Avenue
Alexandria, Virginia 22304

U.S. Army Aviation Materials Laboratories
Fort Eustis, Virginia 23604

(3 copies)
Air Force Materials Laboratory
Code LLM (1 copy)
Code LLN (1 copy)
Code LLP (1 copy)
Wright-Patterson Air Force Base
Dayton, Ohio 45433

Aerospace Research Laboratory
Metallurgy and Ceramics Division
Attn: Dr. H. G. Graham
Wright-Patterson Air Force Base
Dayton, Ohio 45433

Air Force Propulsion Laboratory
Code TBP
Wright-Patterson Air Force Base
Dayton, Ohio 45433

National Aeronautics and Space Administration
Code RWM
Washington, DC 20546

(4 copies)
National Aeronautics and Space Administration
Lewis Research Center
C. M. Ault (1 copy)
H. P. Probst (1 copy)
W. A. Sanders, MS 49-1 (1 copy)
S. J. Klima, MS 106-1 (1 copy)
21000 Brookpark Road
Cleveland, Ohio 44135

U.S. Atomic Energy Commission
Division of Reactor Development
Mail Station F-309 (A. Van Echo)
Washington, DC 20545

Oak Ridge National Laboratory
Attn: R. W. McClung
P.O. Box X
Oak Ridge, Tennessee 37830

Metals and Ceramics Information Center
Battelle Memorial Institute
505 King Avenue
Columbus, Ohio 43201

The Johns Hopkins University
Applied Physics Laboratory
(Maynard L. Hill)
8621 Georgia Avenue
Silver Spring, Maryland 20910

AVCO RAD
201 Lowell Street
Wilmington, Massachusetts 01887

ITT Research Institute
10 West 35th Street
Chicago, Illinois 60616

Detroit Diesel Allison Division
General Motors Corporation
Materials Laboratories
Indianapolis, Indiana 46206

Pratt and Whitney Aircraft
(Mr. A. Magid)
Florida Research and Development Center
West Palm Beach, Florida 33402

Chief, Materials Engineering Dept.
Dept. 93-39M
AiResearch Manufacturing Co. of Arizona
402 South 36th Street
Phoenix, Arizona 85034

Lycoming Division
AVCO Corporation
Stratford, Connecticut 06497

Curtis Wright Company
Wright Aeronautical Division
Wood-Ridge, New Jersey 07075

Bell Aerosystems Company, Technical Library
P.O. Box 1
Buffalo, New York 14240

General Electric Company
Aircraft Engine Group
Materials and Processes Technology Laboratories
Evendale, Ohio 45215

Solar
(Dr. A. Metcalfe)
2200 Pacific Highway
San Diego, California 92112

Teledyne CAE
1330 Laskey Road
Toledo, Ohio 43601

Stellite Division
Cabot Company
Technical Library
P.O. Box 746
Kokomo, Indiana 46901

(2 copies)
General Electric Co.
Corporate Research and Development
Attn: W. Hillig (1 copy)
R. Charles (1 copy)
Schenectady, New York 12301

Norton Company
Protective Products Division
(N. J. Ault)
Worcester, Massachusetts 01606

Westinghouse Electric Company
Materials and Processing Laboratory
(Ray Bratton)
Beulah Road
Pittsburgh, Pennsylvania 15235

Library
Research & Development Div.
The Carborundum Company
P.O. Box 337
Niagara Falls, New York 14302

Ford Motor Company
Product Development Group
(E. A. Fisher)
2000 Rotunda Drive
Dearborn, Michigan 48121

General Electric Company
AEG Technical Information Center
Mail Drop N-32, Bldg. 700
Cincinnati, Ohio 45215

Professor Richard E. Tressler
Ceramic Science Section
Pennsylvania State University
201 Mineral Industries Bldg.
University Park, Pennsylvania 16802

Dr. T. D. Chikalla
Ceramics and Graphite Section
Battelle - Northwest Laboratories
Richland, Washington 99352

United Aircraft Research Labs.
East Hartford, Conn. 06108

Pratt & Whitney Aircraft
East Hartford, Conn. 06108

NTDSC
Southwest Research Institute
P.O. Drawer 28510
San Antonio, TX 78284

SKF Industries
(Harish Dalal)
1100 First Avenue
King of Prussia, PA 19406

Ceramic Finishing Company
(H. P. Kirchner)
P.O. Box 498
State College, PA. 16801

FINAL REPORT ONLY

(12 copies)

Commander, Naval Air Development Center
Code 302A, A. Fletcher - for DDC
Warminster, PA 18974

(3 copies)

Commander, Naval Air Development Center
Code 813
Warminster, PA 18974